Heat Transfer Analysis of a Fin-tube Heat Exchanger using Shear-thinning Fluid and Winglet Type Vortex Generators

A thesis submitted
in partial fulfillment of the requirements
for the Degree of

Doctor of Philosophy

by

Dheeraj Kumar

Department of Mechanical Engineering

Indian Institute of Technology Guwahati

Guwahati - 781 039

April 2024

CERTIFICATE

It is certified that the work contained in the thesis entitled **"Heat Transfer Analysis of a Fin-tube Heat Exchanger using Shear-thinning Fluid and Winglet Type Vortex Generators"**, by **Dheeraj Kumar** has been carried out under my supervision and that this work has not been submitted elsewhere for a degree.

Dr. Amaresh Dalal
Professor,
Department of Mechanical Engineering,
IIT Guwahati, 781039, Assam.

Date: April, 2024
Place: Guwahati

Abstract

The present work investigated the effect of winglets on the flow behavior of an aqueous solution of carboxymethylcellulose (CMC) through a rectangular channel with and without the inbuilt cylinders. Three-dimensional numerical simulations have been performed on a fin-tube heat exchanger (FTHE) using delta winglet (DW), rectangular winglet (RW), and curved rectangular winglet (CRW) using an aqueous solution of CMC as a shear-thinning fluid in the range of Reynolds number (Re) 50 to 200. These winglets were positioned at various attack angles (β) in several combinations, such as common flow up (CFU) and common flow down (CFD). For each winglet, the Nusselt number (Nu), friction factor (f_{app}), and the combined impact of both, known as the quality factor (Q_f), of FTHE, were calculated and compared. Additionally, the comparison is also made with the base channel considering a dimensionless number (η) defined as $(Nu_m/Nu_o)(f_o/f)^{0.33}$. Furthermore, the effect of attack angle, winglet placement, and tube placement (staggered and inline) were examined. The performance parameters of FTHE were compared using an aqueous solution of CMC and water. It was discovered that the inclusion of DWPs in FTHE improves overall performance compared to the inclusion of RWP in FTHE. Still, when only heat transfer applications are considered, RWP outperforms DWP. When considering heat transfer, friction factor, or both, using CRWP is a better option than RWP. CRWVG in an FTHE heat exchanger increases the Nu_{av} and Q_f by 10-18% and 8-22% respectively, and decreases the f_{app} by 1-5% compared to the conventional RWVG. It was seen that reducing the attack angle up to a certain limit increases the performance parameter, and a further decrease in attack angle decreases the performance parameter. Using an aqueous solution of CMC as a working fluid increases the Nu and Q_f and decreases the f_{app}. The inclusion of winglets in the FTHE reduces the wake zone behind the cylinder and generates secondary flow, resulting in an increase in heat transfer at the cost of pressure drop compared to the base channel. Considering the overall performance, FTHE with winglets outperforms the base channel. Compared to the inline tube configurations, the staggered tube configurations of FTHE increase the Nu, f_{app} and Q_f.

Dedicated to all

who made me

what I am today

Acknowledgements

The process of research is a journey that requires the contributions of many individuals, both personally and professionally. If one had to work independently on their complete doctoral research, they would never be able to achieve their goal. In the past three years, many people have contributed to the thesis work presented here. It is difficult to name every individual and their contributions on a short note, but I am forever grateful to all of them. However, I would like to take this opportunity to acknowledge a few of my well-wishers who have helped me immensely during my doctoral research at the Indian Institute of Technology Guwahati.

I would like to express my sincere gratitude to my supervisor, Professor Amaresh Dalal, for his invaluable guidance and unwavering support throughout my thesis work. His selflessness and constant presence have significantly lightened the burden of this enormous task and aided me in completing my dissertation. His constructive ideas and input regarding the objectives of my thesis have been instrumental in shaping it into its final form. Professor Dalal has always been understanding of my limitations, providing a conducive research environment and encouraging me to look at the brighter side of things. I consider myself extremely fortunate to have had the opportunity to work under his supervision. I would also like to thank my doctoral committee members - Prof. Vinayak Kulkarni, Prof. Atul Kumar Soti, and Prof. Pankaj Kumar Mishra for their insightful contributions during my progress seminars have been instrumental in shaping my growth and development.

I would also like to thank the management of Sikkim Manipal Institute of Technology, Majhitar for providing me the opportunity to complete my thesis work at IIT Guwahati.

I couldn't have made it this far without my amazing friends. They have been my support system all along, cheering me on every step of the way. I am truly grateful to have such wonderful people in my life. I feel so lucky to be a part of such an incredible team here at Anupravaha lab. I just wanted to take a moment to express my sincere gratitude to each and every member for making this a truly delightful workplace. I am specially thankful to Dr. Santanu kumar Das, Niraj Kumar Prasad and Rupresha Deb for being so generous and always available for any kind of help, without you people I would never have been completed this Ph.D. journey. I am quite thankful to Ashok Kumar Gond for helping me to learn ANSYS FLUENT. I thoroughly enjoyed the company of Kaustabh Chatterjee, Abhijit Pal, and Rumi Das to make my stay on the IITG campus comfortable and enjoyable. I am very thankful to my badminton family in IITG, Mrs. Swapnali Bora mam, Akshay Namdeo, Vivek Kumar, Sukanta Das, Vivekananda Halder, Suraj Tat Arun and Sukhjeet Aurora for always being there in my ups and down.

My family is the sole reason for my accomplishments; however small it may be. I feel a deep sense of gratitude towards my parents, who have been extremely patient, understanding, and supportive throughout this journey and beyond. I sincerely appreciate the sacrifices you have made during this journey for turning my dream into reality. I am also thankful to my sisters and brother-in-laws for their constant motivation and support.

Dheeraj Kumar

Contents

List of Figures

List of Tables

Nomenclature

Acronyms

CFD common flow down

CFU common flow up

CMC carboxymethyl cellulose

CRWP curve rectangular winglet pair

CRWVG curve rectangular winglet vortex generator

DWP delta winglet pair

DWVG delta winglet vortex generator

FTHE fin-tube heat exchaner

LVG longitudinal vortex generator

PEC performance evaluation criteria

RWP rectangular Winglet pair

RWVG rectangular winglet vortex generator

VG vortex generator

Greek symbols

α inclination angle of CRWVG (°)

β attack angle (°)

Δp pressure difference (N/m^2)

η efficiency (–)

μ dynamic viscosity (kg/(m $\cdot$ s))

ν kinematic viscosity (m^2/s)

ρ density (kg/m^3)

Roman symbols

$\dot{m}$ mass flow rate (kg/s)

$\dot{q}$ heat flux (W/m^2)

A area (m^2)

c_p specific heat (kJ/kg $\cdot$ K)

D cylinder diameter (m)

f friction factor (–)

H channel height (m)

h heat transfer coefficient (W/(m^2·K))

j mean colburn factor

l_{vg} length of vortex generator (m)

Nu Nusselt number (–)

p pressure (N/m^2)

Pr Prandtl number (–)

Q_f quality factor (–)

Re Reynolds number (–)

T temperature (K)

u velocity (m/s)

W channel width (m)

x axial coordinate (m)

K consistency index (kg/(m $\cdot$ s^{2-n}))

k thermal conductivity (W/(m $\cdot$ K))

L channel length (m)

n power law index (–)

Subscripts

in inlet

m, av mean. average

o base channel

out outlet

p plane channel

sa span-average

w wall

Chapter 1

Introduction

There have been various developments in heat transfer with the evolution of industrial technologies, as it plays a vital role in producing different components. Improvement of heat transfer is of significant importance in fields such as power plants, the automotive industry, heating, ventilation and air conditioning and aeronautics devices, etc. [1]. Heat transfer equipment is being used for conversion and heat recovery in many applications in manufacturing and domestic purposes [2]. The heat exchanger is a device that allows the exchange of heat between the two fluids. The wide-ranging of heat exchangers are based on their types of compact architecture, flow arrangements, compact surface, heat transfer method, pass arrangement, fluid phase, application, and mechanism for heat transfer [3]. Available surface area for heat transfer is a critical determinant of total heat transfer. Fin-tube heat exchangers (FTHE) are known by design to maximize the surface area of heat transfer.

1.1 Fin-tube heat exchanger

The FTHE is a heat exchanger with extended surfaces that are commonly used when heat is needed to transfer between liquid and gas. The medium with poor heat transfer quality is supported by an arrangement of extended surfaces, i.e., fins or other essentials such as pins or needles. Such elements can be added to the surface to a considerable height, or they can be small and made from the material of the tube itself. Fins can be found in tubes both indoors and outdoors and are usually transverse or around the shaft axis of a jacket.

FTHE are manufactured in various designs from several materials or combinations of fin-tube materials; based upon their proposed application, fin-tubes were used as the initial concept for economizers. Just a limited number of fin tubes were made for testing purposes using solid materials. All were made of ringed fins shown in Fig. 1.1, where h, P_t, t, and D_A are the height, pitch, thickness and annular diameter of the fin, respectively.

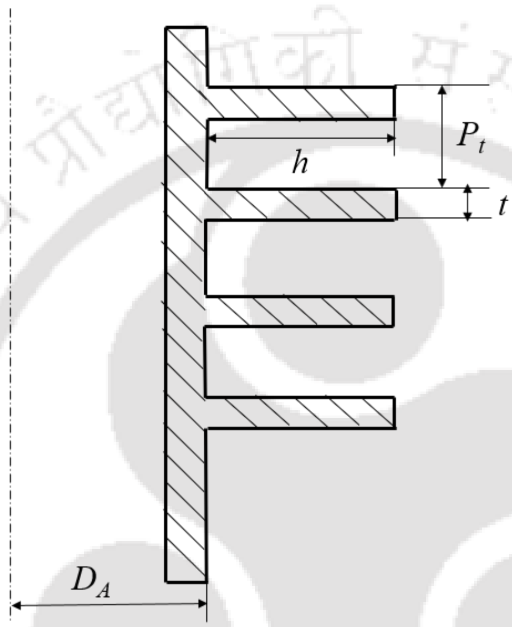

Figure 1.1: Fin-tube with annular fins

1.1.1 Design of fin-tubes

Spiral tubes are still used in the thermal and chemical industries. Fins in the form of steel strips are wrapped around a boiler tube and connected with the help of either resistance or laser welding to the core tube Fig. 1.2.

Fin-tubes with fins wrapped around the tube only by pressure are often used in cases with reduced heat transfer requirements and not too high gas temperatures Fig. 1.3. These fins are also zinc-plated for greater resistance to corrosion after processing. This also results in a tighter bond between the fins and the tube, which enhances heat conduction.

The applications of these finned pipes with copper (Cu) tubes with Cu or aluminum fins or steel tubes with aluminum fins are also used in the field of heating,

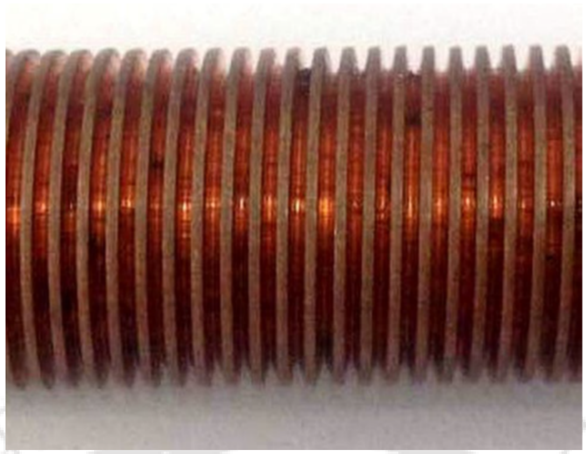

Figure 1.2: Fin-tube with spiral fins [4]

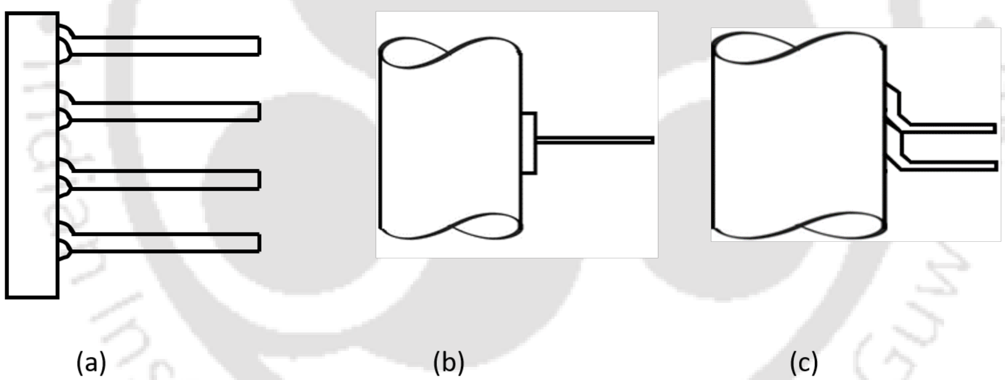

Figure 1.3: (a)Fin-tubes with spiral fins attached by pressure, (b)Fins with t-shaped fin base and (c) Fins with L-shaped fin base

ventilation, and air conditioning (HVAC). For better conduction at the base of the tube, fins are often wrapped by pressure Fig. 1.3(a), fixed around the tube, and fitted with a T-shaped Fig. 1.3(b) or L-shaped base Fig. 1.3(c). Non-circular cross-section tubes are used to reduce the pressure drop on the gas side. Generally, oval or flat tubes and fins are also attached to these tubes. Fins that pass through numerous tubes are also used in the heating, ventilation, and air conditioning as well as in refrigeration fields. To improve heat transfer, wavy fins are mounted orthogonally to the flow direction. FTHE are now employed as fundamental devices in heat transfer processes in a wide range of engineering applications, including vehicles, cooling systems, air conditioning, chemical engineering, aerospace, electronic chip cooling, and power systems. The power requirements for heat exchangers are continuously increasing in order to maintain the heat transfer capacity of heat exchangers. Energy usage, efficiency optimization, and compactness enhancement are critical for this. Thermal resistance leads to the air side of the compact heat exchanger, as per basic knowledge of heat transfer. As a result, the thermal resistance on the air side must be reduced. Passive heat transfer devices, such as rough surfaces, dimples, or cavities, are frequently utilized in micro heat exchangers or other energy converters on micro sizes. Guidance boards, diverter strakes, and vortex generators are examples of larger-scale tools. The vortex generator (VG) is vital for enhancing the air-side heat transfer coefficient.

1.2 Vortex generator

The VG, also known as flow manipulators, is an impressive technique that enhances the thermal performance of FTHE. It can be mounted on the fin surface to create resultant flow and to improve heat transfer. VGs are often embossed, punched, welded, or extruded. VG-induced vortices are classified into two types: transverse vortices and longitudinal vortices. Longitudinal vortex generators (LVGs) produce longitudinal vortices parallel to the main flow direction with their axes, and transverse vortex generators (TVGs) produce transverse vortices perpendicular to the main flow direction.

1.2.1 Mechanism

Longitudinal vortices are formed once the fluid passes over VGs due to the friction and pressure difference on the leading and trailing edges of the VG. Once the fluid passes over VGs, the pressure difference between both sides of the VGs is different, which creates boundary layer separation, further leading to enhanced turbulence and proper fluid mixing. These vortices impart heavy swirling action that leads to thermal boundary layer disruption and, in some cases, to unstable oscillatory motion. VGs improve heat transfer performance by disrupting and deteriorating the boundary layer, resulting in increased turbulence. The generation of transverse vortices controls the heat transfer primarily through flow disruption. In contrast, longitudinal vortices and their generation influence the rate of heat transfer by concerning above all heat transfer mechanisms [3]. The increased mixing of fluids and secondary flow and the interruption of thermal boundary layer development increase the heat transfer coefficient. Amplification of the recirculation zone downstream of the VGs and reinforcement of the induced vortices at elevated *Re* strengthen the fluid mixing and secondary flow in the channel.

1.2.2 Types and arrangements of VGs

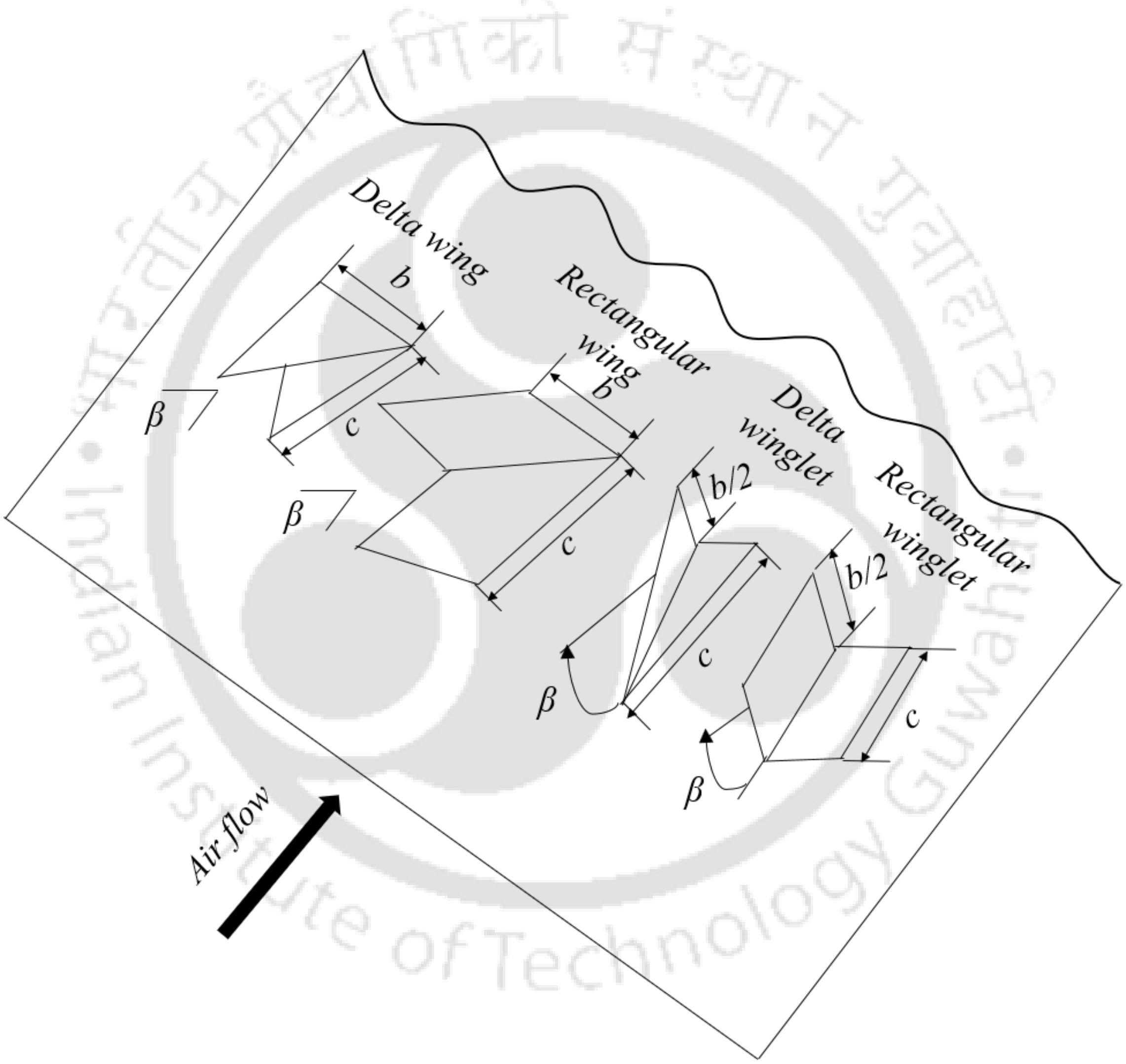

Figure 1.4: Types of Common vortex generators and its geometrical definitions

The VG devices differ in their geometry, dimensions, and integration on the surface of the heat exchanger, resulting in two main categories of the generated vortex: transverse and longitudinal, depending on the particular application. The longitudinal vortices are generally more effective than transverse vortices in improving

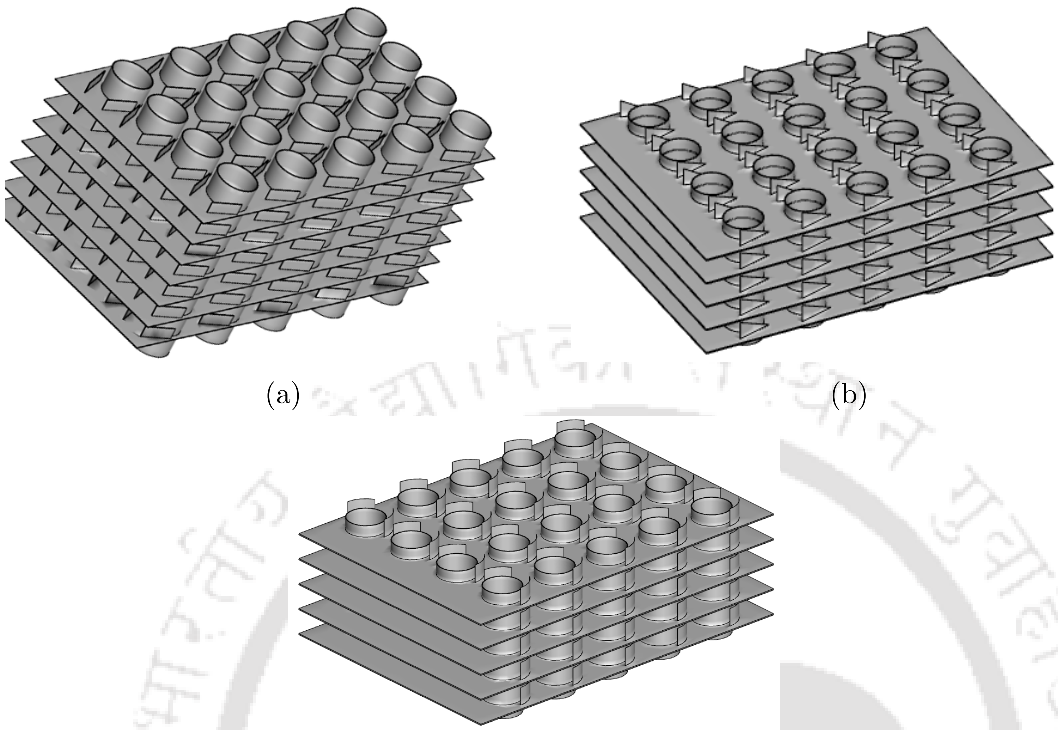

(a) (b)

(c)

Figure 1.5: Fin-tube with (a) RWP, (b) DWP and (c) CRWP

heat transfer with only a small increase in pressure drop. Four surface protrusion designs are commonly used for the heat transfer enhancement induced by longitudinal vortex. They are delta wing, rectangular wing, delta winglet, and rectangular winglet, and their geometrical definitions are shown in Fig. 1.4, where b, c, and β are the width, length, and attack angle of the winglets. There is a key impact on the heat transfer capability of these VGs due to their geometry parameters, such as the angle of attack and aspect ratio [5]. The fin-tube with rectangular winglet pair (RWP), delta winglet pair (DWP), and curve rectangular winglet pair (CRWP) are shown in Fig. 1.5. In addition to the four main styles, several additional VGs have been recently proposed and investigated. Such types of VGs are annular winglet and wave elements, mainly for application in FTHE, and V-deployed VG arrays to emulate the locomotion of animals in nature. Here are several types of vortex generators (VGs) that can be used on both straight and curved surfaces. These include rectangular winglets (RW), trapezoidal winglets (TW), delta winglets (DW), curved rectangular winglets (CRW), curved trapezoidal winglets (CTW), and curved delta winglets (CDW). Some of these winglets have punched holes.

1.2.3 Based on the arrangement of VGs

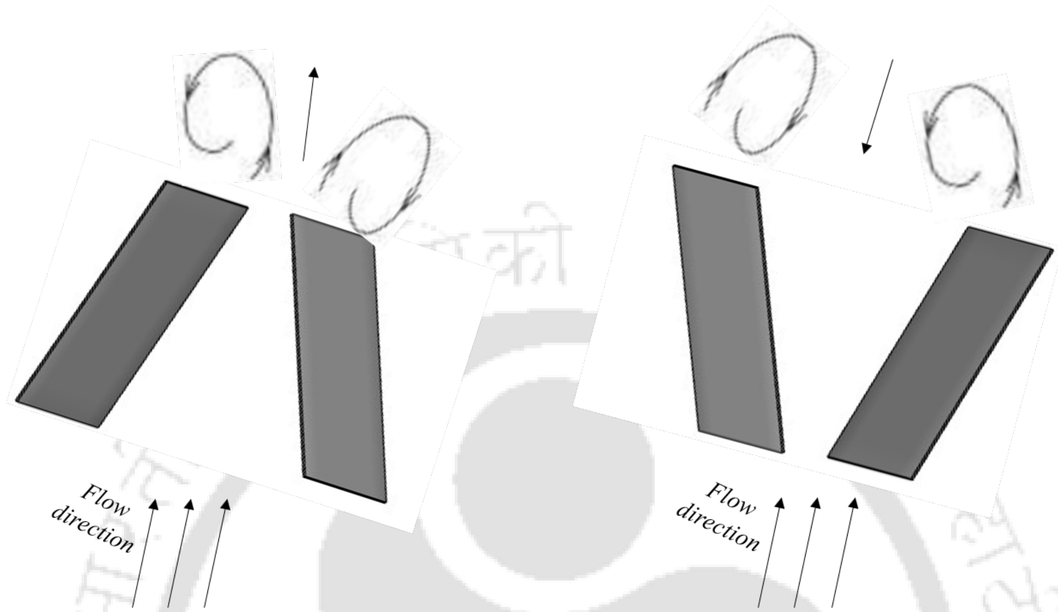

(a) (b)

Figure 1.6: Types of VGs based on placement (a) Common flow up and (b) Common flow down

There are mainly two types of VGs on the basis of placement strategies: common flow down (CFD) and the common flow up (CFU) as shown in Fig. 1.6, approaches for a single fin-tube element. CFU means that the VGs are positioned on the air/gas side in such a way that the consequential vortices rotate to transfer the fluid between them away from the surface they are mounted on, or it generates two anticlockwise antirotating vortices trying to push the fluid toward the upward direction. CFD means that the flux between the two vortices is directed toward the surface they are mounted on, or it generates two clockwise antirotating vortices trying to push the fluid towards the bottom surface of the fin.
Apart from surface modifications, the use of effective coolants is considered to be a rational approach to improve the efficiency of thermal systems in heat transfer. Due to their higher heat transfer coefficient, liquid coolants are preferred over gaseous coolants for heat transfer augmentation applications. Non-Newtonian fluids are of great interest for practical applications as they can be relatively easy to manufacture compared to nanofluids.

1.3 Non-Newtonian fluid

The relationship between shear stress and shear rate in a non-Newtonian fluid is different and can even be time-dependent. Therefore, a constant coefficient of viscosity cannot be defined. Power law fluid is a fluid whose viscosity is variable based on applied stress. Heat transfer processing of viscous power fluids is encountered in various industrial sectors, including chemicals, petrochemicals, food, biomedical, polymers, consumer product industries, and pharmaceuticals. Process food, pharmaceutical, chemical, and biochemical fluid media generally show non-Newtonian behavior, and the shear-thinning or thickening behavior of these fluids significantly affects their thermal-hydraulic performance. There are many different models to describe the rheology of non–Newtonian systems. Non-Newtonian fluids have two-dimensional and three-dimensional behavior quite different from the behavior of Newtonian fluids in similar circumstances.

1.3.1 Types of non-Newtonian fluid

Most real fluids exhibit non-Newtonian behavior, which means that the shear stress is no longer linearly proportional to the velocity gradient. If the viscosity doesn't depend on the forces acting upon it, the fluid is said to be non-Newtonian fluid, as mentioned in Fig. 1.7.

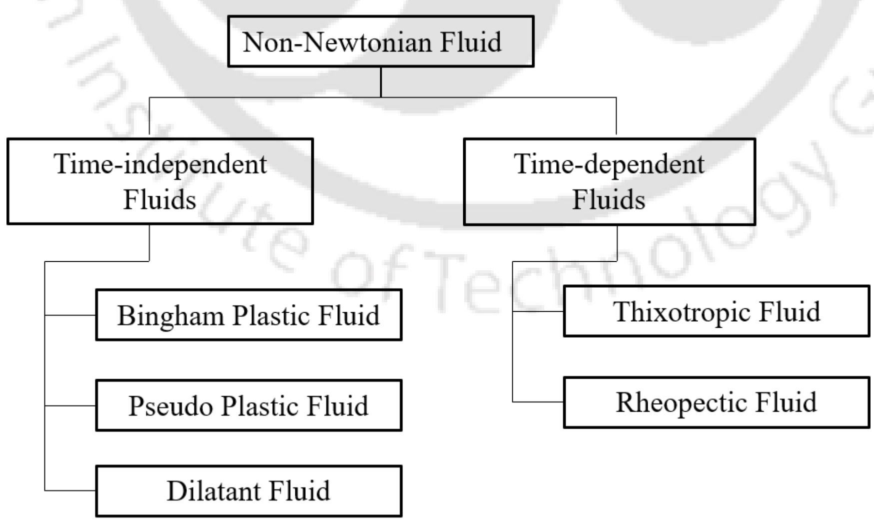

Figure 1.7: Types of non-Newtonian fluids

Table 1.1: Thermal characteristics of water and a CMC solution in water [7]

Sl no	Properties	SI unit	Water	CMC
1	ρ	$[\mathrm{kg\,m^{-3}}]$	1000	1000
2	c_p	$[\mathrm{J\,kg^{-1}\,K^{-1}}]$	4100	4100
3	k	$[\mathrm{W\,m^{-1}\,K^{-1}}]$	0.6076	0.7
4	μ	$[\mathrm{N\cdot s\,m^{-2}}]$	9.55×10^{-4}	equation (1.1)

a. Time independent fluid

Shear-thinning fluid (Pseudo plastic fluid)

(CMC, Xanthan gum, Ketch up, Blood, Nail polish and paints etc.) An increasing shear force gives a more proportional increase in shear rate. The material seems less viscous at high shear rates.

Shear-thickening (Dilatants fluids)

Less common than pseudo plastic fluids. Examples are corn flour-sugar solutions, liquid chocolates, and corn starch in water. Their apparent viscosities increase with increasing shear rate.

Bingham Plastic

These are the fluids which have a linear shear stress-strain relationship as Newtonian fluids but do not go through the origin. A finite shear stress (yield stress) is needed to initiate flow. Examples: clay suspension, drilling mud, toothpaste, soap, greases, and chocolate mixtures. The surface of this type of fluid can hold peaks when it is still.

b. Time dependent fluids

For some fluids, the shear stress may change at a given shear rate as time passes. This is another form of non-Newtonian behaviour.

Thixotropic fluid

Shear stress decreases with time at constant shear rate. The apparent viscosity decreases with time. The change is reversible; the fluid "rebuilds" itself once shearing is removed. Includes some starch paste gels, wet clay soils, paints, egg yolk, synovial fluid and honey etc.

Rheopectic fluid

Shear stress increases with time at constant shear rate. The apparent viscosity increases with time. The change is reversible. Printers ink and sand in water are the example of rheopectic fluid.

1.3.2 Carboxymethycellulose (CMC)

Carboxymethylcellulose (CMC) aqueous solutions are shear-thinning, pseudoplastic, non-Newtonian liquids whose viscosity decreases with an increase in shear stress considered for heat removal applications. CMC is a typical hydrocolloid that is produced by the reaction from a cellulose alkali with monochloro acetate of sodium. Due to its properties, such as solubility in cold and hot water, low to high viscosity in solution, suspending characteristics, retention of water, and resistance to oils, it has wide application in many foodstuffs formulations, product development, and processing. In the food industry, it is used as a stabilizer, binder, thickener, suspending, and water-retaining agent in biscuits, cakes, ice creams, fruit drinks, sauces, dehydrated soups, and dietary foods. It is a microbiological polysaccharide, made from the fermentation of Xanthomonas compestris. It is widely used in food, cosmetics, medicine, etc, because of its physical, chemical, and functional properties. Due to its excellent rheological properties, it is used as a very effective stabilizer for water-based systems. Its various areas of application cover a broad range, from the food industry to oil drilling. Typical food applications of xanthan gum are salad dressing, sauces, gravies, dairy products, desserts, low-calorie foods, and convince foods in general. It is also used in cleaners, coatings, polishes, and agricultural flowable. A power-law model defines the viscosity of the aqueous solution of CMC due to its shear-thinning behavior [6] and is represented by equation (1.1).

$$\mu(\dot{\gamma}) = K(\dot{\gamma}^{n-1}) \tag{1.1}$$

where n represents the power law index, $\mu(\dot{\gamma})$ represents the strain rate [s^{-1}] and K represents the consistency index [$\mathrm{kg}/(\mathrm{m}\cdot\mathrm{s}^{2-n})$].

The thermophysical properties of Newtonian (water) and non-Newtonian (an aqueous solution of CMC) fluids are shown in Table 1.1.

1.4 Literature Review

This research aims to investigate the feasibility of non–Newtonian fluid flow in fin-tube heat exchangers along with the VGs and optimize the heat transfer and pressure drop. However, the importance of using non-Newtonian fluid in the FTHE has already been described in the previous section. Considerable works have already been carried out to propose different techniques to enhance heat transfer by using VGs.

This section discusses prior work done by many researchers to improve heat transfer via channel flow, followed by heat transfer via FTHE. Some literature on the use of various winglet forms of VGs to promote heat transfer has been cited. Additionally, several non-Newtonian fluid heat transfer analysis articles were discussed.

1.4.1 Channel flow with winglets

Datta *et al.* [8] investigated the heat transfer behavior of the delta winglet pairs (DWP) longitudinal vortex generator of three-dimensional fluid flow in a rectangular micro-heat sink. In terms of distances from the inlet, various configurations of two LVG pairs with variable slopes and locations are considered when the LVG heights are equal to the channel height. The best overall outcome was expected with a 30° LVG angle for *Re* above 600, whereas a higher LVG angle was found to be more optimal for lower *Re*. The LVG detected heat transfer enhancement due to improved fluid mixing caused by vortex breakage. Oneissi *et al.* [9] evaluated heat transfer improvements in parallel plate-fin heat exchangers by conducting three-dimensional numerical simulations of LVG. Numerical simulations have been conducted for the classical DWP and added as the reference case for this analysis. Then, a new VG configuration is scrutinized, which is called the IPWP. Deshmukh *et al.* [10] experimented with heat transfer augmentation in a circular tube fitted with an inserted curved delta wing vortex generator (CVWG). Local heat transfer coefficient and overall pressure drop were calculated for the laminar flow regime with water as the working fluid. Fiebig *et al.* [4] investigated the effects of single-vortex generators on flow structure, flow losses, and heat transfer of a rectangular channel using DWP. The vortex structure has been observed, the drag—a measure of flow loss, was determined by a brace, and from unstable liquid crystal thermography, the local heat transfer coefficient was obtained. The geometry of the VG, angle of attack, and *Re* were varied. Wu *et al.* [11] examined experimentally and numerically the average convective heat transfer on the top and bottom surfaces of a plain plate and four plates with a pair of delta winglet LVG perforated directly from the plates at angles of attack of 15°, 30°, 45° and 60°. Experimental outcomes show that the average Nu

on the plate surfaces is enhanced by the increase of the DWP attack angle relative to that of the plain plate without DWP in the test area. Sohankar *et al.* [12] numerically evaluated the efficacy of a vee-shaped VGs in a channel for compact heat exchangers for a range of *Re* between 200 and 2000 and the incidence angle ranging from 10° to 30°. It has been perceived that the flow and heat transfer becomes steady at a low *Re* ($\leq$1000) while it becomes unsteady at a large *Re* ($\geq$1000). With an increase in *Re* and the incidence angles, there is a significant effect on Nu, pressure coefficient, bulk temperature, friction factor, and Colburn factor. The major cause of these changes is the generation of longitudinal and horse-shoe vortices with different strengths and circulation. It is numerically studied that the vortex strength surges with *Re*, and it declines in the streamwise direction. A thermal performance parameter (JF) is calculated to assess the feasibility of the system in measuring the amount of heat transfer augmentation compared to the pressure drop. With an increase in the *Re*, the value of JF also increases. A thermal system shows better performance for heat transfer for the same surface area and pumping power when JF $>$ 1. The value of JF is more than unity for all ranges of *Re* of the present work. Hence, it can be concluded that the VGs enhance heat transfer with a rational pressure penalty. Wu *et al.* [13] experimentally and numerically examined the effect of the location of longitudinal vortex generator (LVG) in the channel, geometric sizes, and shape of LVG on the heat transfer augmentation and flow behavior in a rectangular channel. It has been numerically demonstrated that as the LVG distance from the channel inlet and the gap between the LVG pair decreases, so does the overall Nu. The position of LVG has no significant effect on the channel's total pressure reduction. Heat transmission will be larger, and flow loss will be less with an increase in the length of the rectangular winglet pair (RWP) compared to an increase in the height of RWP for the same area of LVG.

Wu *et al.* [13] presented the numerical computation result of the effect of punched holes and the thickness of the RWP on laminar convection heat transfer in a rectangular channel with a couple of rectangular winglets LVG pierced out from the lower wall of the channel. It has been observed that the heat transfer augmentation in the area near the VG is higher, and the average friction factor is lower in the case with pierced holes instead of the case without punched holes. The thickness of the VG affects heat transfer augmentation near the VG area, and there is no substantial effect on the total pressure drop. Further, it has been observed that the average Nu is slightly higher in the case of LVGs with holes than without holes. The average friction factor with holes is less than without holes. The VGs with attack angle 45° is always a favorable condition than the other attack angles for better heat transfer augmentation while pressure drop increases rapidly with an increase in the attack angle. Wu *et al.* [14] analyzed the average convective heat transfer on the top and bottom surface of the plate embossed with a couple of delta winglet VGs at various attack angles of 15°, 30°, 45° and 60° respectively, experimentally and numerically in a rectangular channel. It has been observed experimentally that the average Nu on the surface of the plate increases with the increase in the attack angle and Re of the delta winglet VG. The average Nu for the plate with delta winglet pair at attack angle 15°, 30°, 45° and 60° is increased by 8-11%, 15-20%, 21-29%, and 21-34% respectively than the plain plate.

Kotcioglu *et al.* [15] investigated the effect of convergent-divergent LVG on the entropy generation and heat transfer through a cross-flow heat exchanger. It has been observed that at the low Re, the entropy generation is affected by the heat transfer, while at the high Re, it is influenced by the pressure drop. The heat transfer augmented from 15% to 30% if compared to heat exchanger without VG, and also a surge in the pressure-loss penalty from 20% to 30%, in comparison with and without VGs, respectively. It has been found that at high Re, the heat transfer rate increases, and the heat transfer irreversibility decreases.

Khoshvaght *et al.* [16] have done the three-dimensional computational fluid dynamics simulation on a plate-fin channel with rectangular wings as a transverse vortex generator (TVG) channel to analyze the heat transfer and fluid flow characteristics. The effect of seven geometrical parameters such as channel length, transverse wing pitch, wing width, wing attack angle, longitudinal wing pitch, wing height, and wing attack angle for three coolants flow like ethylene glycol, water, and oil for the laminar flow regime was assessed. The channels with the rectangular wings show an enhanced value of heat transfer for plate-fin heat exchangers, about 58.3% and 26.2% related to the channels with the trapezoidal and triangular wings, respectively. With a decrease in the height of the wing, longitudinal wing pitch, and transverse wing pitch, the heat transfer coefficient and pressured drop values increase and decrease

with the increase in the wing width, channel length, and wing attack angle.
Abdollahi *et al.* [17] performed a three-dimensional numerical solution to optimize the effect of the shape and the angle of attack of the winglet VG on the fluid flow characteristics and heat transfer in a rectangular channel. A multi-objective genetic algorithm and artificial neural network are used to optimize the result regarding the maximum heat transfer and minimum pressure drop. A channel equipped with VGs augments the heat transfer due to the vertical motions and secondary flow and it also increases the pressure drop mainly due to their form drag. At a low Re, there is no significant effect on the Nu due to the variation of attack angle of the VG, but at a higher Re, this parameter is very vital. It has been seen that with an increase in the angle of attack, pressure drop in the VG location also increases due to increasing the form drag. It has also been investigated that the rectangular vortex generator(RVG) augments the heat transfer and pressure drop maximum, followed by the trapezoidal vortex generator (TVG) and delta vortex generator (DVG) due to having the largest area facing the flow.
Abdollahi *et al.* [18] performed a numerical simulation using computational fluid dynamics to examine the effect of nano-particle and VGs on fluid flow properties and heat transfer for a flow in a rectangular channel. The effect of nano-particle concentration and the shape and geometry of VGs on the thermo-hydraulic performance of rectangular channels has been investigated. It has been observed that adding nano-particle concentration is a preferable option than placing the VG on the heat transfer point of view. Using the combination of both, it enhances the heat transfer as well as friction factor. So, to achieve the optimum value for the concentration of nano-particle and attack angle of VG for the best thermal-hydraulic performance, a combination of computational fluid dynamics, multi-objective genetic algorithm, and artificial neural network is used for the flow through a rectangular channel. Pressure drop increases with an increase in the concentration of nano-particles. Using both nano-particles and a VG makes the thermal boundary layer thinner and hence the heat transfer increases remarkably. The best thermal-hydraulic performance was achieved by using a concentration of 0.3% volume/volume of the nano-particles and a trapezoidal vortex generator (angle 20°) at an attack angle of 51°.
Tang *et al.* [19] performed a three-dimensional computational fluid dynamics simulation to investigate the effect of six different types of LVG arrangements on the fluid friction characteristics and heat transfer of channels. These six types of LVGs are stated as case A, CFD rectangular winglet, case B, CFU rectangular winglet,

case C, CFD delta winglet, case D, CFU delta winglet, case E, CFU rectangular winglet combined with elliptical pole and case F, CFU delta winglet combined with elliptical pole. The thermal-hydraulic performance of case F had the best overall heat transfer performance compared to other cases. Datta *et al.* [8] numerically investigated the effect of inclined LVGs on heat transfer and fluid flow characteristics in a rectangular microchannel. The range of *Re* between 200-1100 and temperature range without involving the phase change considered for the study. The best thermo-hydraulic performance has been expected with 30° LVG angle for *Re* beyond 600, however, for lower *Re*, an elevated LVG angle has been found as more appropriate.

Samadifar *et al.* [20] performed a simulation to analyze the effect of six different types of VGs on the thermo-hydraulic performance of a triangular channel. These VGs are angular rectangular winglet (ARW), simple rectangular winglet (SRW), wishbone winglet (WW), rectangular trapezoidal winglet (RTW), waved vortex generator (WVG) and intended vortex generator (IVG). It has been observed that the SRW augments maximum heat transfer of plate-fin heat exchanger among all models. The best angle of attack of the VG for heat transfer is 45° and increasing the height of the VGs also increases the heat transfer augmentation.

Oneissi *et al.* [9] compared the effect of two types of VGs on the thermo-hydraulic performance of parallel plate-fin heat exchangers. Delta winglet pair(DWP) and modified DWP namely inclined projected winglet pair(IPWP) are considered for the analysis. A three-dimensional simulation is done for different *Re* such as 270, 540, and 1080. A decrease of 50% magnitude in the peak friction factor by using IPWP instead of using DWP and a 30% increase in vorticity relative to DWP. A thermo-hydraulic performance combining both, increases in heat transfer and a decrease in pressure drop is enhanced by about 6% in the case of the IPWP when compared with the DWP configuration.

Dey *et al.* [21] numerically examined the effect of an adiabatic square cylindrical VG on the wall heat transfer augmentation of a channel. It has been seen that the location of VG doesn't affect the heat transfer much but the axial and transverse position of VG has a noticeable impact on the heat transfer augmentation of the channel. Ebrahimi *et al.* [6] numerically investigated the thermo-hydraulic performance of a laminar flow for *Re* (25-200) in a rectangular channel equipped with LVGs. A plain channel and channel with VGs have been considered for three-dimensional numerical simulation. The VGs with various attack angle and locations have been attached within the channel. The flow of the aqueous solution of CMC solution with LVGs are considered and the effect on the thermo-hydraulic performance of the channel has been discussed.

The overall performance of the channel, considering the combined effect of heat transfer and pressure drop, of the channel equipped with delta winglet pairs performs better than that of the base channel. According to Vasudevan *et al.* [22], employing DWPs in the channel improves heat transmission by 20–25% at the expense of a negligible increase in pumping power. Tang *et al.* [19] studied six different orientations of RWPs and DWPs in rectangular channels. It was observed that the thermohydraulic performance of the channel with DWPs in a common flow up orientation outperforms that of the channel with RWPs. Zhou *et al.* [23] experimentally investigated the performance of four different types of winglets, such as RWP, DWP, trapezoidal winglet pairs (TWP) and curved trapezoidal winglet pairs (CTWP). It was observed that the DWP performs best among all the winglets considered in the study for laminar flow. A larger attack angle improves thermohydraulic performance.
Garimella and Eibeck [24] experimentally observed the performance of triangular wings in a rectangular channel. It was found that the VGs installed in the channel experienced a maximum of heat transfer about 40% in the laminar region. Fiebig *et al.* [4] experimentally observed the performance of the heat exchanger using delta wing, DWP, and RWP. Delta wings were shown to have the greatest heat transfer augmentation, followed by DWPs and RWPs. Khoshvaght *et al.* [25] have used two types of arrangements of DWPs in a rectangular channel. Eight uniform sizes of DWPs and eight nonuniform DWPs in increasing and decreasing sizes were considered for experimental and numerical analysis. The outcomes showed that employing non-uniform DWPs improves the thermal performance of the channel over utilizing uniform DWPs.

1.4.2 Fin-tube heat exchanger

Dogan *et al.* [26] discussed the application of FTHE. A variety of heat exchangers have been developed and put into operation by engineers and scientists to increase efficiency of heat exchangers. Out of these, the most widely used heat exchangers are the fin and tube forms of the heat exchanger. This form of heat exchanger is used in a variety of engineering uses; particularly in heating and cooling systems, in-car radiators, engine oil, and air cooling. Kondepudi *et al.* [27] presented a research study about the application of FTHE and their performance under frosting conditions.

A heat exchanger with a larger number of fins has an elevated energy transfer rate due to a greater surface area, more frost gathering, and elevated latent transfer of energy. At the same time, an elevated velocity not only surges the *Re*, and consequently increases the coefficient of airside heat transfer, but also enhances the latent energy transfer, thereby increasing the heat transfer coefficient.

Tso *et al.* [28] developed a general distributed model in this study, with frost development. In the frost model, the equations for the fin-tube heat exchanger were derived in a non-state manner and quasi-form state. To make the model more practical, it included the variance of frost along the fin due to irregular distribution of temperature. The model presented can forecast the dynamic performance of an air cooler both under non-frost and frost conditions. Sun *et al.* [29] proposed a computational model to simultaneously foresee the fluid flow and transfer of heat on the air and water side of an elliptical fin-tube heat exchanger. The numerical results are in perfect agreement with the experimental data reported. Surface response methodology was applied to realize the relations between seven design factors including axis ratio, water volumetric flow rate, longitudinal tube pitch, fin pitch, row number, transversal tube pitch, and air velocity. Analysis of the response surface was used to determine the effect of the axis ratio on the overall thermal-hydraulic efficiency that was calculated by the heat transfer rate per unit power expenditure.

Jacobi *et al.* [30] characterized the efficiency of a condensing heat exchanger by heat and mass transfer. Present research work carried out on a heat exchanger with baffles, copper , direct transfer, total counter flow, and indirect contact. The data on heat and mass transfer is related and an assessment is made with other studies. Interesting behavior and contrasts of low *Re* sensible transfer of heat in condensing and noncondensing cases are observed and a mechanism is hypothesized that explains the physics of those observations.

Hsieh *et al.* [31] performed a series of experiments to investigate the effects of the outer diameter of the fin neck, the pitch of the fin, the number of longitudinal tube rows, the pitch of the transverse tube, the pitch of the longitudinal tube, the height of the louver, the thickness of the fin, the angle of the louver fin on the output of the louver heat exchanger using numerical methods. The louver heat exchanger parameters are optimized using the Taguchi method. Eighteen types of models are rendered for each component by compounding rates. The heat transfer and flow characteristics of each model are analyzed. The findings show that the thermal-hydraulic efficiency of the heat exchanger is greatly determined by the end

collar outside diameter, transverse tube pitch, and fin pitch.
Gu *et al.* [32] have carried out numerical studies to inspect the thermal-hydraulic airside features of the plain fin-tube and bare tube bank heat exchangers anticipated for use in aero-engine refrigeration. In present studies, small diameter tubes (3.0 mm) heat exchangers with a compact tube layout have been used and operate over the exchanger depth at high temperatures with immense temperature changes. Frontal air velocities of 5 to 20 $\mathrm{m\,s^{-1}}$ are calculated and Re found 4898 to 19592 based on tube diameter. Based on the Realizable k-ϵ turbulence model, calculations are made by considering the variations in the physical properties of air caused by the changes in its temperature.

Nemati *et al.* [33] optimized the shape of annular fins in a multi-row air heat exchanger to augment performance, without incurring an expenditure price for manufacturing.
In a regular, four-row heat exchanger, the air-side heat transfer, pressure drop, and entropy generation are forecasted using a steady-state turbulent computational fluid dynamics model and authenticated against experimental data. The authenticated simulation tool is then used to optimize the fin shapes in a model-based manner. The uniqueness of the proposed approach lies in separately optimizing the shape of each fin line, ensuing in a non-homogeneous custom tube bundle. It has been seen that elliptical annular-shaped fins reduce the pressure drop and entropy generation while circular-shaped fins can be used for enhancing heat transfer at the opening region. The findings also show that the pressure drop is diminished by 31% for the situation in which the overall heat transfer rate is enhanced and the pressure drop is reduced, the fin weight is decreased up to 23%, while the gross air-side heat transfer falls by 14%, relative to the situation where all the fins around the tube package are circular.
Chen *et al.* [34] used the commercial package of three-dimensional computational fluid dynamics along with the inverse method and experimental data to inspect the natural heat transfer convection and fluid flow features of the single-tube vertical annular fin-tube heat exchanger for different standards of fin spacing and tube diameter. Distributions of air temperature and velocity, fin surface temperature, and the heat transfer coefficient on the fins are determined by the FLUENT together with the different flow models in the box with the opening upward. The inverse method is applied in conjunction with the finite difference method and the experimental temperature data to determine the finite temperature and heat transfer coefficient for the smaller tube.

Lotfi *et al.* [5] successfully carried out three-dimensional numerical tests on the thermo-hydraulic features of a new flat fin-and-elliptical tube (PFET) heat exchanger with innovatory tube bench forms, namely; a slotted elliptical tube bank (SETB) and a slotted annular elliptical tube bank (SAETB). The goal of this analysis is to establish an optimum staggered tube-bank design to maximize heat transfer rates with limited pressure drop penalties and to evaluate the findings of conventional non-slotted tube-bank heat exchangers. The average heat transfer rate of SETB/SAETB heat exchanger is more than 15% higher than that of the traditional non-slotted elliptical tube heat exchanger.

Singh *et al.* [35] experimentally investigated the absorption and desorption performances of a solid-state (metal hydride) hydrogen storage device with a fin-tube heat exchanger. Storage system output is studied for different operating parameters, such as hydrogen supply pressure, fluid temperature cooling, and fluid temperature heating. Also investigated the effect of copper flakes on absorption performance, and compared it to a similar storage device without copper flakes.

Gray *et al.* [36] discussed heat exchangers on a staggering array of circular tubes having continuous, flat fins. As a function of the *Re* and the geometric variables of the heat exchanger, correlations are developed to predict the air-side heat transfer coefficient and the friction factor. The results apply to any number of tube rows in the direction of airflow. Kim *et al.* [37] provided experimental data that can be used in the optimal design of heat exchangers with a large finned pitch for flat plate. Twenty-two heat exchangers were tested with tube alignment, fin pitch variation, and tube row number. The coefficient of air-side heat transfer decreased with a reduction in the finish pitch and an increase in the number of tube rows. The reduction in the heat transfer coefficient of the four-row heat exchanger coil was about 10% as the finish pitch decreased from 15.0 to 7.5 mm over the 500–900 *Re* range calculated based on the tube diameter.

Taler *et al.* [38] discussed a double-row two-pass plate-FTHE consisting of circular or oval pipes and developed a technique for calculating the air side Nu on each row of pipe by using computational fluid dynamics modeling of the heat exchanger. A heat transfer correlation was also found for the mean heat transfer coefficient for the entire PFTHE, using computational fluid dynamics modeling. Qiu *et al.* [39] studied the application of fin-tube heat exchanger on collector/evaporator under solar radiation and theoretically analyzed the heat transfer characteristics and accuracy of the theoretical expression of fin-tube temperature field is validated by simulation.

Bezaatpour *et al.* [40] investigated about the effect on heat transfer augmentation of a uniform external magnetic field with Fe_3O_4-water nanofluid of a fin-and-tube compact heat exchanger. The results obtained are confirmed by the existing experimental data to exhibit the correctness of the present simulation. It has been observed in this investigation that the local and average heat transfer coefficients enhance around the tubes in the occurrence of an external magnetic field due to the vortex formation at the rear of the tubes as well as the flow pattern variation in the heat exchanger, without considering the pressure drop increment.

Ravi *et al.* [41] designed a double pipe, protracted finned counter-flow heat exchanger for the energy revival capacity of exhaust gases in internal combustion engines to harvest low-grade waste heat energy. It has been observed that with an increase in the number of fins along with its height, the heat transfer rate also augmented which further enhanced the performance of the heat recovery system and increased brake thermal efficiency from 32% to 39.6%.

Abolfathi *et al.* [42] experimentally studied the flow and heat transfer around a tube in mixed tube bundles made up of circular and cam-shaped tubes. The findings demonstrated that the Nusselt number (Nu) increases in all mixed tube banks with an increase in the pitch ratio. Experimental research has been done by Mobedi *et al.*[43] on the thermal-hydraulic performance of a cam-shaped tube with different aspect ratios at two different angles of attack, 0° and 180°. The outcomes demonstrate that the drag coefficient decreases as the aspect ratio rises [43]. The performance of a cam-shaped tube with constant heat flux in crossflow was examined experimentally by Salehi *et al.* [44] to ascertain the impact of the angle of attack on thermal-hydraulic behavior. The findings demonstrated that as the angle of attack is increased from 0° to 180°, the mean Nusselt number (Nu_m) increases for all Reynolds numbers (Re).

Hu *et al.* [45] projected a unique arrangement of staggered concave curved VGs to improve the heat transmission enhancement of wavy FTHE. The wavy channel with concave curved VGs has significantly better overall performance compared to the wavy smooth channel and the wavy channel with plane vortex generators. Aktas *et al.*[46] numerically investigated the heat transfer and pressure drop performance of FTHE using circular, diamond, and optimal enhanced-shaped geometries tube banks in a staggered arrangement. The finding reveals that the heat transfer performance of the diamond-shaped tube was enhanced by 156% compared to the circular tube. The heat transfer performance of the optimal enhanced-shaped geometries tube was augmented by 0.59% and the pumping power requirement was reduced by 21.73% compared to the diamond-shaped tube of FTHE.

1.4.3 Fin-tube heat exchanger with delta winglet pairs

Skullong *et al.* [47] studied the effects of introducing a straight tape with double-sided delta wing pairs also called 'delta-wing tape' (DWT) used as an LVG on forced convective heat transfer and also examined flow friction characteristics in a uniform heat-flux heat exchanger tube experimentally and numerically. Behfard *et al.* [48] conducted a numerical simulation to analyze the characteristics of heat transfer and pressure drop of three-row inline tube bundles as part of a heat exchanger (Re = 1000, Pr = 4.29). A comprehensive study has been conducted to increase heat transfer due to the effects of different geometrical parameters such as the transverse and longitudinal positions of VGs, the length and height of VGs, and the angle of attack of the delta winglets.

Majumder *et al.* [49] numerically studied the thermal performance, pressure drop, and heat transfer characteristics for a tube bank heat exchanger with DWVG at a different angle of attack on the fin. It has been observed that the coefficient of heat transfer and pressure drop increased with the increase in Re. However, a considerable enhancement of about 23.92% in heat transfer was observed for the angle of attack at 35° compared to the plain fin heat exchanger.

Wu *et al.* [11] observed that Delta winglet performs better in enhancing the efficiency of the FTHE than other VGs. In this research work, the effects of the fin pitch, the ratio of the longitudinal pitch to the transverse pitch of the tube, the ratio of both sides V_1, V_h of the delta winglets, and the angle of attack of the delta winglets on the performance of the FTHE has been studied by using response surface approximation.

Awais *et al.* [50] investigated the influence of delta winglet VGs on heat exchanger thermal-hydraulic characteristics. The effect of VGs with a different number of rows, angle of attack heat transfer performance, and pressure drop configuration is shown. In addition, the effect of tube configurations such as inline and staggered tube placement and specific tube form (circular, oval, and rectangular) is also realized.

Wang *et al.* [51] and Salviano *et al.* [52] used an optimization procedure, based on the SIMPLEC method for augmenting the heat transfer performance through a fin-tube compact heat exchanger with two rows of tubes in staggered and inline arrangements along with the VGs to find an optimal arrangement of the VGs for two objective functions connected to the friction factor and Colburn factor. The results signify that for both objective functions, tube arrangements and Re, this optimized-work, arrangement for VGs has achieved a higher heat transfer rate and is more prominent for staggered tube arrangement than for inline tube arrangement. In addition, proper VG shapes to maximize objective functions are more alike to the type of rectangular winglet than the type of delta winglet, and the best ratio between the height and the fin pitch of the VGs is 0.6.

Lei *et al.* [53] used a new type of circular tube with delta-winglet VG to boost thermal-hydraulic efficiency for energy conservation. The fins are punched out with the delta-winglet VGs and inserted into the circular tube center. The impact of attack angle 15°, 30°, 45°, and 60° and pitch (P = 1D, 2D, 3D, and 4D) of delta-winglet VGs on fluid flow and heat transfer are observed in detail. It has been observed that delta-winglet VGs produce swirling flow motion to advance fluid flow mixing in the circular tube causing heat transfer augmentation with a reasonable pressure drop punishment. The results of experimental studies by Valencia*et al.* [54] demonstrated that the best position for VGs concerning the tube is with the winglets symmetrically placed downstream to avoid the wake region formed in arrears of the tubes. Further analysis by Biswas *et al.* [55] and Gentry and Jacobi [56] revealed that raising the angle of attack of DWVG and Re enhances the strength of the vortices and, consequently, increases the performance of thermal energy transmission. In their computational work by Li *et al.* [7], considering rectangular and delta winglet VGs, found that the best possible attack angle at which the studied system performs best is 25° for the RWVG and 45° for the DWVG. Kumar *et al.* [57] investigated the heat transfer efficiency of solar air heaters along with the winglet VGs in the range of attack angle 30° to 60°. The study provides insight into the enhancement in Nusselt number (Nu_m) with a rise in attack angle. Ramanathan *et al.* [58] analyzed the thermohydraulic performance of solar water collectors using a winglet type of VG. The system performs best at an ideal attack angle of VGs which is 30° and 60°. Fu *et al.* [59] analyzed the thermohydraulic performance of a mini channel using DWVG at different heights of the channel. The findings demonstrate that the channel height and winglet arrangement mostly influence the primary vortex behavior downstream of LVGs, but have the least impact on the vortex orientation close to winglets. Tian *et al.* [60] examined the heat transfer performance and flow behavior of a rectangular channel using DWVG and RWVG at a range of Re = 180 - 1130. The results show that the DWVG outperforms the RWVG considering the overall performance of the channel.

1.4.4 Fin-tube heat exchanger with rectangular winglet pairs

Kong *et al.* [61] presented two types of rectangular slot configurations, continuous and irregular slots, and the effect of these slot configurations on the air-side thermo-flow performance of the plain bundles has been analyzed in in-line and staggered configurations by using numerical simulations, which further validated by the experiment. The bundles in a staggered pattern are superior to those in an in-line one for overall performance. The staggered bundles of fin tubes with continuous rectangular slotted strips have the best overall performance.

Wu *et al.* [14] presented numerical calculation results on laminar convection heat transfer in a rectangular channel with a pair of LVG rectangular winglets punched out of the lower wall of the channel. The effect of perforated holes and the thickness of the RWP on fluid flow and heat transfer are studied numerically. It has been observed that heat transfer enhancement is more in the case with punched holes and lower average frictional flow coefficient compared to the case without punched holes near the VG region. There is less heat transfer enhancement caused by the thickness of the rectangular winglet in the region close to the VG and almost has no major effect on the total pressure drop of the channel.

Fiebig *et al.* [4] investigated the dependency of the vortices on how they are made and also discussed the development of boundary layers on the surface of the VG, flow destabilization, and swirl. VGs of wing-type are usually integrated into heat transfer surfaces, for augmenting the heat transfer and cost of pressure loss in fully developed and developing channel flows. Observations made through experimental calculations that: rectangular and delta winglets give similar performance and winglets are more effective than wings. A detailed investigation has been made for a base configuration with RVG. Longitudinal vortices are more efficient than transverse vortices at all ranges of Re, i.e., higher heat transfer augmentation has been observed with longitudinal VGs for the same pressure loss as TVGs.

Wu *et al.* [11] presented the impact of key parameters of the LVG on heat transfer augmentation of the rectangular channel and flow resistance. The parameters include LVG position in the channel, LVG shape, and geometric sizes. Findings through the numerical study indicate that the overall Nu of channels decreases with the position of the LVGs away from the channel inlet, and also decreases with the space decreasing between the LVG pair. No considerable effect on pressure loss due to the LVG location. With the fixed LVG area, heat transfer increases with an increase in the length of RWP VG, and with increasing the height of RWP VG, flow loss also increases.

DWP is more effective than RWP for the identical area of LVG, on heat transfer enhancement of the channel. It is found that a rectangular channel improves the heat transfer if it is attached to VGs and this heat transfer enhancement is achieved at the cost of a larger pressure drop. It has been observed that with an increase in the attack angle and the lateral distance of the LVGs, the heat transfer also increases [62].

Jacobi and Shah [63] analyzed the heat transmission and flow behavior of an FTHE utilizing rectangular and delta VG winglets. Wu *et al.* [14] experimentally and computationally explored the impact of the position, size, and arrangement of the longitudinal vortex generator (LVG) on the heat transmission and the friction loss behavior of a rectangular channel. The mean value of Nu for a pair of winglets on a plate at attack angles of 15°, 30°, 45°, and 60° increases by 8-11%, 15-20%, 21-29%, and 21-34%, respectively, than the plain plate in the absence of VG. Valencia *et al.* [54] have used winglet pairs in FTHE and observed an improvement of 50% in Nu compared to those without winglet pairs. The flow pattern was shown to be significantly influenced by the inclination angle of geometry [64].

Rectangular winglets have been shown to enhance heat transmission, albeit at the expense of significantly higher flow resistance. [10, 65–68]. However, employing a delta winglet results in a minimal gain in pressure drop but a considerable increase in heat transmission. [4, 19, 22, 23, 69–71]

1.4.4.1 Fin-tube heat exchanger with curved winglet vortex generator

Song *et al.* [72] studied experimentally the effect of curved delta winglet VG of various geometric sizes on the heat transfer performance and pressure drop for circular tube-and-fin heat exchanger. A total of 15 tests of circular tube-fin exchangers with two tube pitches, three fin pitches, and two types of curved delta winglet VGs with varying base lengths are carried out to see their effect on heat transfer and pressure drop. To evaluate the performance of circular tube-and-fin heat exchangers with various parameters, the Colburn factor and friction factor are calculated. The observation made through the results is that the smaller size of VG near the tube has the beneficial heat transfer improvement for low Re flow and the bigger VG is more favorable to heat transfer augmentation for large Re flow. There is less effect on the Colburn factor by changing the fin pitch, whereas the friction factor is affected by the change in fin pitch. Reducing the pitch of the tube is helpful for heat transfer at the expense of increased pressure loss and the total heat output improves with a 2.3 mm fin pitch.

Shi *et al.* [73] have numerically discussed the impact of the position of curved winglet VGs on the thermal-hydraulic performance of a heat exchanger. It has been observed that the frictional loss of the curved VGs is comparatively lesser than that of the equivalent plane VG. Shifting the VGs towards the inlet aids in postponing the separation of the fluid and reducing the less-heat transfer zone size, as a result, heat transfer performance improves. The variation of Nu_{local} throughout the channel also has been discussed. A significantly higher value of Nu_{local} has been observed in front of the tubes as the flow area gets contracted due to the presence of the tube, hence the kinetic energy of the fluid increases, and the fluid moves with elevated velocity. Owing to the recirculation behind the tubes, the amount of Nu_{local} in the low heat transfer zones appears to be the lowest.

Modi *et al.* [74] studied the heat transfer and flow characteristics of FTHE considering rectangular winglets along with circular stamped holes with varying *Re*. Various types of rectangular winglets with inbuilt and without inbuilt circular holes have been considered in this study and the thermo-hydraulic performance of this case is contrasted with the baseline (without VG) and VG in the absence of the punched hole. It has been found that the heat exchanger's thermo-hydraulic performance is significantly enhanced by rectangular winglet VG with circular punched holes. The Nu is slightly lower for all conditions when the flow resistance has been reduced by the punched holes. Comparing rectangular winglet VG with 6 holes to other cases, it performs better. Lu and Zhai [1] discussed the impact of CVG on the thermo-fluid behavior of heat exchangers. At varied attack angles, the effectiveness of VGs with diverse curvatures is assessed. Additionally, the impacts of variables like location, extent, and attack angle are also examined. The numerical outcome demonstrates that the value of overall performance increases with the surge in *Re*, indicating that for the current investigation, a larger *Re* yields superior thermal-hydraulic performance. Additionally, it is discovered that VGs with a curvature of 0.25 work best thermally and hydraulically, and the greatest value of overall performance 1.06 is attained at an inclination angle of 15°. A better heat transfer performance can be obtained by using a CVG with considerably less pressure loss owing to its efficient design.

Gong *et al.* [75] compared the thermo-hydraulic performance of heat exchangers with curved rectangular VGs. It has been observed that curved rectangular VGs might boost secondary flow intensity and decrease the low heat transfer zone. An improved heat transfer performance can be attained by mounting the leading edge of the VG in the transversal axis of the tube, the base arc length of the VG must be large, and the height of the VG must be 0.8 times that of the channel height and the base arc length of the VG is 3.04 times that of the channel height. Naik *et al.* [76] numerically examined the thermo-hydraulic characteristics of the curved rectangular winglet. The influence of curvature in concave and convex RWVGs on thermo-hydraulic performance has been contrasted with flat RWVGs. A maximum of 22% of heat transfer enhancement has been observed at a curvature angle of 75° for concave shape RWVG in comparison to plane channel in the absence of RWVGs. The local secondary flow variation along the channel length for concave, convex, and plane RWVG shapes has also been observed. Both lower and higher peak values of span average secondary flow variation for concave shape RWVG are relatively higher than that of the plane and convex RWVG.

Nowadays, most industrial instruments use liquids for efficient heat transfer performance of the heat exchangers. The thermal resistance for liquids is quite low, according to a basic understanding of heat transfer. However, sometimes it is quite necessary to augment the thermal energy transfer on the liquid side such as cooling the nuclear reactor core and cooling the electronic components such as the electronic chip. Since liquid cooling is more effective than air cooling, high-performance computers and gaming systems frequently use liquids to cool their components. Meanwhile, there has been a lot of interest in studies on the thermohydraulic performance of non-Newtonian fluids all around the world. Shear-thinning fluid is used as a coolant in most industries, including pharmaceutical and drug industries, distilleries, food industries, petrochemical industries, and food and biological industries. The aqueous solution of CMC acts as a non-Newtonian shear thinning fluid and provides better results when used for heat removal applications [6, 77].

1.4.5 Placement of VGs in FTHE

The placement of the VG is also crucial to enhance heat transmission. Common flow up (CFU) and common flow down (CFD) are two different placement strategies of VGs for heat transfer claims. The CFU configuration refers to the placement of the VGs to ensure that the ensuing rotating vortices transport the fluid amid them far from the surface of the fin where it is situated. CFD configuration signifies the path of the fluid flow amidst the two vortices in the direction of the surface where they are installed [62]. The CFU technique significantly delays separation, lessens form drag, and eliminates the region of inefficient heat transmission behind the tubes [78]. Tian *et al.* [60] examined the thermohydraulic features of a flat-plate channel utilizing different LVG configurations. The results demonstrated that the overall performance of the CFD configuration is superior to that of the CFU configuration for RWPs. VGs are positioned in a CFD configuration behind the cylinder in the closed-wake zone to inject high-energy fluid behind the cylinder and reduce the area of weak heat transmission. The VGs are often deployed during the CFU approach somewhat upstream of the tube such that the winglet and tube form a restricted path, which causes the fluid to accelerate close to the tube [79].

Tori *et al.* [79] anticipated a new VG configuration called CFU along with inline and staggered tube configurations in the FTHE and observed a remarkable improvement in heat transmission with a decrease in the substantial value of pressure loss. Staggered tube arrangements outperform inline tube arrangements in terms of thermohydraulic performance. The CFU technique significantly delays separation, lessens form drag, and eliminates the region of inefficient heat transmission behind the tubes [78].

Zeeshan *et al.* [80] has investigated to find the best location of RWPs for improving the heat transfer and flow characteristics of a fin and tube compact heat exchanger at the low *Re* ranges between 500 and 900. The RWPs are located at two different locations, one, adjacent to the tubes and another, behind the tubes named CFU and CFD orientations respectively. The effect of the angle of attack, angle of span, and position of RWPs on thermal-hydraulic efficiency on the air side is studied numerically. Area goodness factor and heat transfer rate per unit of fan power are known as parameters of performance evaluation. It has been observed that the heat transfer rate increases with the increase in attack angle and span angle also causing an increase in pressure drop penalty. Behind the tube, the VGs may diminish the pressure drop but with a significant drop in heat transfer.

Thermohydraulic investigation of an FTHE along with the pairs of DWVGs in common flow up (CFU) and common flow down (CFD) configuration at considerably low *Re* done by Tori *et al.* [79]. The sidewise and CFU placement of VGs nearby tubes performs best considering the convective heat transfer coefficient. The computational work done by Tiwari *et al.* [81] informs the enhancement of the performance of FTHE utilizing two braces of DWVG in a CFD configuration downstream along with the oval tubes. Considering only the heat transfer, a larger attack angle performs better in FTHE [82].

Tang *et al.* [19] analyzed the performance of a rectangular channel using DWVG and RWVG in CFU and CFD configurations. The findings show that the DWVG in the CFU configuration performs best in comparison to all other configurations of DWVG and RWVG. The CFU design has a higher Nu_m than the CFD configuration for channels with rectangular or delta winglet pairs. The JF factor for a channel equipped with a delta winglet is higher compared to the rectangular winglet [19].

1.4.6 Newtonian and non-Newtonian fluid

Garimella and Eibeck [24] studied the water channel using five pairs of DW. It was observed that the heat transfer near the first row of DWPs is not very promising. Heat transfer near the second row of DWPs is the maximum and is around 30%. The experimental investigation carried out by Islam *et al.* [83] in a rectangular water channel with repeated ribs. Heat transfer was observed to be enhanced by 200-250% compared to the channel in the absence of ribs along with 2.5 times increase in pressure drop. Ahmed *et al.* [84] considered a triangular channel equipped with DWP in their study using an aqueous solution of nanoparticles as a working fluid. The research revealed that employing DWPs and nanofluid increases heat transmission by approximately 33% as compared to the base channel and base fluid. Ebrahimi *et al.* [85] used four different orientations of RWPs in rectangular microchannels to evaluate thermohydraulic performance using deionized water as a working fluid. It was observed that the combination of common flow up and common flow down of RWPs performs best considering heat transfer as well as thermal efficiency. Wang *et al.* [86] conducted experimental research in a rectangular channel along with longitudinal vortex generators (LVGs) using water as working fluid to cool the core of the nuclear reactor. It was observed that the heat transfer greatly improved by using LVGs. Ebrahimi *et al.* [6] considered five pairs of RWPs in a rectangular channel using an aqueous solution of CMC as a working fluid for laminar flow. It was observed that the heat transfer enhancement of this channel is increased by 24-135% compared to the channel in the absence of RWPs. The results also showed that the use of an aqueous solution of CMC as a working fluid enhances heat transfer by 39-188% compared to the Newtonian fluid. The heat transfer is greater at higher attack angles while thermal efficiency is greater at lower attack angles.

Kurnia *et al.* [87] investigated the thermal performance of the laminar flow of aqueous CMC solution in a square-shaped tube numerically. The results demonstrated that, when an aqueous solution of CMC was used as the working fluid, the channel's thermal performance improved by 200% as compared to water.

Esmaeilnejad *et al.* [88] have explored the thermal and hydraulic performance of a rectangular microchannel using an aqueous solution of CMC and Al_2O_3 and Cuo nanoparticle as working fluid. It was found that adding nanoparticles to the non-Newtonian fluid improved the channel's thermal performance.

Sasmal and Chhabra [89] investigated the laminar heat transfer of a heated square cylinder submerged in shear-thinning and shear-thickening fluid. Shear-thinning fluids perform better compared to shear-thickening fluids considering the thermal performance. Kumar and Dalal [90] have done the numerical simulation in an FTHE using an aqueous solution of CMC and reported the enhancement in Nu by 124-186%. Furthermore, the shear thinning property of the CMC solution was observed to have an impact on the shape of the vortex, improving the heat transfer efficiency of a heat exchanger [7, 55, 91].

Smith and Promvonge [65] have used delta wings in a circular cylinder to observe the heat transfer and pressure drop characteristics of the channel. It was observed that although there is an enhancement in Nu, at the same time there is a huge enhancement in friction factor i.e. 14.8 times the plain circular channel. Deshmukh *et al.* [10] have also seen this increase in heat transfer at the expense of a very significant rise in the friction factor using curved delta wings in a circular tube for laminar flow. Sun *et al.* [66] used multiple numbers of RWs in a circular-shaped heat exchanger with varying height and pitch ratios. Compared to the smooth channel, they found that the ratio of Nu numbers fell between 1.15 and 2.32 and the friction factor between 1.46 and 11.63. Zhang *et al.* [67] used parallel and V-shaped arrangements of rectangular wings in a circular tube. It was observed that the parallel configuration of RWPs augments the thermal energy transfer and pressure drop by 1.54-2.18 times and 2.52-6.18 times compared to the base channel whereas, V-shaped orientations improve the thermal performance and pressure drop by 1.6-2.18 times and 2.41-7.44 times compared to the base channel.

The thermal processing of viscous non-Newtonian fluids is of vital importance in today's food industry as various sauces, purees, slurries, and concentrations exhibit non-Newtonian behavior. Since non-Newtonian fluids often tend to be very viscous, most thermal process development methods assume the flow of these types of foods in tubes is laminar [92]. The application of non-Newtonian fluids has spread in many areas of the industrial and engineering field such as in the production of drugs, food, drug delivery, and drilling and processing of crude oil. Further, the application of these fluids for compact heat exchangers in electronic modules is a booster of heat transfer. Hence, the study of the use of non-Newtonian fluids in electronic module heat exchangers has great significance economically and technologically [93]. CMC acts as a non-Newtonian fluid a distinctive hydrocolloid that conveys a prominent effect on mixing and aroma retaining, gel formation, and water retaining with no straight impact on the sense of taste and flavor of foodstuffs. CMC plays the role of a pacifier, adhesion, stiffener, dangling, and water-retaining agent, in ice cream and frozen desserts, fluid and powdered fruit drinks, sauces and creams, cake mixes, and healthy and nutritive foods. Therefore, a thorough investigation is required for different concentrations of CMC solution as a fluid medium for different industrial applications [87, 94, 95].

There is a considerable difference between the viscosity of Newtonian and non-Newtonian fluids which results in low Re and high Pr for non-Newtonian fluids. While considering the flow and heat transfer process of the non-Newtonian fluid, there is a comparatively higher pressure loss and low heat transfer coefficient than Newtonian fluid. Hence the heat transfer augmentation of non-Newtonian fluids is rather important in the designing of efficient heat exchangers [96]. Cheng *et al.* [95] experimentally investigated the laminar heat transfer analysis of different concentrations of aqueous CMC solutions in a square duct with its heated top wall. The experimental results show that the aqueous CMC solution is a preferable option for laminar heat transfer augmentation in a non-circular channel. It has been observed that a considerable heat transfer augmentation has been produced at a certain range of CMC concentration and Re. The Reynolds number (Re) for the fully developed flow of the aqueous CMC solutions is determined by linear relations with the Kozicki generalized Re by equation (1.2)

$$Re = \rho U^{2-n} D_h^n / \left[8^{n-1} K \left(0.6766 + \frac{0.2121}{n} \right)^n \right] \tag{1.2}$$

and the viscosity of aqueous CMC solutions can be well defined by the following power law equation.

$$\eta = K(\dot{\gamma})^{n-1} \tag{1.3}$$

where K and n are consistency index and power-law index in the power-law model, and ρ, U and D_h are density [$\mathrm{kg\,m^{-3}}$], inlet velocity [$\mathrm{m\,s^{-1}}$] and hydraulic diameter [m] of the channel respectively. The value of the consistency index and power-law index depends upon the CMC concentration at a particular temperature. The range of n, K, and Re for the current power-law fluid is estimated as 0.66-0.78, 0.05-0.28 [$\mathrm{N\,s^n\,m^{-2}}$], and 1-500 respectively for the present research work.

Shin *et al.* [97] addressed the challenges in the field of phase separation, aggregation of expanded graphite, and supercooling. Sodium acetate trihydrate (SAT), containing expanded graphite and CMC has been considered for the study, and its thermal property and latent heat energy storage behavior for phase change material have been investigated. It has been seen that with an increase in the concentration of expanded graphite and CMC, the thermal conductivity of SAT increases. The heat transfer analysis of the laminar flow of aqueous CMC for different square coiled tubes such as helical spiral ducts, in-plane spiral ducts, and conical spiral ducts has been discussed by Kurnia *et al.* [87]. The effects of tube geometries, the power-law index for different concentrations of CMC, and other parameters on flow characteristics and heat transfer performance have been discussed and compared with the straight tubes of equal length. The thermo-hydraulic performance factor is defined to compare the heat transfer performance of different geometries concerning the pressure drop. It has been observed that the CMC solution exhibits superior heat transfer enhancement around twice that of water at Re = 1000. The different concentration of CMC affects the shear thinning behavior as well as the thermo-physical properties of the working fluid. The effect of CMC concentration on heat transfer also has been discussed and observed that the heat transfer performance of the system increases with the increase in the concentration of CMC. It has been observed that the CMC solution gives a better heat transfer performance than the water. The best heat transfer performance has been observed in the case of the helical coil but at the same time pressure drop is also maximum. The plane spiral coil gives the best thermal-hydraulic performance when combining both heat transfer and pressure drop in comparison with the straight tube.

Varnaseri *et al.* [98] have examined the effect of four drag-reducing agents (DRA), comprising CMC with high molecular weight (DRA1), and medium molecular weight (DRA2), polyacrylamide (DRA3) and the natural polymer, xanthan gum (DRA4) by adding it to water on thermo-hydraulic performance of a heat exchanger. Laminar flow of fluid under with Re less than 1400 was considered to exchange the heat between water and air in the heat exchanger. It is found that DRA1 shows a maximum percentage of drag reduction value of 26%, and DRA4, with a minimum percentage of drag reduction of 5%, were the topmost and the bottommost obtained results, respectively and temperature range of 40 °C – 65 °C.

Ebrahimi *et al.* [6] performed a three-dimensional numerical solution to investigate the effect of CMC as a non-Newtonian fluid in a rectangular channel. More studies are essential to attain an insight into the effects of non-Newtonian fluid flow behavior in channels furnished with LVGs and accordingly on the heat transfer augmentation of the channel. Using CMC aqueous solutions as the working fluid in rectangular channels increases heat transfer augmentation. Additionally, it was noticed that the shear-thinning nature of the CMC solution affected the structure of vortices, resulting in a better heat transfer performance of a heat transfer device [7, 55, 91]. Tso *et al.* [99] numerically analyzed the viscous flow and thermal energy transfer performance of an aqueous CMC solution between parallel plates. The outcome suggests that the non-Newtonian behavior of an aqueous solution of CMC has a remarkable impact on heat transfer. The viscous flow and thermal energy transfer of a rectangular cylinder immersed in a non-Newtonian fluid were investigated by Sasmal and Chhabra [89]. According to the findings, heat transmission was improved in fluids that had undergone a shear-thinning nature by 100%. The viscous flow and thermal energy transmission of CMC solutions in a helical coil have been investigated by Primenta and Campos [100]. The findings reveal that aqueous CMC solution provides a much lesser f_{app} than Newtonian fluid.

Poh *et al.* [101] considered an aqueous solution of CMC as a power-law fluid in their study and found the elevated value of the Nusselt number (Nu) by lowering the power law index. Kurnia *et al.* [87] addressed the CMC as a power law fluid in a coiled tube and the findings imply that at $Re = 1000$, the CMC solution produces a heat transfer performance nearly 200% as good as water. Nanofluids are conventional techniques for improving heat transfer. Performance evaluation criteria (PEC) increase approximately three times when using alumina/water nanofluid (5%) under optimal simultaneous conditions.

Furthermore, it was shown that with increasing volume fractions of nanofluids (Al_2O_3 *and* CuO), the Nu_m and friction coefficient tended to increase, and the PEC tended to decrease. [102–104]. Esmaeilnejad *et al.* [88] numerically explored the analysis of heat transmission of a microchannel using a non-Newtonian shear–thinning fluid along with nanoparticles and experienced increased thermal performance of the channel.

The aqueous solution of CMC was considered as the working fluid in a computational study by Li *et al.* [7] to examine the three-dimensional laminar flow-induced convection of a dimpled microchannel and observed an increase in relative Nu and frictional loss along with the increase in CMC concentration and depth of the dimple.

The thermohydraulic performance of a square cylinder immersed in static shear-thinning fluids was improved by 100% compared to water [89]. The laminar thermal performance and the friction factor of the aqueous solution of CMC in a helical coil were examined by Pimenta and Campos [100]. It was found that friction factors were significantly reduced. In their study, Shah *et al.* [105] performed an experiment using an aqueous solution of CMC at various concentrations and a Prandtl number of around 100, and Re from 10^2 to 10^4 and informed the local Nu of an aqueous solution of CMC was much larger than for fluids with Newtonian behavior. The aim of the experiment was to analyze the transfer of thermal energy from a cylinder to an aqueous solution of CMC. Using an aqueous solution of CMC as a working fluid reduces drag by 26% compared to distilled water in an FTHE for laminar flow ($Re \leq 1400$) [98]. The addition of additives like CMC to some antifreeze formulations in order to increase their stability and rheological properties may have an indirect effect on the performance of heat exchangers in cold conditions.

1.5 Research Gap

According to the literature study mentioned above, the majority of the research has been conducted concerning the thermohydraulic performance of varying channel shapes and sizes along with a variety of winglets and wings using air as a working medium. Very little work has been done using the winglets in a channel using water. It was concluded from the surveyed literature review that the non-Newtonian fluid especially an aqueous solution of CMC (2000 ppm) showing shear-thinning behaviour performs better than water considering the thermohydraulic performance of the channel. To the best of the author's knowledge, no studies have been conducted to investigate the impact on the thermohydraulic performance of the rectangular channel with inbuilt winglets using shear-thinning fluids. Hence, it requires a thorough investigation to understand the behavior of shear-thinning fluid on the heat transfer and frictional loss of a rectangular channel and fin-tube using various types of winglets.

1.6 Objectives

Based on the above literature survey, recent consideration has been given to the heat transfer of Newtonian and non-Newtonian fluids in the heat exchanger and different channels but there is not sufficient information available for heat transfer analysis of heat exchanger using non-Newtonian fluid equipped with winglet type VGs. It requires analyzing the thermo-hydraulic performance of FTHE using non-Newtonian fluid and various types of winglets while combining both the heat transfer and pressure drop. Hence it is a great scope of discussion among the society of researchers to discuss the effect of winglet type VG on fin-tube while considering the shear-thinning fluid as a working medium. The present study aims at the three-dimensional numerical solution of a fin-tube heat exchanger equipped with RWVG, DWVG, and CRWVG using non-Newtonian fluid as a working fluid. Based upon these discussions the following objectives have been decided which are mentioned below:-

1. To analyze the heat transfer and frictional loss characteristics of a rectangular channel using delta winglets and shear-thinning fluid.

2. To understand the influence of delta winglets on the thermal and fluid flow characteristics of shear-thinning fluids through a fin-tube heat exchanger.

3. To investigate the thermo-hydraulic performance of a fin-tube heat exchanger using rectangular winglet and shear-thinning fluid.

4. To examine the behavior of shear-thinning fluid on the fluid flow and thermal performance of a fin-tube heat exchanger equipped with curved rectangular winglet vortex generators.

1.7 Thesis overview

The current chapter offers a brief introduction to the fin-tube heat exchanger, various types of winglets, and shear-thinning fluids. In addition, this present chapter also provides a detailed literature review on heat transfer through fin-tube using various types of winglets and heat transfer through the shear-thinning fluid. Further, the research gap is highlighted, and based upon this the objectives have been discussed. This thesis only uses numerical analysis to comprehend the thermal performance of fin-tube heat exchangers using shear-thinning fluid and various types of winglets. The remainder of the work discussed in this thesis is organized in the following chapters.

Chapter 2 presents the details of the numerical methods and solver settings used to solve the governing equations in Ansys fluent. Additionally, a detailed validation of previously known result to verify the relevance and accuracy of the process adopted to get the result so that it can be used for further analysis are also discussed.

Chapter 3 presents a detailed discussion about the analysis of the heat transfer and frictional loss characteristics of a rectangular channel using delta winglets and shear-thinning fluid.

Chapter 4 explores the understanding of the influence of delta winglets on the thermal and fluid flow characteristics of shear-thinning fluids through a fin-tube heat exchanger.

Chapter 5 focuses on the investigation of the thermo-hydraulic performance of a fin-tube heat exchanger using rectangular winglet and shear-thinning fluid.

Chapter 6 discusses the behavior of shear-thinning fluid on the fluid flow and thermal performance of a fin-tube heat exchanger equipped with curved rectangular winglet vortex generators.

Chapter 7 concludes the work presented in the thesis, along with recommendations for future work.

Chapter 2

Numerical methods and validation

2.1 Governing equation

To model the fluid flow and heat transfer inside the heat exchanger, continuity, momentum and energy equations are solved.

To develop the mathematical model of a single-phase flow of fluid, the following assumptions have been made.

- The effects of body forces are negligible.
- There are no radiation heat losses.
- Compressibility effect is negligible.
- The flow is laminar and steady.

Based on these assumptions the continuity, momentum, and energy conservations equations are written below:

Continuity equation

$$\nabla \cdot \vec{V} = 0 \tag{2.1}$$

Momentum equation

$$\nabla \cdot (\rho \vec{V}\vec{V}) = -\nabla p + \nabla \cdot \left[\frac{\mu}{2}(\nabla \vec{V} + (\nabla \vec{V})^T)\right] \tag{2.2}$$

Energy equation

$$\nabla \cdot (\rho C_p \vec{V} T) = k \nabla^2 T \tag{2.3}$$

Where, $\vec{V}$, ρ, μ, p, C_p, T, and k are velocity vector, density [$\mathrm{kg\,m^{-3}}$], dynamic viscosity [$\mathrm{kg\,m^{-1}\,s^{-1}}$], static pressure[Pa], specific heat capacity [$\mathrm{J\,kg^{-1}\,K^{-1}}$], temperature [K] and thermal conductivity [$\mathrm{W\,m^{-1}\,K^{-1}}$] of flowing fluid element.
The viscosity of power-law fluid showing shear-thinning behaviour relating to the function of strain rate γ has been defined by equation (2.4), where the power-law index is represented by n and consistency index [$\mathrm{kg/(m \cdot s^{2-n})}$] is represented by K [106]

$$\mu(\dot{\gamma}) = K(\dot{\gamma}^{n-1}) \tag{2.4}$$

The objective of this analysis is to gain an understanding of how non-Newtonian fluid flows impact the thermal and fluid flow characteristics of FTHE with DWPs. In order to assess the effectiveness of an FTHE, it is necessary to quantitatively measure a series of dimensionless numbers. These numbers are clearly defined as follows:
The Reynolds number (Re) and Prandtl number (Pr) of a shear-thinning non-Newtonian fluid are determined by the hydraulic diameter ($2H$) and the average axial velocity (u_m) [62] of the channel as

$$Re = \frac{\rho u_m^{2-n} (2H)^n}{K} \tag{2.5}$$

$$Pr = \frac{C_p K (u_m/2H)^{n-1}}{k} \tag{2.6}$$

The numeric values of K and n are 0.02792 and 0.7051 respectively for the aqueous solution of CMC of concentration 2000 ppm [101] while u_m is the average axial velocity of the fluid at the entrance of the channel, in [$\mathrm{m\,s^{-1}}$].
Span average Nusselt number (Nu_{sa}) [107], the apparent friction factor (f_{app}) [62] and the average Nusselt number (Nu_m) [6] are defined as follows:

$$\overline{Nu}_{sa} = \left(\frac{\dot{q}_{[x,y]|_{z=0}}}{T_w - T_x} + \frac{\dot{q}_{[x,y]|_{z=H}}}{T_w - T_x} \right) \left(\frac{H}{k} \right) \tag{2.7}$$

$\dot{q}_{[x,y]|_{z=0}}$ and $\dot{q}_{[x,y]|_{z=H}}$ is length-weighted average heat flux at a various locations along the direction of flow on the upper and lower wall respectively, T_w is constant wall temperature and T_x is the mass-weighted average temperature of the fluid along the flow direction.

$$Nu_m = \frac{h(2H)}{k} \tag{2.8}$$

$$h = \frac{\dot{m}C_p(T_{out} - T_{in})}{A_h \Delta T} \tag{2.9}$$

$$\Delta T = \frac{(T_{wall} - T_{in}) - (T_{wall} - T_{out})}{\ln[(T_{wall} - T_{in})/(T_{wall} - T_{out})]} \tag{2.10}$$

$$f_{app} = \left(\frac{P_1 - P_2}{0.5\rho U_{av}^2}\right)\left(\frac{2H}{\Delta x}\right) \tag{2.11}$$

$$P_{pump} = Q\Delta p \tag{2.12}$$

$$\Delta p = (P_1 - P_2) \tag{2.13}$$

The expression of mean colburn factor(j) and friction factor (f) [62] are given below

$$j = \frac{\overline{Nu_x}}{Re\ Pr^{0.33}} \tag{2.14}$$

$$f = \frac{f_{app}}{8} \tag{2.15}$$

The quality factor (Q_f) represents the collective impact of heat transmission augmentation and pressure drop in the flow domain with the VG and is represented by equation (2.15) [62].

$$Q_f = \frac{j}{f} \tag{2.16}$$

where the heat transmission area of the channel and mass flow rate of the CMC solution is represented by A_h [m^2] and $\dot{m}$ [kg s^{-1}]. T_{out} [K] is the average mass-weighted temperature of the CMC solution at the exit of the channel, and P_1 and P_2 are the area weighted-average static pressures at the inlet and outlet of the flow domain, respectively.
The hydraulic diameter (D_h) is represented as:

$$D_h = \frac{2WH}{(W + H)} \tag{2.17}$$

The efficiency (η) is expressed as:

$$\eta = \left(\frac{Nu_m}{Nu_o}\right)\left(\frac{f_{app,o}}{fapp}\right)^{0.33} \tag{2.18}$$

where m and o represent mean value and base channel, respectively. $\eta > 1$

represents better overall performance campared to the base channel.

Selection of steady and unsteady process solver

The selection of steady and unsteady process solutions in ANSYS Fluent 2021 R1 [108] is entirely based on comparing the results of the two processes. Numerical solutions for CRWP-embedded FTHE were performed using CMC aqueous solution at Re = 200, considering steady and unsteady processes. The outcomes for Nu_{sa} for steady and unsteady process is represnted by Fig. 2.1. It was observed that the the outcomes for steady and unsteady process coincides with each other leaving no difference. However, considering unsteady process solver required a much more solution time compared with steady process. To save the computational cost, it is advisable to use steady process solver of ANSYS Fluent.

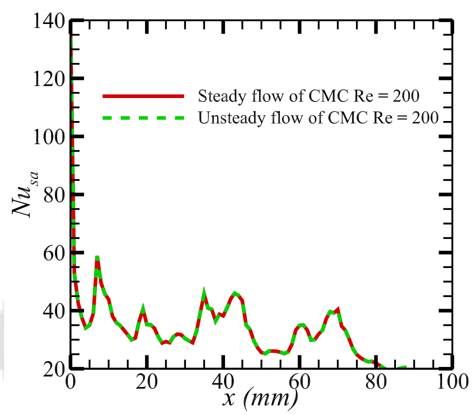

Figure 2.1: Comparison of Nu_{sa} for steady and unsteady process for the inline tube row with CRWP for the aqueous solution of CMC (2000 ppm) at Re = 200

2.2 Numerical methodology and solver settings

The finite volume approach is used in conjunction with a prescribed boundary condition to solve the equations for continuity, momentum, and energy. The SIMPLEC algorithm is used to link the pressure and velocity as it is well-known for its stability and convergence. It provides stable solutions, even in complex flow conditions, and tends to efficiently converge to a solution [107]. It is quite important to choose an appropriate solver (pressure-based or density-based), spatial discretization scheme (Upwind scheme, Quick scheme, and CDS scheme), and other settings to get to know whether the numerical scheme is consistent, convergent, and stable in computational fluid dynamics simulations. Following solver configuration parameters for ANSYS FLUENT are mentioned below:

- Second order upwind scheme was used to discretize the convective terms of momentum and energy equations.
- Double precision, steady state and pressure based solver was used.
- The convergence criteria for continuity, momentum, and energy were set as $10^{-8}, 10^{-8}$, and 10^{-10} respectively.

2.3 Validation Results

The main aim of solver verification is to verify the relevance and accuracy of the process adopted to get the result so that it can be used for further analysis. Hence it is required to compare the known result or analytical result with the result obtained by using the present adopted model to verify the solution process.

2.3.1 Simulation of air through a rectangular channel

A rectangular channel of length 200 mm, height 3 mm, and width 12 mm has been considered for this validation process. The fluid enters the channel with constant velocity and temperature. The top and bottom wall of the channel is fixed at 320 K and the side walls have been considered as symmetry. The hydraulic diameter of the channel is considered as twice the height of the channel. The analysis has been done for the $Re = 1000$. Mass-weighted average temperature and the length-weighted average heat flux are calculated. Local Nu is calculated using the equation (2.17) [60]

$$Nu_x = \left(\frac{\dot{q_x}}{T_w - T_x}\right)\left(\frac{2H}{k}\right) \tag{2.19}$$

where, Nu_x is local Nusselt number, $\dot{q_x}$ is length-weighted average heat flux at different location in x-direction, T_w is fixed wall temperature and T_x is mass-weighted average temperature at different location in x-direction in [K].

The analytical value of Nu of this channel has been reported as 7.54 while adopting the present solver process the Nu value is 7.534. The analytical and

Table 2.1: Variation in analytical and present solution for average Nu

	Analytical solution	Present solution	% Change
Nu	7.54	7.534	0.07

present result variation for Nu is 0.07% mentioned in Table 2.1. The variation in the analytical result and the present result is quite small and it can be assumed as negligible.

2.3.2 Simulation of Newtonian fluid through a rectangular channel with inbuilt cylinder

Two flat plate fins form a channel of height $= H$, width $= 5H$, length $= 15H$ and the tube of diameter $D = 5H$ is located at the center of the fins was considered for the validation process. The geometry for the validation is shown in Fig. 2.2. Heat transfer analysis of fin-tube elements at different Re has been carried out to calculate the combined effect of convective and conductive heat transfer and average pressure distribution throughout the system. The results have been validated by comparing it with the results of Fiebig *et al.* [109] for average pressure concerning channel length for a Newtonian fluid.

The comparison of the results has been shown in Fig. 2.3. The results of the present simulation for average pressure are almost close to the Fiebig *et al.* [109], which validates the results obtained. From Fig 2.3 it has been observed that the pressure near the tube decreases sturdily while it decreases gently before and behind the tube area. There is a slight deviation between the results of Fiebig *et al.* [109] and the current simulation. This deviation of pressure values from the Fiebig *et al.* [109] can be considered due to the difference in numerical schemes, and convergence criteria.

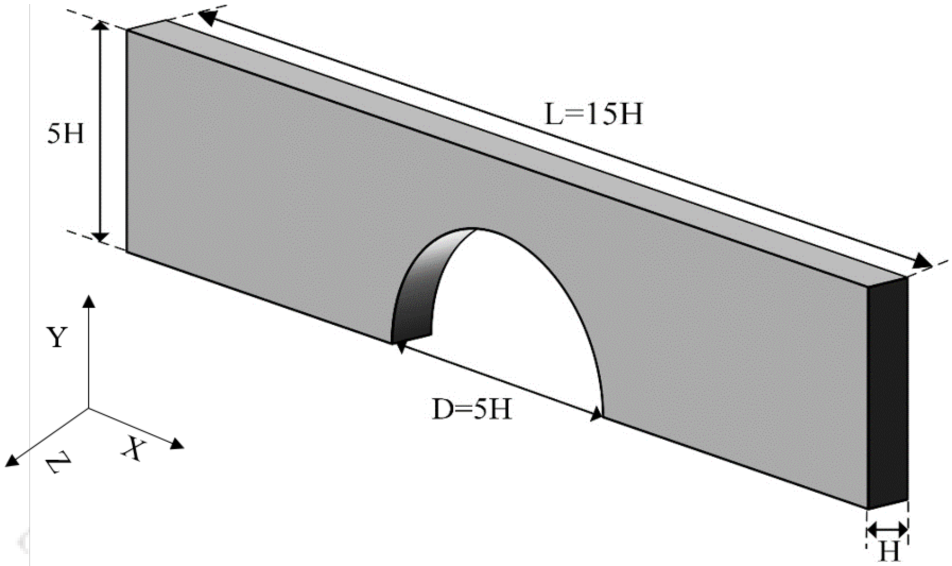

Figure 2.2: Fin-tube model geometry

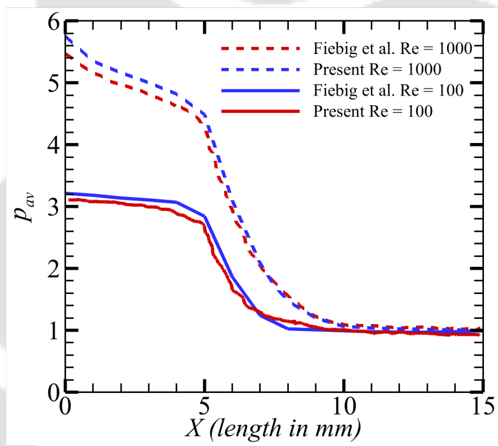

(a)

Figure 2.3: Comparison of the average pressure along the length of the channel for Re = 100, and 1000

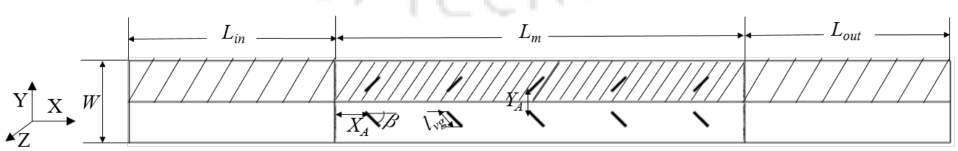

Figure 2.4: Computational domain

Table 2.2: Difference in analytical and present solution for average Nu and pump power

	Nu_{av}	P_{pump}
Ebrahimi *et al.*	29.41	0.007178
Present solution	28.9987	0.007121
% change	1.41	0.8

2.3.3 Laminar convective heat transfer of shear-thinning liquids in rectangular channels with LVGs

Thermo hydraulic performance of a rectangular channel furnished with rectangular vortex generators has been discussed by Ebrahimi *et al.* [6]. Three-dimensional numerical simulations have been performed on a channel equipped with five pairs of rectangular winglet vortex generators represented by Fig. 2.4. An aqueous solution of carboxymethylcellulose (CMC) with a concentration of 2000 ppm is considered a working fluid. The hydraulic diameter of the channel is 8 mm calculated by using Eq^n. 2.17. The height of the channel is considered as $H = 5$ mm and width $W = 4H$. The computational domain is divided into three parts, namely inlet zone, main zone, and outlet zone, corresponding lengths of these zones are $L_{in} = 10H$, $L_m = 20H$, and $L_{out} = 10H$ respectively. The main zone consists of five couple of rectangular winglet vortex generators kept at equal distances in the flow direction, mounted in CFU pattern at an attack angle of 45° and lateral distance of $Y_A = 5$ mm. The inlet and outlet zone walls are considered adiabatic walls and the main zone walls are heated at a fixed temperature of 320 K. VGs are also maintained at a fixed temperature of 320 K. Due to symmetry, half of the channel is considered a computational domain. Three-dimensional numerical simulation has been performed to solve the problem using carboxymethylcellulose as a shear-thinning fluid. SIMPLEC scheme was used for pressure-velocity coupling. Second order upwind scheme was used to discretize the convection terms of momentum and energy equation and convergence criteria for continuity, momentum, and energy were set as 10^{-8}, 10^{-8}, and 10^{-10}. The Nu_{av} and pumping power have been calculated by using the equations (2.8) and (2.12) and compared with the result of Ebrahimi *et al.* [6]. The variations in the result of Nu_{av} and pumping power are 1.3%, and 0.79% respectively. The difference between Ebrahimi *et al.* [6] result and the present result is quite small and mentioned in

Table 2.2.

2.3.4 Simulation of air through a staggered fin-tube heat exchanger

The accuracy of the simulation and the implemented process was confirmed by comparing the present simulation results with the experimental results of Wang and Chi [110] and the numerical results of Lu and Zhai [111]. The present simulation results for convective heat transfer coefficient (h_c) and pressure drop at various frontal velocities (V_{fr}) have been validated by comparing the experimental results of Wang and Chi [110] and the numerical study of Lu and Zhai [111]. Fig. 2.5 represents the computational domain.

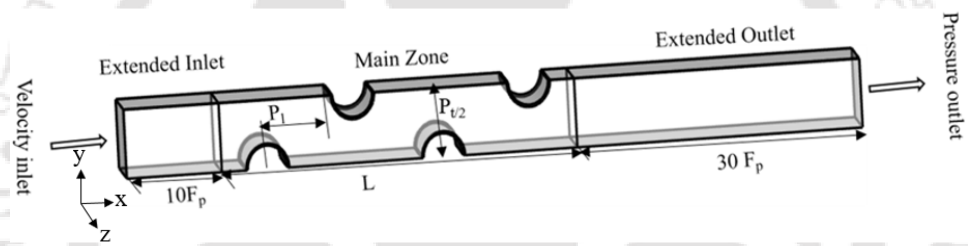

Figure 2.5: Computational domain

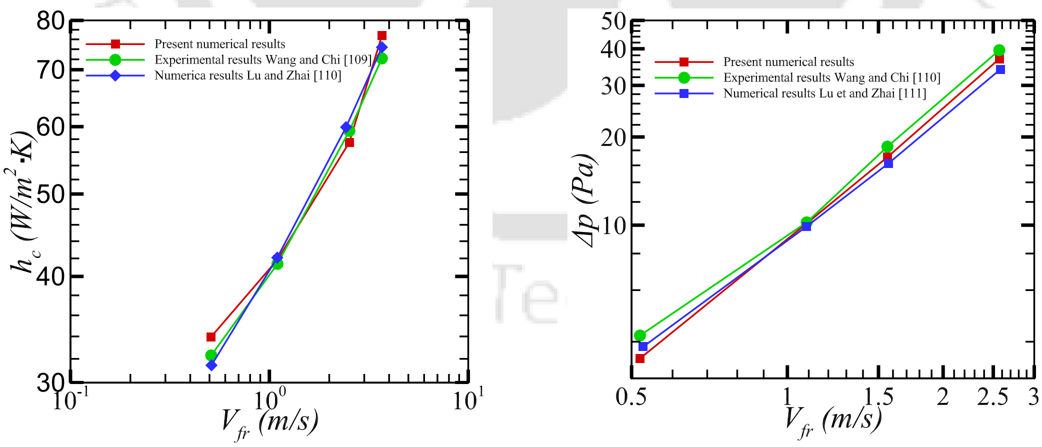

(a) (b)

Figure 2.6: Comparisons among the present numerical results, experimental results by Wang *et al.* [110] and numerical results of Lu *et al.* [111] (a) h_c, and (b) Δp

Table 2.3: Geometrical details of the geometry considered by Wang and Chi [110] and Lu and Zhai [111]

Parameter	Symbol	Values (mm)
Longitudinal tube pitch	P_l	19.05
Transverse tube pitch	$P_{t/2}$	12.9
Fin collar outside diameter	D_c	8.61
Fin pitch	F_p	2.06
Fin length	L	77

The geometrical details for the validation problem are mentioned in Table 2.3. The geometry considered by Wang and Chi [110] and Lu and Zhai [111] is a rectangular channel with the inbuilt cylinders in staggered configurations. The mean absolute error (MAE) expressed in equation (2.18) for pressure difference and heat transfer coefficient of numerical work done by Lu and Zhai [111] and present numerical work is 0.908 and 0.565, respectively. The MAE for the pressure difference and the heat transfer coefficient of the experimental work done by Chi and Wang [110] and the present numerical simulation are 1.211 and 1.233 respectively. The maximum deviation in percentage for pressure difference and heat transfer coefficient of numerical work done by Lu and Zhai [111] and present numerical work is 8.83% and 7.43%, respectively, and for pressure difference and heat transfer coefficient of experimental work done by Chi and Wang [110] and present numerical work is 11.49% and 5.96% respectively. The comparisons for h_c and Δp are shown in Fig. 2.6.

$$\text{Mean absolute error (MAE)} = \frac{\sum_{i=1}^{n} \mid Y_i - X_i \mid}{n} \tag{2.20}$$

Chapter 3

Heat transfer analysis of a rectangular channel with delta winglets and shear-thinning fluid

The efficient and economical use of energy is essential to prevent the release of hazardous gases into the atmosphere and to prevent climatic change and environmental degradation. Heat transfer applications are used in a variety of industries, including chemical industries, chilling industries, pharmaceutical industries, food industries, clothing industries, heating ventilation and air conditioning devices, cooling of electronic components, nuclear power plants, and thermal power plants. It is important for these industries to focus on efficient and innovative heat transfer techniques to maximize productivity with reduced costs. It is a splendid project for researchers to enhance the overall performance of heat exchangers to meet the demand of these industries for efficient heat transfer. Several types of research have been carried out to improve the efficiency of heat removal capacity of heat exchangers [2, 112–119]

3.1 Introduction

A vortex generator (VG) in the form of delta winglet pairs (DWP) is a very efficient approach to increasing the capacity of heat exchangers to remove heat passively [34, 120–124]. It may be placed on the surface of the fins to improve heat transmission and generate the resulting secondary flow. VGs are indispensable for increasing the heat transfer coefficient by generating vortices when fluid passes over them, because of the pressure differences of their leading and trailing edges.

This high-energy fluid tries to penetrate the boundary layer, diminishes it, and mixing takes place, leading to high heat transmission. The overall goal of vortex generators in improving heat transfer is to increase convective heat transfer by promoting efficient fluid mixing, boundary layer disruption, and increased turbulence. These generated vortices impart swirling motion and transfer their energy to the remaining fluid.

DWPs perform better than RWPs in a plate-fin heat exchanger at higher attack angles [69]. However, employing a delta winglet results in a minimal gain in pressure drop but a considerable increase in heat transmission [4, 19, 22, 23, 69–71].

The majority of industrial instruments use liquids to improve the heat transfer performance of heat exchangers. The thermal resistance for liquids is quite low, according to a basic understanding of heat transfer. However, sometimes it is quite necessary to augment the thermal energy transfer on the liquid side such as cooling the nuclear reactor core and cooling the electronic components such as the electronic chip. Since liquid cooling is more effective than air cooling, high-performance computers and gaming systems frequently use liquids to cool their components. Meanwhile, there has been a lot of interest in studies on the thermohydraulic performance of non-Newtonian fluids all around the world. Shear-thinning fluid is used as a coolant in most industries, including pharmaceutical and drug industries, distilleries, food industries, petrochemical industries, and food and biological industries. The aqueous solution of CMC acts as a non-Newtonian shear thinning fluid and provides better results compared to water when used for heat removal applications [6, 77].

According to the studied literature, the majority of the research has been conducted concerning the thermohydraulic performance of varying channel shapes and sizes along with a variety of winglets and wings using Newtonian fluid as a working medium. It was concluded from the surveyed literature review that the DWPs perform better than RWPs considering the thermohydraulic performance of the channel. To the best of the author's knowledge, no studies have been conducted to investigate the impact on the thermohydraulic performance of the rectangular channel with inbuilt DWPs using shear-thinning fluids. It requires a thorough investigation to understand the behavior of shear-thinning fluid on the heat transfer and frictional loss of a rectangular channel using DWPs.

3.2 Problem definition

The main aim of this study is to investigate heat transfer and frictional loss in a rectangular channel equipped with punched delta winglets (DWPs) concerning the viscosity of an aqueous CMC solution. The channel consists of five pairs of DWPs at regular intervals mounted on the bottom plate of the channel. These winglets are arranged in a common flow down configuration at various inclination angles, viz. 30°, 45°, and 60° to obtain the optimum value of heat transfer and frictional loss [6]. An aqueous solution of CMC with a concentration of 2000 ppm showing shear-thinning behavior is considered a working fluid to investigate laminar heat transfer through the channel with a range of Reynolds numbers Re 50 to 200 [90]. Additionally, the performance of the channel was compared to that of the base channel. In addition, this work used a comparison analysis to analyse the heat transfer and pressure drop properties of flow channels employing CMC aqueous solutions against water. The research findings will provide valuable insights into selecting suitable winglets based on specific requirements.

3.2.1 Computational model

Fig. 3.1 represents the schematic and isometric view of the geometry considered for the analysis. Due to the symmetry of the model, only half of the geometry is considered to be a computational domain. The hatched region of Fig. (a) represents the computational domain for further analysis. The height (H) of the channel is 5 mm. All dimensions of the channels are expressed in the form of the channel height. Full length and width (W) of the channel are $20H$ and $4H$ respectively. Five pairs of DWPs are attached on the bottom surface of the channel with the angle of inclination 30°, 45°, and 60° from the direction of fluid flow. The apex height and base length (l_{vg}) of the DWPs are equal to the height of the channel. The computational model has been divided into three parts, namely, the primary zone of length (L_1), the main zone of length (L_2), and the secondary zone of length (L_3). To maintain the uniform flow at the entry of the main zone the inlet part has been extended to $L_1 = 10H$ and to avoid the flow reversal at the exit of the main zone the outlet is extended to the $L_3 = 10H$. The lateral (Y_A) and longitudinal distance between two consecutive DWPs is equal to H and $5H$, respectively. The

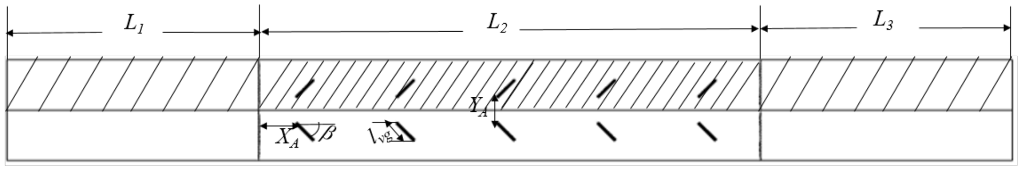

(a)

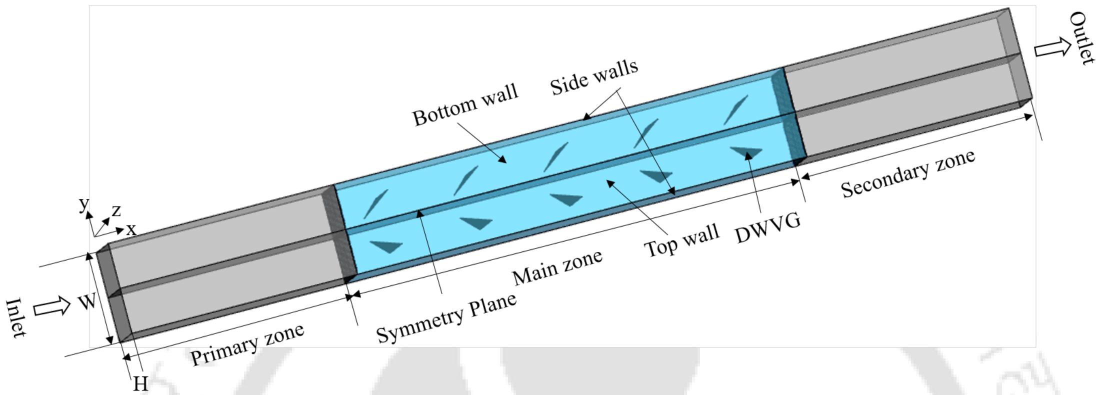

(b)

Figure 3.1: Computational domain with DWPs (a) Schematic view of the Computational domain and (b) Isometric view of the Computational domain

distance of the leading edge of the first pair of DWPs from the entrance of the main zone is $(X_A) = 1.5H$. Five pairs of DWPs are evenly spaced along the primary flow direction in the main zone.

3.2.2 Boundary conditions

This work compares the thermal and hydraulic performances of non-Newtonian CMC solutions to water in a rectangular channel using DWPs and RWPs. The findings of this investigation will provide insights into the distinctions between these two winglets and their individual impacts on the thermal and hydraulic performance of the channel.

The velocity inlet and outflow boundary condition is applied at the entry and exit of the channel respectively. The solid walls and the DWPs in the main zone are maintained at a fixed temperature of 320 K. The walls of primary and secondary zones are maintained at adiabatic boundary conditions. The temperature of the fluid at the inlet remains constant at 298 K throughout the operation. Owing to the symmetrical nature of the channel, only half of the channel is utilized as a computational domain, and thus the symmetry boundary condition is applied to the symmetry plane. No slip boundary condition is applied on all solid walls of the channel.

The boundary conditions for the various parts of the channel are mathematically represented as follows:

Channel entry: $u = u_{in}, v = w = 0, T = T_{in} = 298$ K, $\frac{\partial p}{\partial n} = 0$,

Channel Exit: $p = 0$, $\frac{\partial u}{\partial x} = \frac{\partial v}{\partial x} = \frac{\partial w}{\partial x} = 0$, $\frac{\partial T}{\partial x} = 0$,

Wall of main zone: $u = v = w = 0, T = T_{wall} = 320$ K, $\frac{\partial p}{\partial n} = 0$,

Central Symmetry plane: $\frac{\partial v}{\partial y} = \frac{\partial w}{\partial y} = 0$, $\frac{\partial T}{\partial y} = 0$, $u = 0$, $\frac{\partial p}{\partial n} = 0$ and

Walls of primary and secondary zone (adiabatic walls):

$u = v = w = 0$, $\frac{\partial T}{\partial z} = 0$, $\frac{\partial p}{\partial n} = 0$

3.3 Mesh generation and grid independency test

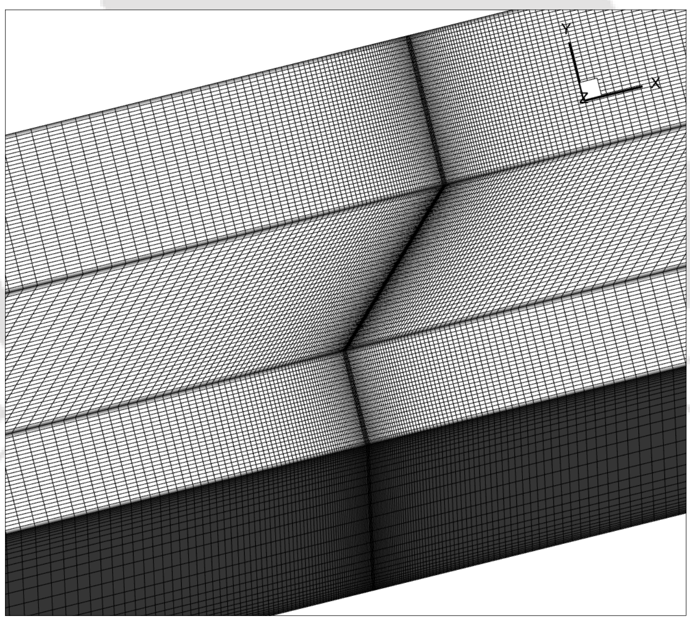

Figure 3.2: Magnified representation of the computational grid

The flow domain discretization comprises a non-uniform, unstructured mesh composed of multi-block hexahedral cells that follow the flow direction, as depicted in Fig. 3.2. These cells were made to cluster around the VG, particularly in regions with steep gradients. To ensure result accuracy and to investigate the influence of cell size, four different meshes were generated, each with a varying number of

Table 3.1: Results of a mesh independence study on the flow of 2000 ppm aqueous CMC solution in a channel equipped with DWPs. at $Re = 200$

element counts	f_{app}	% Diff.	Nu_m	% Diff.
748534	0.410	-	30.47	-
1261621	0.411	0.24	30.9	1.39
1991805	0.412	0.24	30.97	0.23
4709230	0.412	0.09	30.99	0.065

cells. The comparison of Nu_m and f_{app} for different grid sizes are presented in Table 3.1. The comparison indicates that the system comprising of 1991805 cell count can produce satisfactory results with minor variations in Nu_m and f_{app}, while also maintaining a reasonable processing time. Therefore, this mesh was chosen for additional analysis. The calculations were performed on an HP machine with 8 CPU cores, each with 3 GB memory, with each case taking approximately 6 to 8 hours to compute.

3.4 Results and discussion

The study involved determining the average changes in performance parameters such as the Nusselt number (Nu), the apparent friction factor (f_{app}), and the quality factor (Q_f) caused by the addition of DWP to the rectangular channel at various angles of attack (β). Then, these data were compared to the performance of a similar channel with RWPs and with the base channel (without the winglets). Additionally, the performance of the channel was compared for Newtonian as well as non-Newtonian fluid. Figs. 3.3 and 3.4 show the velocity and temperature distribution of a rectangular channel equipped with DWPs at various angles of attack in the midplane ($z = 0.5H$).

Fig. 3.3 clearly shows how the size of the wake zone reduces behind the winglets as the inclination angle lowers. However, as the angle of attack increases, so do the fluid temperature and pressure drop. The flow loss increases as the angle of attack increases, generating a barrier in the flow creating more pressure loss. The temperature distributions at various angles of attack at the mid plane of the channel are depicted in Fig. 3.4. As the attack angle increases, the fluid has more

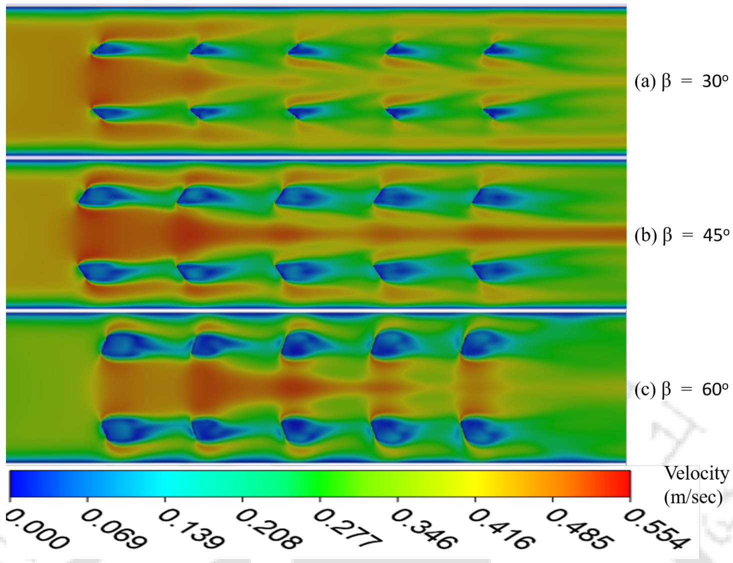

Figure 3.3: Velocity distribution of a rectangular channel along with DWP at various attack angles (a) $\beta = 30°$, (b) $\beta = 45°$ and (c) $\beta = 60°$ at a cross-section z = $0.5H$ and $Re = 200$ for the aqueous solution of CMC (2000 ppm)

time to come into contact with the heated surface of the DWPs, increasing heat transfer. The thermal gradient grows as the attack angle increases, as does the exit temperature of the fluid.

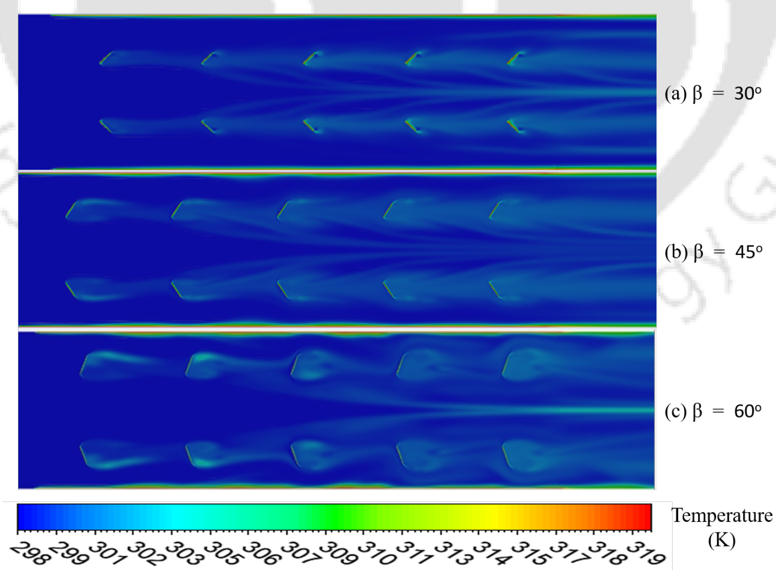

Figure 3.4: Temperature distribution of a rectangular channel along with DWP at various attack angles (a) $\beta = 30°$, (b) $\beta = 45°$ and (c) $\beta = 60°$ at a cross-section $z = 0.5H$ and $Re = 200$ for the aqueous solution of CMC (2000 ppm)

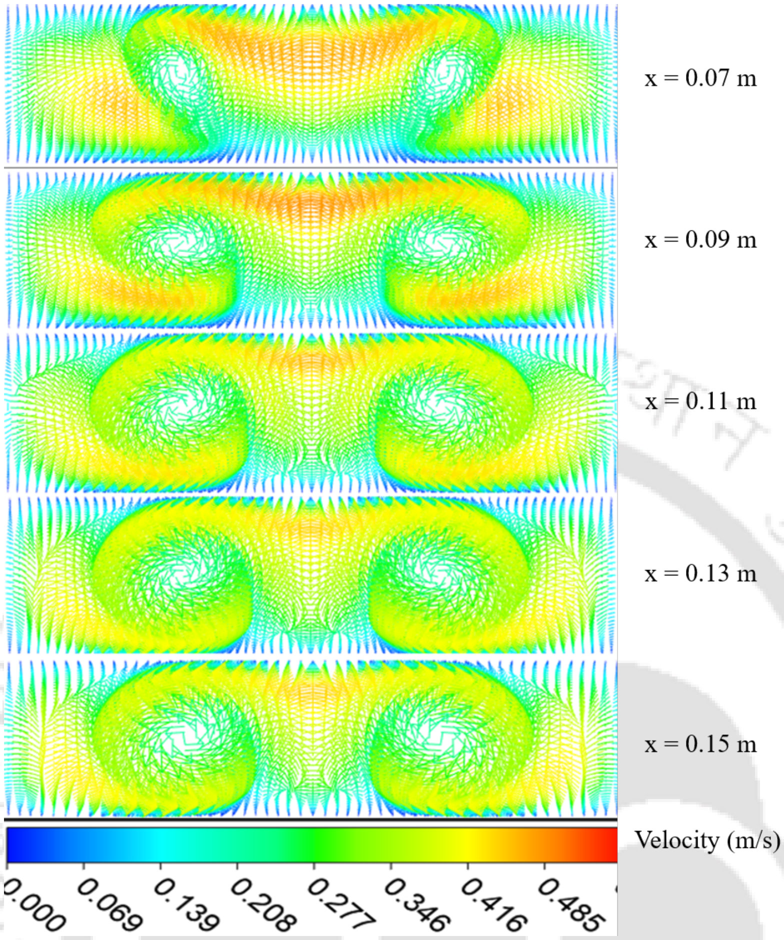

Figure 3.5: Velocity vector at various cross sections along the direction of flow for the rectangular channel with DWVG at an attack angle of 30° and $Re = 200$ for the aqueous solution of CMC (2000 ppm)

Fig. 3.5 shows the velocity vectors at different cross-sections along the flow direction. The propagation of longitudinal vortices was observed along the length of the channel. Two pairs of counterclockwise antirotating vortices propagating in the direction of flow were trying to lift the fluid toward the top wall of the channel. The fluid near the side wall of the channel tries to push the fluid toward the bottom wall of the channel. This upward and downward movement of fluid enhances the fluid mixing.

Fig. 3.6 represents the average variation of Nu, f_{app}, P_{pump} and Q_f with Re at various attack angles for the flow of an aqueous solution of CMC (2000 ppm). It was observed that the average Nusselt number Nu_{av} for RWVG and DWVG at various attack angles increases with Re. Higher Re generates strong longitudinal vortices at

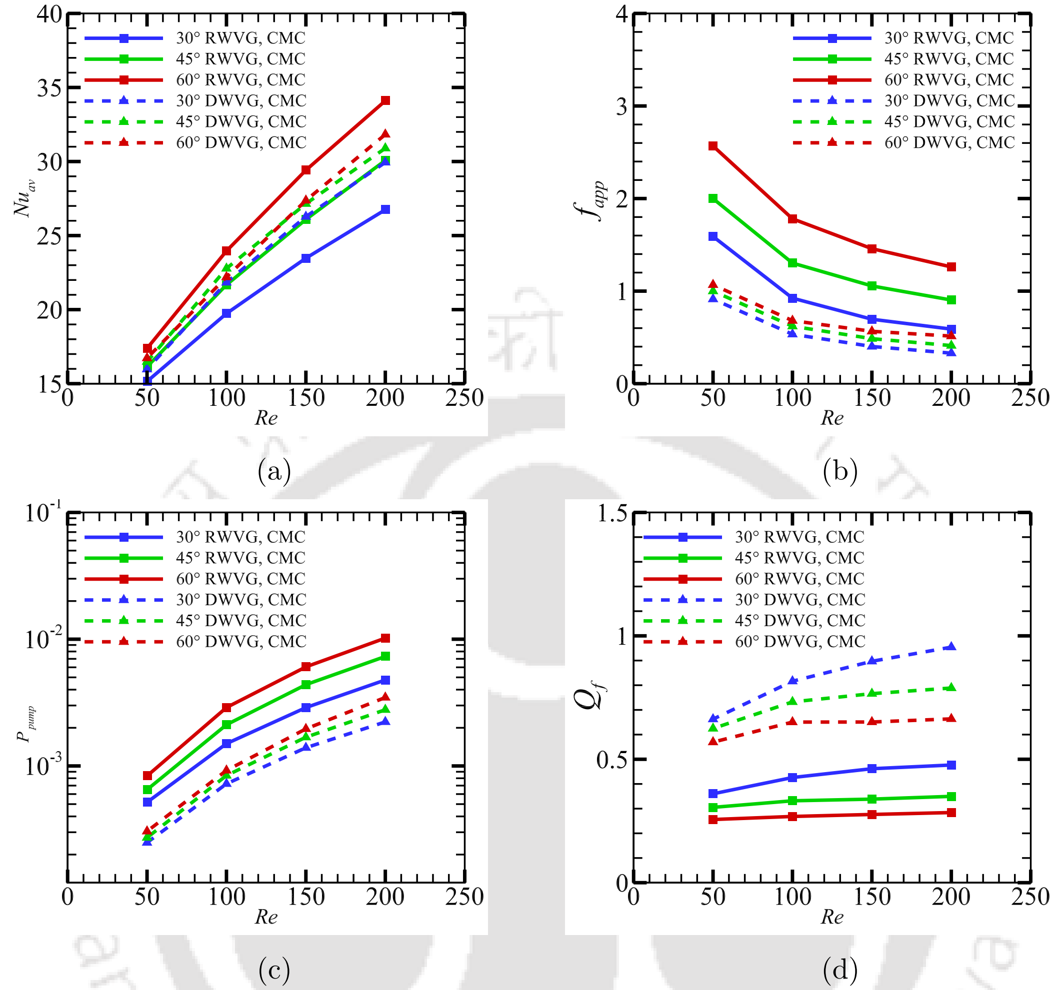

Figure 3.6: Variation of average (a) Nu_{av}, (b) f_{app}, (c) P_{pump} and (d) Q_f with Re for a rectangular channel with DWPs and RWPs at various angle of attack for CMC (2000 ppm)

elevated velocities. These high-energy vortices penetrate the boundary layer, disrupt it, and enhance the fluid mixing resulting in enhanced heat transfer. The Nu_{av} also increases with an increase in attack angle for RWVG and DWVG. A higher attack angle provides more time for the fluid to be in contact with heated winglet surfaces to absorb more heat resulting in high heat transfer at the cost of a large pressure drop. Higher Nu_{av} has been observed for RWVG at a higher attack angle but at the lower attack angle, DWVG outperforms RWVG. The channel equipped with RWVG has a large wake zone behind the winglet surface compared to the DWVG, resulting in lesser Nu_{av} at a lower attack angle. Compared to the DWVG, the RWVG exhibits a higher frictional loss because its larger surface area causes more obstacles in the fluid's flow, which raises the pressure drop. The friction factor decreases with an increase in Re for a laminar flow of fluid. P_{pump} for RWVG shows a higher value compared to the DWVG as the pressure drop for RWVG is higher. P_{pump} increases with increase in Re and attack angle. Considering the Q_f DWVG outperforms the RWVG. Although the RWVG generates more heat transfer but at the same time it creates a larger pressure drop resulting in lower Q_f.

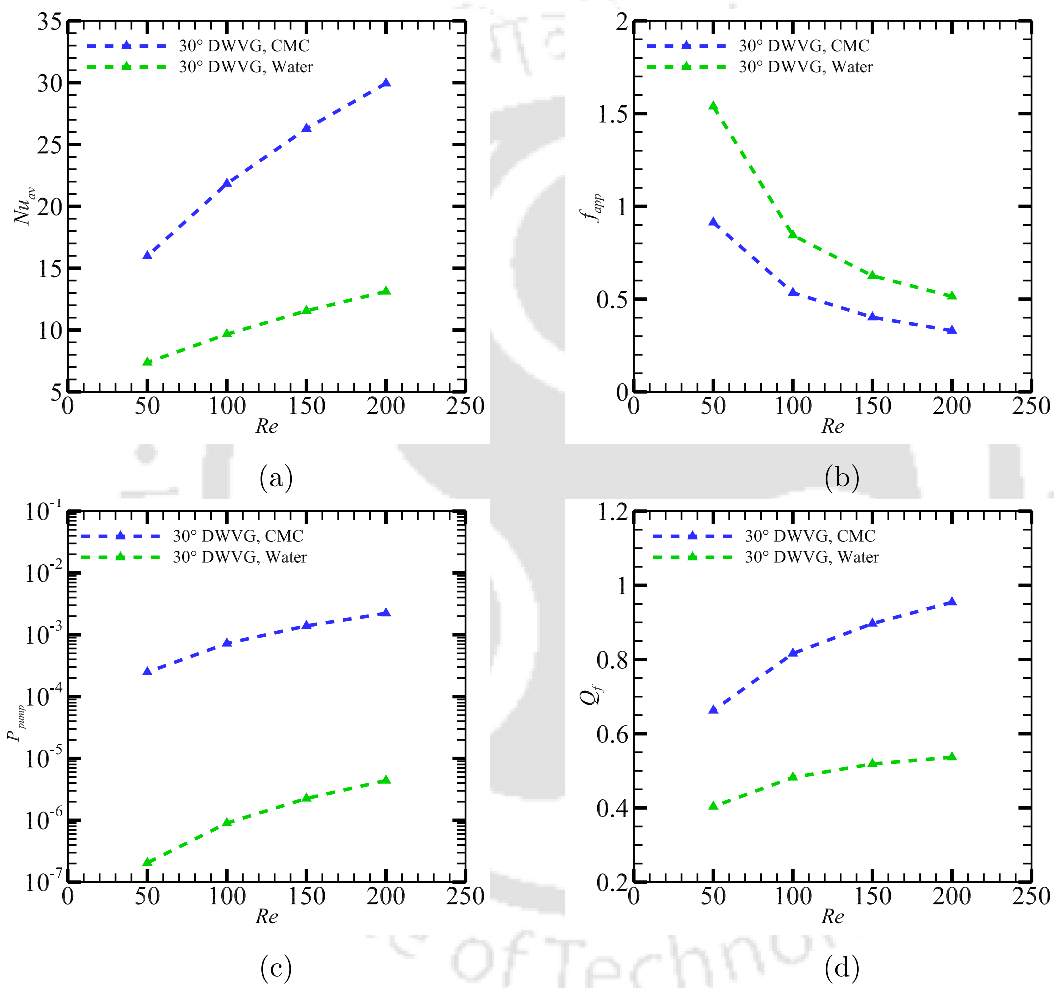

Figure 3.7: Average variation of (a) Nu_{av}, (b) f_{app}, (c) P_{pump} and (d) Q_f with Re for a rectangular channel with DWPs at an attack angle of 30° for CMC(2000 ppm) and water

Fig. 3.7 represents the average variation of Nu, f_{app}, P_{pump} and Q_f with Re for CMC solutions and water. The Nu_{av} for CMC is substantially higher than that of water, as seen in Fig. 3.7a. The aqueous solution of CMC can absorb more heat from the heated surface as its thermal conductivity is greater than the water. Using an aqueous solution of CMC is the main cause of effective heat transfer, it enhances the wetting characteristics of surface and boosts liquid-surface contact. This leads to improved overall performance in heat transfer applications. Fig. 3.7b represents the variations in average f_{app} for water and a CMC aqueous solution with Re. The results show that the average frictional loss in the channel decreases when a CMC aqueous solution is used as the working fluid. This is explained by the fact that a CMC aqueous solution has drag-reducing properties and a cushioning effect because of its molecular arrangement, which lowers frictional loss in comparison to water. Spherical and cylindrical micelles are generated when CMC is present in water, and the cylindrical shape of the micelles grows as the concentration of CMC increases. These micelles give the fluid a dampening effect that improves the drag-reducing ability of the fluid and helps to lower the frictional loss. The P_{pump} for CMC is significantly higher than the water as the viscosity of CMC is higher resulting in a higher pressure drop represented in Fig. 3.7c. Fig. 3.7d represents the combined effect of heat transfer and frictional loss. The aqueous solution of CMC performs well compared to the water for a given Re.

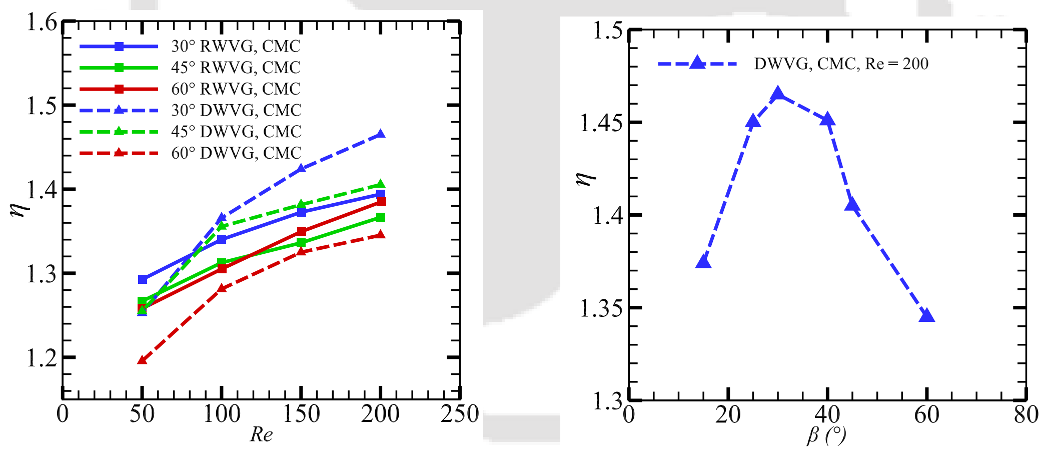

(a) (b)

Figure 3.8: Average variation of (a) η, with Re for a rectangular channel punched with RWPs and DWPs at various attack angles and (b) η, with attack angle for a rectangular channel equipped with DWP at $Re = 200$ for CMC (2000 ppm)

Fig. 3.8a represents the variation of efficiency (η) with Re for RWVG and DWVG at various attack angles for the flow of the aqueous solution of CMC. η represents the overall performance of the channel compared to the base channel. The value of η greater than unity represents the better performance of the channel. It was observed that the η for the channel equipped with DWVG outperforms the channel equipped with RWVG. Increasing the attack angle decreases the η. The channel equipped with VGs performs better than the base channel at all the range of Re considered for the present study. Fig. 3.8b represents the variation of η with attack angle. It was observed that initially with increase in the angle of attack enhances the η up to a certain limit, beyond this, it decreases. However, with increase in β increases the heat transfer but at the same time it increases the large pressure drop results in lesser η for the channel at the $\beta > 30°$. The channel equipped with DWVGs performs best at an optimum angle of 30°.

3.5 Summary

The aim of this study was to analyze the impact of DWVG on the performance of a rectangular channel that uses a non-Newtonian fluid. Numerical simulations were conducted for a rectangular channel equipped with five pairs of DWVGs in common flow down configurations using a specific type of liquid known as CMC with a concentration of 2000 ppm, which is viscous in nature. The apex height of the DWVGs was set at half the height of the channel. The inclusion of VGs affects the heat transfer and fluid flow performance of the channel. This is evaluated by comparing the Nusselt number (Nu), apparent friction factor (f_{app}), and quality factor (Q_f) of the channel with and without the VGs. Incorporating VGs into the channel improves fluid mixing, destabilizes the thermal boundary layer, and increases heat transfer. It was observed that increasing the inclination angle of the VG increases Nu and f_{app}, and decreases the Q_f of the channel. The channel performs best at 30° of attack angle considering the overall performance. Based on these observations, the conclusion have been made that DWVGs can be used to improve the heat transfer performance of channels at slight increase in pressure drop compared to the base channel using non-Newtonian fluids.

Chapter 4

Analysis of heat transfer and frictional loss of fin-tube heat exchanger with delta winglet and shear-thinning fluid

Heat transfer augmentation is a significant concern for industries involving heat transfer applications. FTHE are used in industries like heating, ventilation, air conditioning, petrochemicals, automotive and food industries to transmit heat from high-temperature surfaces to fluids. Enhancing heat transfer while meeting the demands of elevated efficiency and least cost with the minimum volume and lightest feasible weight is a significant problem for the research community; thus, the topic of heat transfer augmentation is of considerable attention. Numerous approaches are routinely used to improve heat transmission. One of them is the recurrent fracas of the creation of thermal boundary layers near heat transfer surfaces using DWVGs, providing better intermixing of the fluid. Investigation of the thermal and fluid flow characteristics of non-Newtonian fluids is crucial for various shear-thinning fluid applications in the food, medical, molecular biology, petrochemical, and chemical sectors. In the realm of heat exchangers, there has been a growing need to eliminate considerable amounts of heat by utilizing shear-thinning power-law fluids at low-pressure drops for various applications. This crucial requirement emphasizes the significance of efficient heat transfer in various industries and highlights the importance of finding the most effective methods to achieve it. Moreover, these materials are typically used in laminar flow regimes due to their high viscosity levels.

The aqueous solution of carboxymethyl cellulose (CMC) behaves as a shear-thinning fluid and reduces viscosity with applied shear stress.

4.1 Introduction

A vortex generator (VG) is a passive technique to enhance heat transmission using various shapes of wings and winglets. Several experimental and computational work has been reported involving the delta winglet vortex generator (DWVG) to improve heat transfer enhancement [34, 120–124].

Using effective coolants is a smart move to augment the performance of the FTHE along with the surface alterations. Since liquids have a higher heat transfer coefficient than gases, they are better suited for heat removal applications [60, 125]. Meanwhile, there has been much interest in studying non-Newtonian fluid flow behavior and heat conduction. One of the most intriguing aspects of the non-Newtonian fluid is that they may significantly improve heat transfer in laminar flows without appreciable increases in friction drag [90]. It was noticed that utilizing the aqueous solution of CMC in heat transfer devices enhances the capacity of the system to increase the transfer of thermal energy [6, 7, 87, 88].

According to the current literature, various research studies have successfully focused on improving heat transmission in an FTHE with winglets while minimizing the pressure penalty and utilizing air as the working fluid. As far as the author is aware, and based on the literature that has been looked at, the behavior of non-Newtonian fluid on the heat transfer and friction loss characteristics of an FTHE embossed with DWVG has yet to be investigated. More research is needed to completely understand the impact of non-Newtonian flow behaviour on the ability of the channel to carry heat.

4.2 Problem definition

The present analysis aims to investigate how the viscosity of an aqueous CMC solution affects the performance of FTHE equipped with DWVGs. The FTHE includes three lines of cylinders arranged in a row, with or without the DWVG attached to the bottom plate of the channel at regular intervals. The simulations are conducted at different Re values, ranging from 50 to 200 because the transition from laminar to turbulent flow occurs at a *Re* of about 200 for a flow inside the circular tube as reported by Gunter *et al.* [126]. The winglets have been thoughtfully placed in an inline tube configuration that follows a CFU arrangement. Additionally, they have been inclined towards the flow at various attack angles i.e. 160°, 165° and, 170° to ensure optimal performance. It is noteworthy to mention that the winglets are designed to be half the height of the channel, thus providing efficient aerodynamics and structural stability. The working liquid used in the simulations is an aqueous CMC solution with a concentration of 2000 ppm. The study compares the heat transfer and friction loss characteristics of channels with DWVGs and base channels. Moreover, a comparative analysis of the heat transfer and pressure drop attributes of flow paths utilizing CMC aqueous solution and water is conducted in this study. The results of the analysis will provide valuable insights into the thermodynamic performance of these two fluids and will aid in identifying the most efficient and effective fluid for a given application.

4.2.1 Computational model

Fig. 4.1 displays a rectangular channel with three rows of inbuilt cylinders having stamped DWPs near the tubes [90]. The channel dimensions are clearly defined, with a channel height (H) of 3.6 mm. The width (W) and the length (L) of the channel are $7.06H$ and $24.7H$, respectively. The three rows of tubes have the same diameters (D) of $2.96H$ and are equally spaced from the channel entry. The center distance between the first tube and the inlet is $L_1 = 3.53H$, the center distance between the first and second tube is $L_2 = 7.06H$, and the center distance between the second and third tube is $L_3 = 7.06H$, respectively. The height (h), chord length (l), and thickness (t) of the DWPs are $0.5H$, $2.93H$, and $0.027H$, respectively. The front end of the DWP is located at $X_1 = 1.28H$ distance from the inlet and $Y_1 = 0.63H$ from the side wall. The angle at which the DWP surface is inclined towards the direction in which fluid flows, also known as the attack angle (β), has three distinct values – 160°, 165°, and 170°. These numerical values determine the angle of attack of the DWP in relation to the fluid flow. The second and third pairs of winglets are located $7.06H$ behind the leading edge of the first and second pairs, respectively. The computational domain, winglet, and cylinder surfaces are all maintained at a constant temperature of 330 K, and the fluid temperature at the channel entrance is maintained at a constant temperature of 300 K. Since the temperature variation

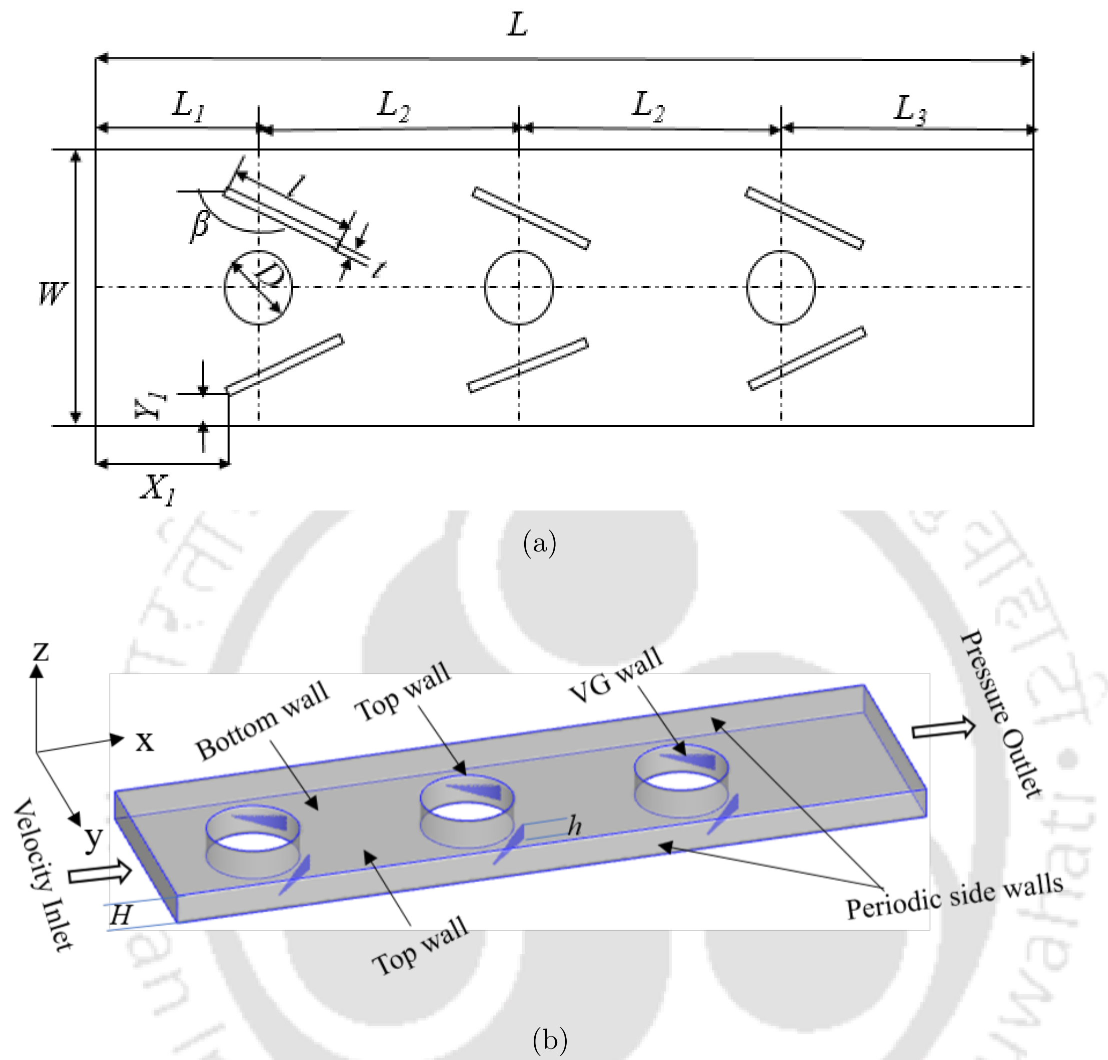

Figure 4.1: Computational domain with DWPs (a) Schematic view of the Computational domain and (b) Isometric view of the Computational domain

along the channel is minimal (less than 30 K), the material properties are considered temperature invariant [62].

4.2.2 Boundary conditions

The main aim of this analysis to compare the thermal and hydraulic performance of non-Newtonian CMC solutions with that of Newtonian fluids, especially water. The results of this study will shed light on the differences between these two fluid types and their respective effects on thermal and hydraulic performance.

Table 4.1: Boundary conditions are used in different parts of the channel

Boundary name	Boundary conditions
Entry	$u = u(z)$, $v = w = 0$, $T_{in} = 300$ K, $\frac{\partial p}{\partial n} = 0$
Exit	$p = 0$, $\frac{\partial T}{\partial x} = \frac{\partial u}{\partial x} = \frac{\partial v}{\partial y} = \frac{\partial w}{\partial z} = 0$
top, bottom, DWPs, and cylinder walls	$u = v = w = 0$, $T_w = 330$ K, $\frac{\partial p}{\partial n} = 0$
Side walls	$u(x_1, y_1, z_1) = u(x_2, y_2, z_2)$ and $p(x_1, y_1, z_1) = p(x_2, y_2, z_2)$

The velocity profile is fully developed and consistent at the inlet of the flow channel. The pressure-outlet boundary condition is maintained at the exit of the channel. The walls of the channel, cylinders, and VG are kept at a constant temperature and no-slip boundary conditions. The side walls have periodic boundary conditions. Table 4.1 mathematically represents the boundary conditions for different channel parts.

Where, n represents the direction normal to the boundary. (x_1, y_1, z_1) and (x_2, y_2, z_2) are corresponding points on the opposite boundaries.

4.3 Mesh generation and grid independency test

The discretization of the flow domain involves an unstructured, non-uniform, multi-zone hexahedral cell that aligns with the flow, as shown in Fig. 4.2. The finer mesh were made in the vicinity of the VGs and tube surfaces, where the gradient is greater. To ensure the accuracy of the results and test the impact of cell sizes, five meshes with different cell counts were created. As indicated in Table 4.2, the comparison of Nu_m and f_{app} for various grid sizes revealed that the mesh with 766919 and 1164458 mesh components showed the least variation in Nu_m and f_{app}, generating decent outcomes with adequate computational time. Therefore, the mesh with cell count 766919 was chosen for additional analysis. The calculations were performed on an HP machine with 8 CPU cores, each with 3 GB memory, with each case taking approximately 5 to 7 hours to compute.

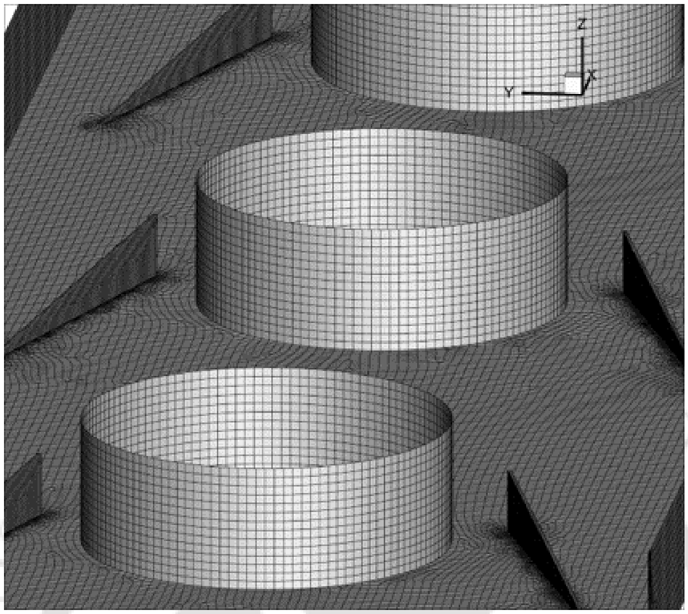

Figure 4.2: Magnified representation of the computational grid

Table 4.2: Mesh independence test results for the flow of a 2000 ppm aqueous solution of CMC in the channel fitted with cylinders and DWPs at $Re = 200$

element counts	f_{app}	% Diff.	Nu_m	% Diff.
300713	0.663	-	28	-
404161	0.670	1.06	29.13	4.04
532551	0.674	0.60	30.03	3.09
766919	0.678	0.59	30.88	2.83
1164458	0.680	0.29	31.70	2.66

4.4 Results and discussion

The study evaluated the average variation in performance parameters resulting from the placement of winglets in the FTHE. The findings were then compared to the performance of the same channel without winglets.

It is observed from Fig. 4.3 that the wake zone formation behind the tubes is significantly large in the base channel due to flow separation behind the tubes. Placing the winglets in FTHE behind the tubes reduces the wake zone formation represented in Fig. 4.3. Owing to its palcement and surface area, DWVG produces stronger longitudinal vortices compared to the base channel, thus retarding flow separation significantly and hence penetrating the wake zone efficiently compared

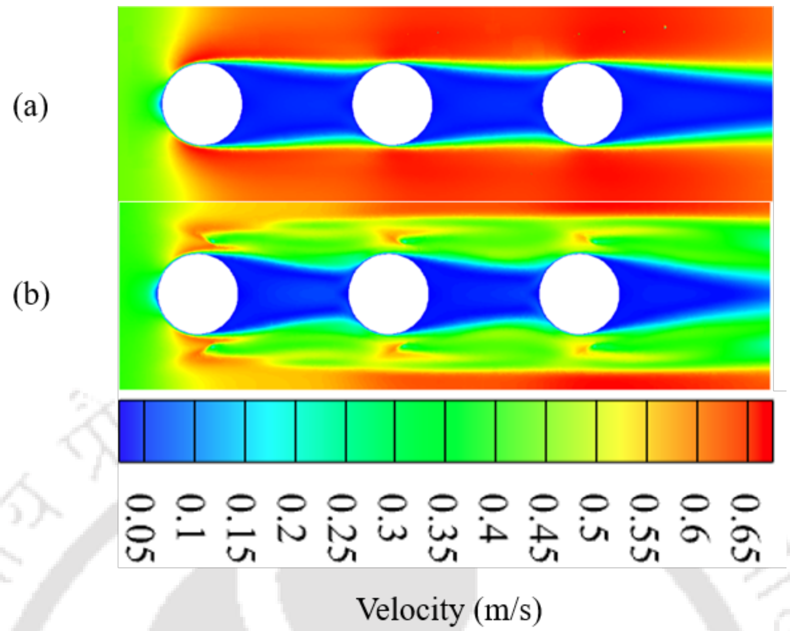

Figure 4.3: Velocity distribution of (a) Base channel, and (b) DWVG, $\beta = 160°$ at a midplane ($z = 0.5H$) and $Re = 200$ for the aqueous solution of CMC (2000 ppm)

to the base channel. However, there is a very small wake zone formed behind the DWVGs which resulting a liitle larger pressure drop compared to the base channel.

Fig. 4.4 represents the temperature distributions in (a) the base channel, and (b) the channel with DWVGs of attack angle 160° at the midplane of the channel ($z = 0.5H$). The thermal gradient was significantly less in the base channel compared to the channel with the winglets. Compared to the DWVGs, the outlet temperature of the base channel is lesser. The surface of the DWVGs allows the fluid to be in contact with the hot surface for longer resulting in more heat transfer than the base channel.

Fig. 4.5 shows the velocity vectors at different cross sections along the flow direction. Two pairs of counterclockwise rotating vortices were observed near the cylinder and VG surfaces. These vortices create an upwash zone by forcing fluid between the winglet pair and the cylinder toward the top wall. The fluid near the side walls of the channel tries to move towards the bottom wall of the channel hence, creates a downwash zone. This vertical movement of the liquid is entirely due to the presence of DWVG in the channel, which ensures better mixing of the liquid. In a typical CFU arrangement, the DWVGs are spaced at regular intervals, so this up-and-down movement of fluid continues further downstream to the channel exit.

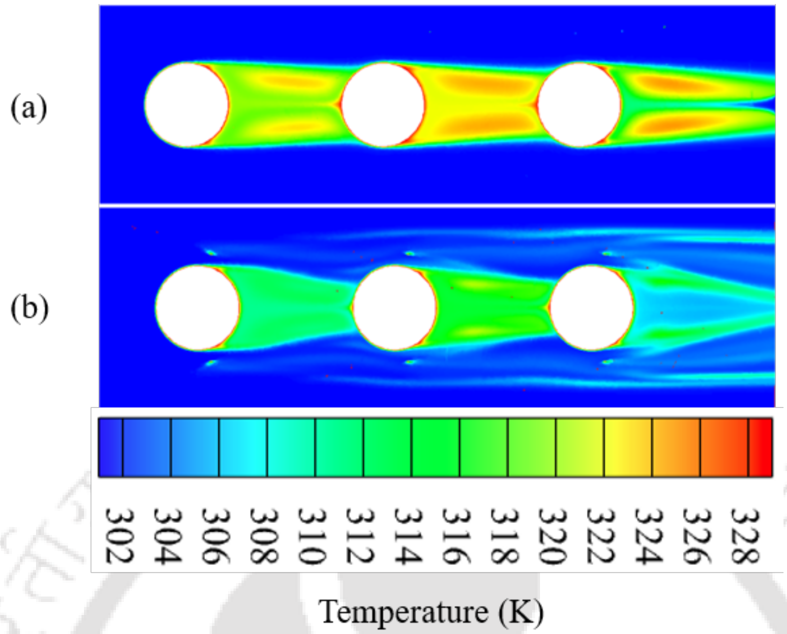

Figure 4.4: Temperature distribution of (a) Base channel, and (b) DWVG, $\beta = 160°$ at a midplane ($z = 0.5H$) and $Re = 200$ for the aqueous solution of CMC (2000 ppm)

The first pair of vortices generated by the arrangement of the winglet pairs moves further downwards and imparts their energy to the next pair of vortices downstream making it stronger.

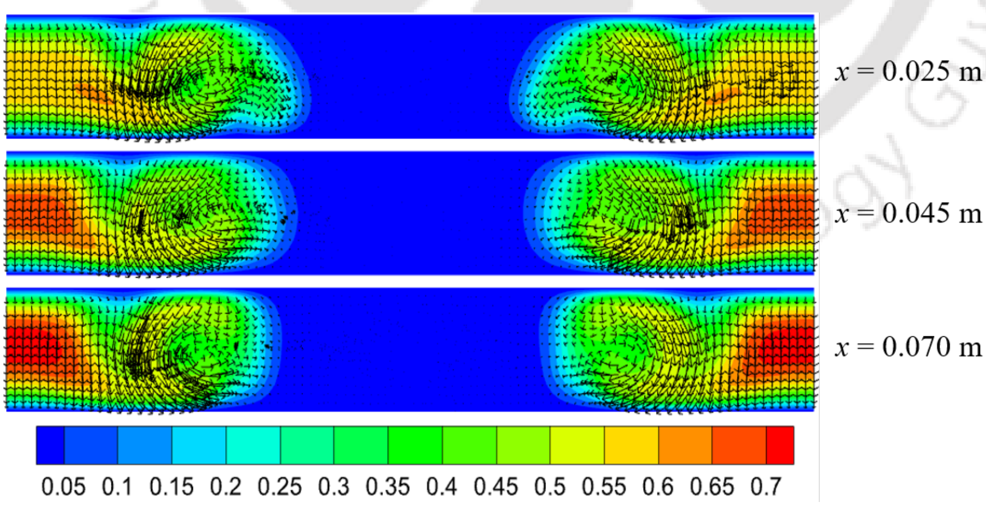

Figure 4.5: Velocity vector at various cross sections along the direction of flow for the rectangular channel with DWVG at an attack angle of 160° and $Re = 200$ for the aqueous solution of CMC (2000 ppm)

Fig. 4.6 represents the span-wise variation of Nu_{sa} and viscosity in relation to attack angles. The variations that occur in the local Nu_{sa} and viscosity within the channel are predominantly attributed to the existence of tubes and winglets. These elements can influence the flow dynamics and alter the heat transfer properties of the fluid. The existence of DWVGs and tubes inside the channel changes the fluid flow area and, as a result, locally changes the performance parameters [90]. Nu_{sa} is largest at the inlet and then decreases rapidly with the development of the thermal boundary layer. Before each cylinder, Nu_{sa} achieves its maximum value as the fluid quickly changes its direction and passes around it. The lowest Nu_{sa} value is achieved in the recirculation area behind each cylinder. The highest values are also achieved in areas where VGs are installed. Due to the presence of VG in various locations, the peak of Nu_{sa} caused by the longitudinal vortex also shifts. The Nu_{sa} of a channel with VG is larger than that of a simple fin due to the longitudinal vortex and reduced wake area. Fig. 4.6a clearly shows the Nu_{sa} values increasing with the decrease in attack angle. Based on Fig. 4.6b, it is clear that the presence of VGs and cylinder surfaces creates an increased flow resistance which in turn increases the velocity gradient at the axial location aligned with the leading edge of the VGs. This leads to a sharp decrease in viscosity at these specific locations. In the downstream space between the two cylinders at the rear portion of the VG, the viscosity increases. This drop in viscosity at the leading edge of the winglets and cylinder surfaces and rise in viscosity towards the following edge of the winglets persists till the channel exit due to the consistent arrangement of cylinders and DWVGs. The shear stress generated by the winglet and cylinder surfaces increases the velocity gradient and reduces the viscosity of the shear-thinning fluid, but away from the winglet and cylinder surfaces, the shear stress is not as strong, resulting in a drop in the velocity gradient, providing a rise in the viscosity of CMC solution.

Fig. 4.7 illustrates how the Nu_m, average f_{app}, and average Q_f of the channel with DWVGs and the base channel vary in relation to the Re. Fig. 4.7a depicts the increase in Nu_m with the rise in Re for a channel equipped with DWVGs and a base channel. As the Re increases, the resulting shear stress also increases. This, in turn, leads to a higher velocity gradient in the vicinity of the tubes and winglets. The behavior of shear-thinning fluid is greatly affected by the velocity gradient. Increasing the velocity gradient further reduces the viscosity of the shear-thinning fluids resulting in better intermixing and increasing the heat transfer in the form of Nu_m. It is clearly evident that the presence of VGs enhances the Nu_m compared

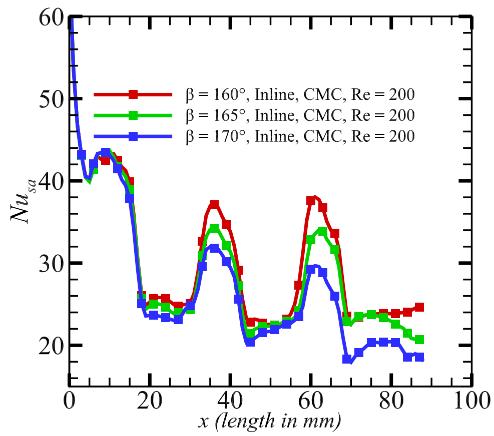

(a)

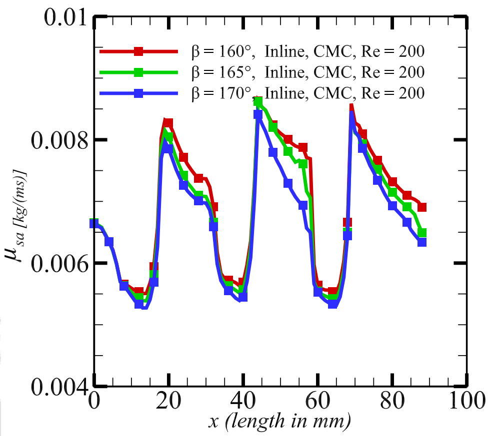

(b)

Figure 4.6: Span average variation of (a) Nu_{sa}, and (b) μ_{sa}, for the channel equipped with DWVGs with attack angles for CMC (2000 ppm) at $Re = 200$

to the channel without the winglets. The integration of vortex generators (VGs) in the vicinity of cylinders can significantly enhance heat transfer by curtailing the wake zones beneath the cylinders and promoting increased liquid-surface interaction with the heated surface of the wall and cylinders. This results in an augmented heat transfer coefficient, which is an important factor in applications where efficient cooling or heating is a critical requirement. Therefore, the use of VGs can be considered a promising strategy to improve the thermal performance of systems. The presence of DWVGs in the channel creates upward and downward movement of fluid and provides better intermixing assuring enhanced heat transfer rate. The existence of a VG in the flow regime increases shear stress, which has a remarkable impression on heat transmission and pressure drop in the channel. However, since the winglet drag is greater than the base duct drag, the existence of the VG also raises the pressure difference in the duct compared to the base channel represented by Fig. 4.7b. Fig. 4.7c represents the changes in average Q_f for a channel equipped with DWVGs and a channel without DWVGs. The compound effect of heat transfer and frictional loss of the channel is quantified by average Q_f. The average Q_f of the channel equipped with DWVGs increases by 36% compared to the base channel.

Fig. 4.7 also represents the variation of Nu_m for different attack angles of the winglets. The Nu_m and average f_{app} increase with a decrease in attack angle represented in Figs. 4.7a and 4.7b. The presence of winglets creates an obstacle

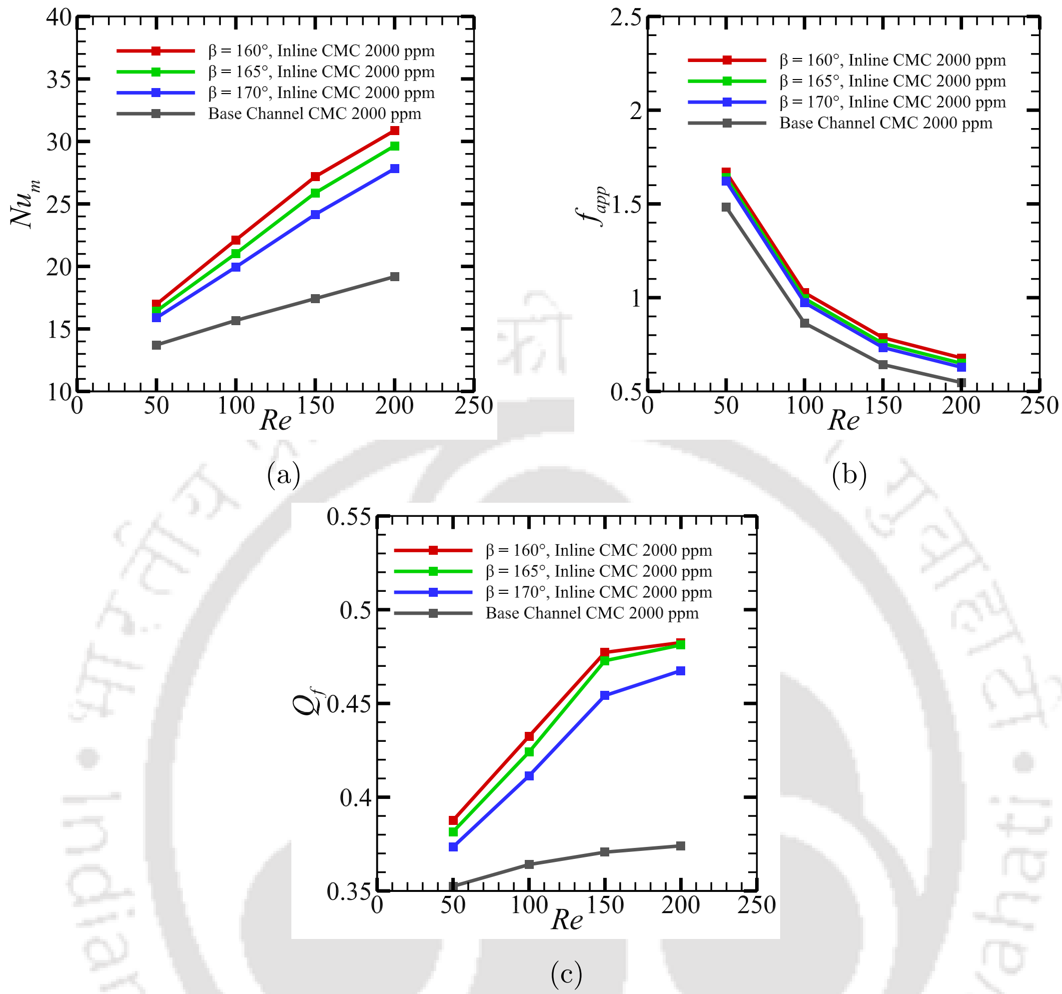

Figure 4.7: Variation of average (a) Nu_m, (b) f_{app}, and (c) Q_f with Re for different arrangements of DWPs and base channel for CMC (2000 ppm)

in the fluid flow, resulting in better intermixing and providing more heat transfer at the cost of considerable pressure penalty. Decreasing the attack angle provides more blockage of fluid flow inside the channel and increases the shear strain rate, reducing the viscosity near the winglets and cylinder surfaces, and providing better intermixing of fluid resulting in enhanced heat transfer. However, decreasing the attack angle simultaneously increases the pressure drop, which increases the average f_{app}. This increase in Nu_m and average f_{app} does not ultimately mean that the final comments lead to the selection of the best attack angle of the winglet. Therefore, it requires a new parameter that can consider the compound effect of heat transfer, and frictional loss is defined as Q_f. Based on the data presented in Fig. 4.7c, it is evident that a decrease in the attack angle results in a significant increase in the value of Q_f. Out of all the attack angles considered in the study, 160° performs best for heat transfer application.

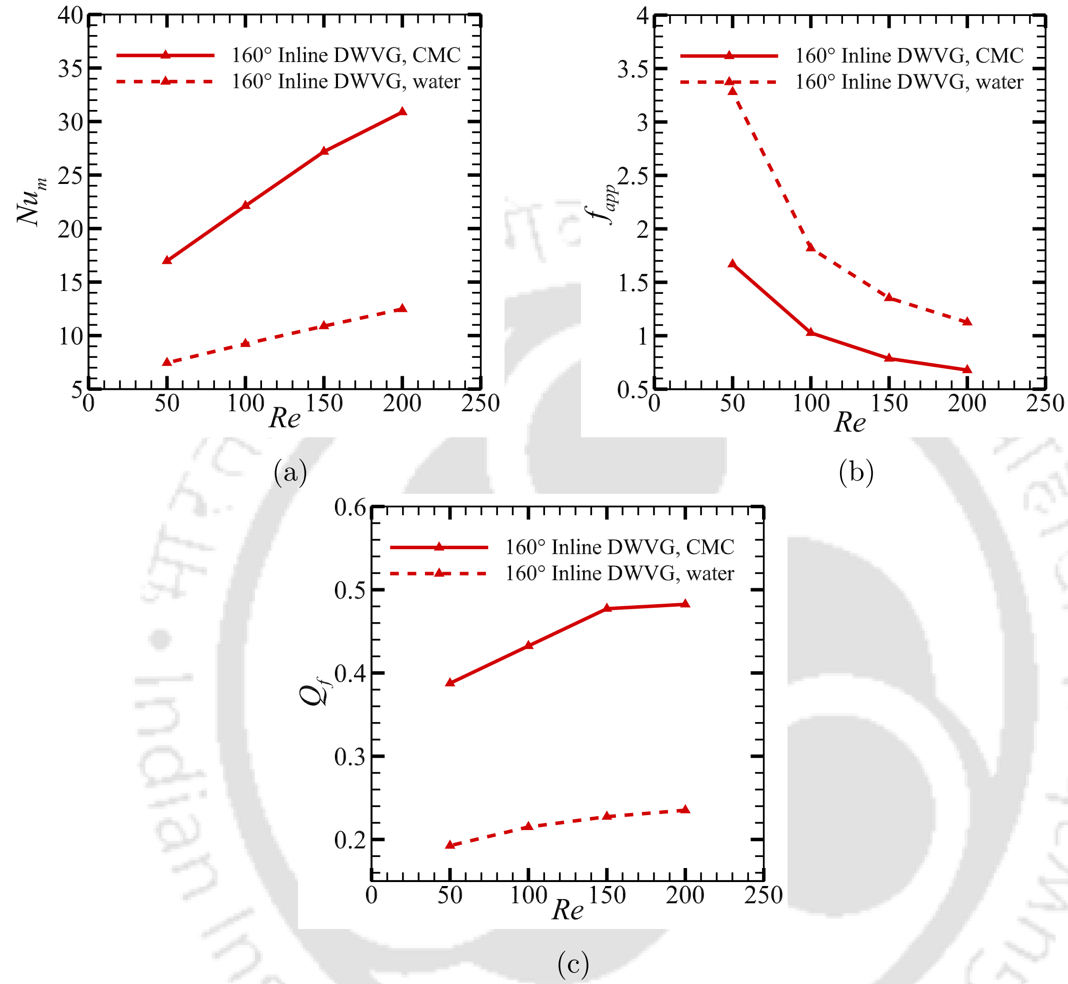

Figure 4.8: Average variation of (a) Nu_m, (b) f_{app}, and (c) Q_f for the channel equipped with DWVGs at an attack angle of 160° for CMC (2000 ppm) and water at various Re

Fig. 4.8 represents the variation of Nu_m, f_{app} and Q_f with respect to Re for CMC solutions and water. Fig. 4.8a depicts that the Nu_m for CMC is significantly higher than the water. The thermal conductivity of the aqueous solution of CMC is relatively larger than the water, which helps the CMC to better absorb heat from the heated surface. CMC improves the wetting properties of the surface and increases the liquid-surface contact for more efficient heat transfer. This leads to improved overall performance in heat transfer applications. Observed the alterations in average f_{app} for water and a CMC aqueous solution in Fig. 4.8b. The findings indicate that implementing a CMC aqueous solution as the working fluid leads to a reduction in the average frictional loss within the channel. This can be attributed to the drag-reducing characteristics of a CMC aqueous solution and provides a cushioning effect due to its molecular arrangement, reducing the frictional loss compared to water. The joint effect of heat transfer and frictional loss is represented by Fig. 4.8c. It was shown that the average Q_f employing an aqueous solution of CMC is considerably higher than the water.

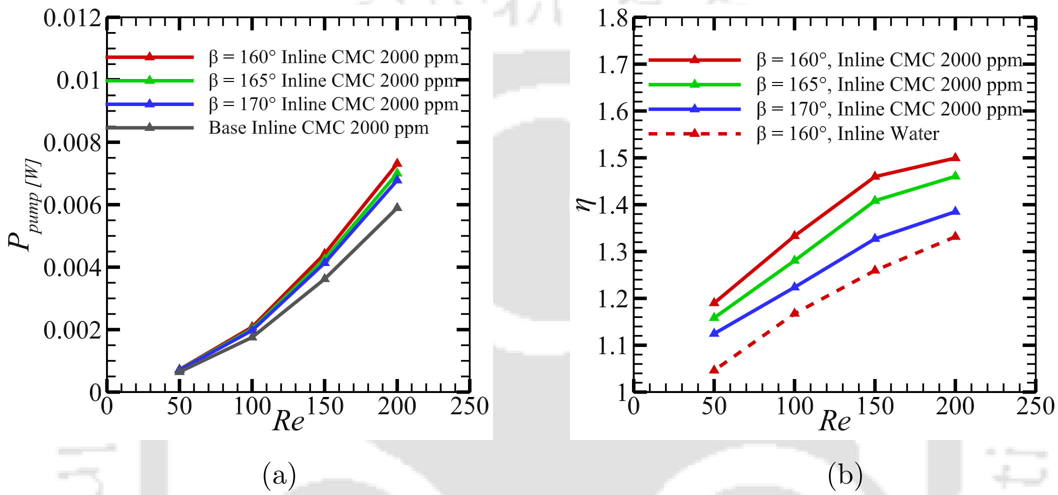

Figure 4.9: Variation of (a) P_{pump} of the FTHE with DWVGs and without DWVGs at various Re and (b) η using aqueous solution of CMC and water as a working fluid at various Re in a channel for CMC (2000 ppm) at Re = 200

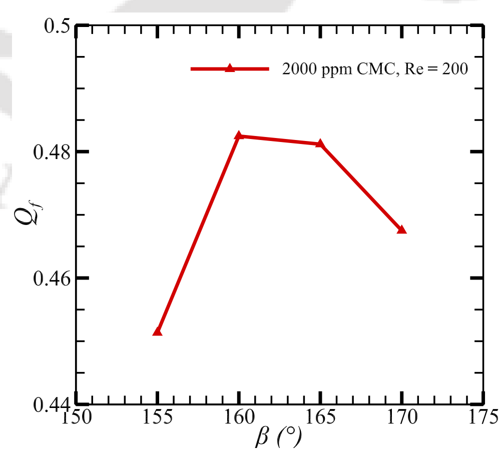

Figure 4.10: Variation of Q_f at various attack angle in a channel for CMC (2000 ppm) at Re = 200

Fig. 4.9a represents the variation of P_{pump} with respect to Re for the channel equipped with DWVGs using a CMC solution in water as a working fluid at various attack angles. This figure shows the increase in P_{pump} with increasing Re for all configurations examined. As Re increases, so does the mass flow rate, requiring more energy to keep the fluid flowing. Since winglets increase the pressure drop in the channel, more power is needed to move the fluid, hence P_{pump} is much larger for channels with winglets than for simple base channels. P_{pump} increases with decreasing angle of attack. The reduced angle of attack creates a significant pressure drop in the channel.

Fig. 4.9b represents the variation in the efficiency η of the channel with DWVG at different angles of attack employing an aqueous solution containing CMC and water. η is a measure of the efficiency of the system relative to the base duct taking into account the combined effects of heat transfer and pressure loss. Efficiency rises as the angle of attack decreases. The CMC aqueous solution shows higher efficiency compared to water in channels with DWVG at different Re.

Fig. 4.10 represents the variation in average Q_f for the channel equipped with DWVGs at various attack angles employing CMC solution as a working fluid. It was observed from Fig. 4.10 that the reduction in attack angle up to a specific limit, i.e., 160°, increases the overall performance, and a further reduction in attack angle decreases the overall performance. Therefore, the channel performs best at an attack angle of 160°, taking into account both heat transfer and frictional loss.

4.5 Summary

The purpose of this study was to examine how DWVG affects the performance of FTHE using a non-Newtonian fluid. In order to conduct the analysis, a set of numerical simulations were performed. A specific type of liquid was employed i.e. an aqueous solution of CMC with a concentration of 2000 ppm, which is known for its viscous nature. The tubes were arranged in a straight line and the height of DWVG was set at half the height of the channel. The inclusion of VGs affects the heat transfer and fluid flow performance of the FTHE. This is evaluated by comparing the Nu, f_{app}, and Q_f of the channel with and without the VGs. Incorporating VGs into the channel improves fluid mixing, destabilizes the thermal boundary layer, and increases heat transfer. Diminishing the inclination angle of the VG increases Nu_m, vorticity, f_{app}, and Q_f of the channel up to $\beta = 160°$, beyond $\beta = 160°$ it decreases.

Chapter 5

Analysis of the thermal and hydraulic parameters of a fin-tube heat exchanger using shear-thinning fluid and rectangular winglet

Fin-tube heat exchangers (FTHEs) are indispensable for heat transfer in various engineering applications, such as auto sectors, chilling devices, air coolers, biochemical industries, aerospace, electronic cooling chips, and control systems. Energy usage, efficiency optimization, and compactness improvement are crucial to reducing the continuously increasing power requirements of an FTHE to maintain its heat transmission capacity. One aspect of heat transfer exchange optimization is increasing heat transfer capacity with a relatively small increase in pumping power [127]. It is necessary to improve the heat transmission efficiency of FTHE as the thermal resistance acts as a great barrier as per the basic knowledge of heat transfer [2].

The contents in this chapter have been published as Kumar, D., and Dalal, A. (2023) "A numerical study of the thermal and hydraulic parameters of a fin-tube heat exchanger using shear-thinning fluid and rectangular winglet", *International Journal of Thermal Sciences*, vol. **195**, p.108653.

5.1 Introduction

Passive devices such as rough surfaces, dimples, or cavities are accustomed to improve heat transmission, often in micro-heat exchangers or other microscale energy converters [1]. VG is a very effective way to improve the heat transmission characteristics of FTHE. It may be placed on the surface of the fins to improve heat transmission and generate the resulting flow. The vast majority of current research on the VGs available now has focused on winglets, as they can be quickly connected to or punched out of fins. The thermal transmission and frictional loss behavior of fin tube heat exchangers have been discussed in various computational and experimental studies considering the types of winglets of VGs. The computational work done by Fiebig *et al.* [128] using rectangular and triangular wings and winglets in a channel, observed better thermal performance of winglets than wings. The presence of winglets enhances the local thermal performance by 100%, while global thermal performance is enhanced by 50%.

Tian *et al.* [60] examined the thermohydraulic features of a flat-plate channel utilizing different LVG configurations. The results demonstrated that the overall performance of the CFD configuration is superior to that of the CFU configuration for RWPs.

In addition to the surface modifications, the use of efficient coolants is considered a wise course of action to enhance the performance of the FTHE. In the meantime, research on heat transmission and flow behavior of non-Newtonian fluids has received much interest worldwide. Liquids are preferable to gases for heat removal applications due to their increased heat transfer coefficients [125, 129]. Non-Newtonian nanofluids have attracted a lot of attention because of their potential to speed up heat transfer rates in convective flows [130]. An aqueous solution of carboxymethyl cellulose (CMC)(2000 ppm) is considered a working fluid for the present study. Ebrahimi *et al.* [6] numerically observed the heat transmission and pressure drop characteristics of a laminar flow for a range of Re (25-200) in a rectangular conduit furnished with LVG. Compared to water, an aqueous solution of CMC shows an improved heat transfer performance by 39-188%, and compared to a plane channel, the addition of LVGs to rectangular channels improves the heat transfer performance by 24-135%. Furthermore, non-Newtonian fluids as active ingredients are adopted mostly in the laminar flow regime owing to their elevated viscosity and reduced velocity level [7].

A conclusion drawn from the aforementioned literature review is that winglet-type VGs have been thoroughly investigated to enhance the thermohydraulic characteristics of FTHE using Newtonian fluid.

As far as the author is aware, no research has been done on how non-Newtonian fluid flow behavior affects the heat transmission and frictional loss features of FTHE fitted with RWVGs. More investigation is necessary to comprehend the effects of non-Newtonian fluid flow behavior on the fluid flow and heat transfer characteristics of FTHEs fitted with winglet-type VGs.The results of this study might spark innovative approaches for enhancing heat augmentation in FTHE.

5.2 Problem definition

The main objective of the present study is to understand how the thermal-hydraulic performance of FTHE equipped with RWPs is affected by the shear–thinning behavior of an aqueous CMC solution. An FTHE comprises three lines of the integrated cylinder in an inline and staggered configuration, with and without the RWP, and is considered for numerical simulations at various Re ranging between 50 to 200. These RWPs are mounted to the bottom plate of the channel nearby tubes at regular intervals. The height of these RWPs is half the height of the channel placed in CFU arrangement in an inline tube configuration and a combination of CFU-CFD-CFU configuration in staggered tube arrangements of the channel. These RWPs have various degrees of inclination with the flow direction, including 160°, 165°, and 170°. A 2000 ppm concentration of the aqueous solution of CMC is considered a working fluid. The thermal transmission and frictional loss characteristics of the channel furnished with winglet VGs are emulated with those of the channel without the winglet VGs. Furthermore, the heat transmission and pressure loss characteristics of the channel using an aqueous solution of CMC and water are compared.

5.2.1 Computational model

A three-dimensional rectangular duct equipped with three rows of built-in cylinders with punched RWPs near the tubes is considered the computational domain shown in Fig. 5.1 and 5.2 for the inline and staggered tube configurations respectively [62]. All channel dimensions are represented in the form of the channel height H = 3.6 mm. The length (L) and width (B) of the channel are 24.7H and 7.06H respectively. The three rows of tubes of equal diameter (D) = 2.96H are located at a regular interval from the entry of the channel. The center distance of these tubes from the inlet is $L_1 = 3.53H$, $L_2 = 10.59H$, and $L_3 = 17.65H$, respectively.

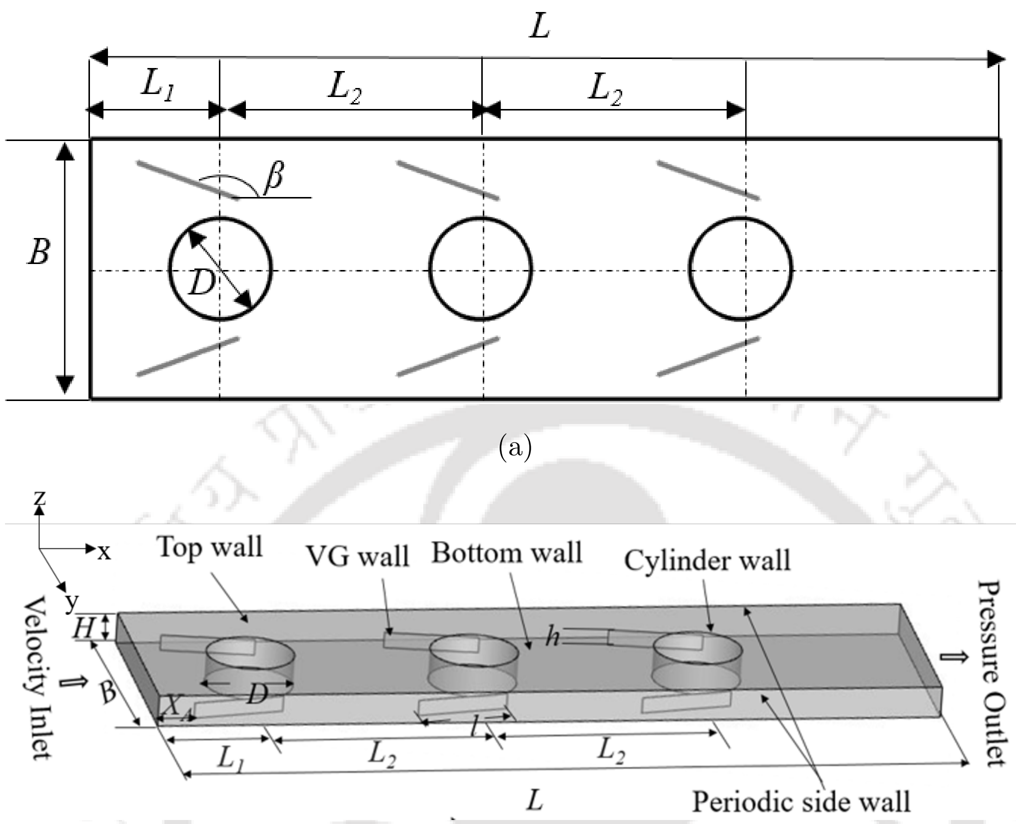

Figure 5.1: Computational domain with RWVGs with inline tube configurations (a) Schematic view and (b) Isometric view

The chord length (l), height (h), and thickness (t) of the RWPs are $2.93H$, $0.5H$, and $0.027H$ respectively. The foremost edge of the winglet is $X_A = 1.28H$ away from the entrance and $Y_A = 0.63H$ away from the side wall. The inclination angle (β) of the RWP surface towards the flow direction of the entering fluid is 160°, 165°, and 170°. The foremost edge of the second and third sets of winglet pairs is $7.06H$ distance away from the front edge of the first and second sets of winglets. The *Re* is defined in accordance with the hydraulic diameter ($2H$) of the channel [62]. The surfaces of the computational domain, the winglets, and the cylinders are kept at a fixed temperature of 330 K, while the fluid temperature at the inlet of the channel is kept at a fixed temperature of 300 K. The characteristics of the material were considered to be invariant in temperature due to the minimal temperature fluctuations along the channel (less than 30 K) [62].

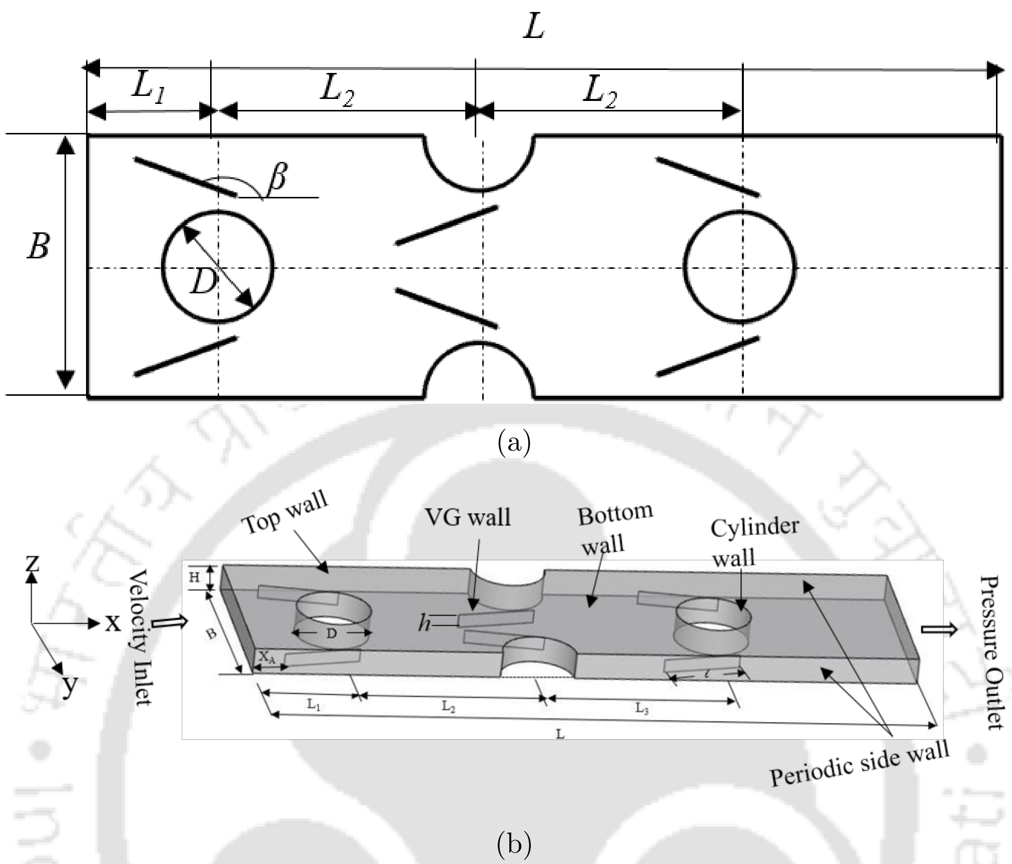

Figure 5.2: Computational domain with RWVGs with staggered tube configurations (a) Schematic view and (b) Isometric view

5.2.2 Boundary conditions

The present paper emphasizes the comparison of the thermohydraulic performance of a non-Newtonian shear–thinning aqueous solution of CMC with Newtonian fluid (water). A mathematical model was created considering that the generated vortices are quasi-steady [6].

At the inlet of the channel, a fully developed velocity profile is maintained in the flow path, while the outlet of the channel is maintained under pressure-outlet boundary conditions. The top and bottom walls of the channel, the wall of the cylinders, and the VG walls are maintained under isothermal and no-slip boundary conditions. Side walls are maintained at periodic boundary conditions. The boundary conditions for various part of the channel is mathematically represented in Table 5.1.

Where, n represents the direction normal to the boundary. (x_1, y_1, z_1) and (x_2, y_2, z_2) are corresponding points on the opposite boundaries.

Table 5.1: Boundary conditions are used in different parts of the channel

Boundary name	Boundary conditions
Entry	$u = u(z)$, $v = w = 0$, $T_{in} = 300$ K, $\frac{\partial p}{\partial n} = 0$
Exit	$p = 0$, $\frac{\partial T}{\partial x} = \frac{\partial u}{\partial x} = \frac{\partial v}{\partial y} = \frac{\partial w}{\partial z} = 0$
top, bottom, DWPs, and cylinder walls	$u = v = w = 0$, $T_w = 330$ K, $\frac{\partial p}{\partial n} = 0$
Side walls	$u(x_1, y_1, z_1) = u(x_2, y_2, z_2)$
	and $p(x_1, y_1, z_1) = p(x_2, y_2, z_2)$

5.3 Mesh generation and grid independency test

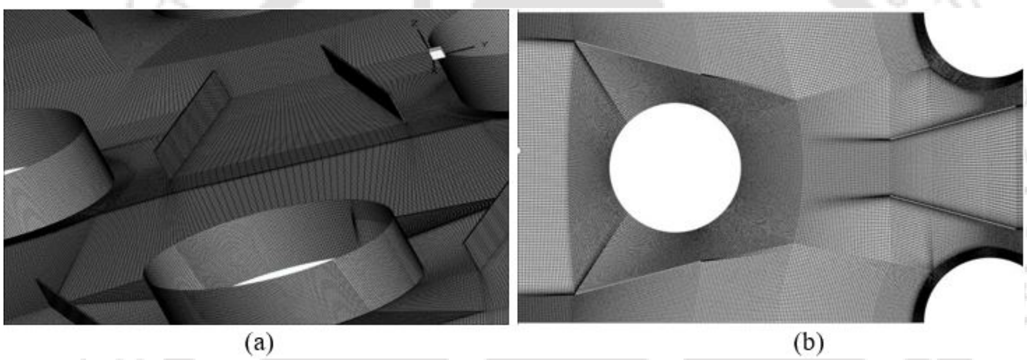

Figure 5.3: Enlarged view of the computational grid (a) isometric view of nearby tube and winglets (b) bottom plate

The structured, non-uniform multiblock hexahedral cell aligned with the flow shown in Fig. 5.3 discretizes the flow domain. Since the gradient will be greater in these zones, the cells are clustered close to the VG and tube surfaces. In order to test how sensitive the findings were to the size of the cells and to establish the bare minimum number of cells needed to get accurate results, four meshes with varying cell counts were created. The results of Nu_m and f_{app} for different grid sizes were compared with the largest grid (6305285) and are presented in Table 5.2. As can be seen in Table 5.2, the least variation in Nu_m and f_{app} for the mesh with 5892642 mesh components. Therefore, the mesh with 5892642 mesh components produces respectable results and requires an appropriate amount of processing time, which has been selected for further analysis. The computations were carried out on an HP machine using 8 CPU cores with 3 GB memory in each core. Each of these cases took roughly 25 to 30 hours to calculate.

Table 5.2: Grid sensitivity test outcomes for the flow of water in the rectangular channel equipped with cylinders and RWVGs at $Re = 200$

Number of elements	Nu_m	% Diff.	f_{app}	% Diff.
2191176	14.85	-	0.4699	-
4798176	15.35	0.36	0.5481	16.64
5892642	15.39	0.26	0.5478	-0.036
6305285	15.41	0.13	0.5479	-0.018

5.4 Results and discussion

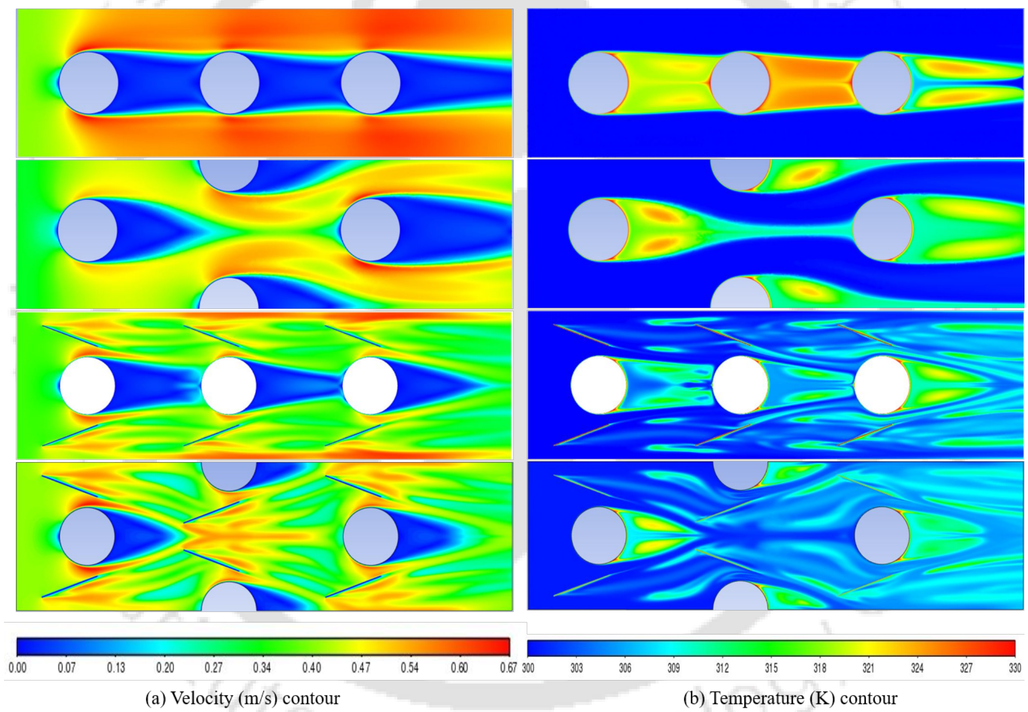

Figure 5.4: Comparison of (a) velocity ($\mathrm{m\,s^{-1}}$) distribution and (b) temperature (K) distribution at a midplane z = $0.5H$ and $Re = 200$ for (i) base in-line, (ii) base staggered, (iii) in-line tube row with RWP, (iv) staggered row with RWP (angle of attack = 160°) for the aqueous solution of CMC (2000 ppm)

The local and overall variation in performance parameters due to winglet placement and tube arrangements have been evaluated and compared with the channel in the absence of winglets. Fig. 5.4 displays the velocity and temperature contours at the midplane of the channel ($z = 0.5H$) for inline and staggered configurations

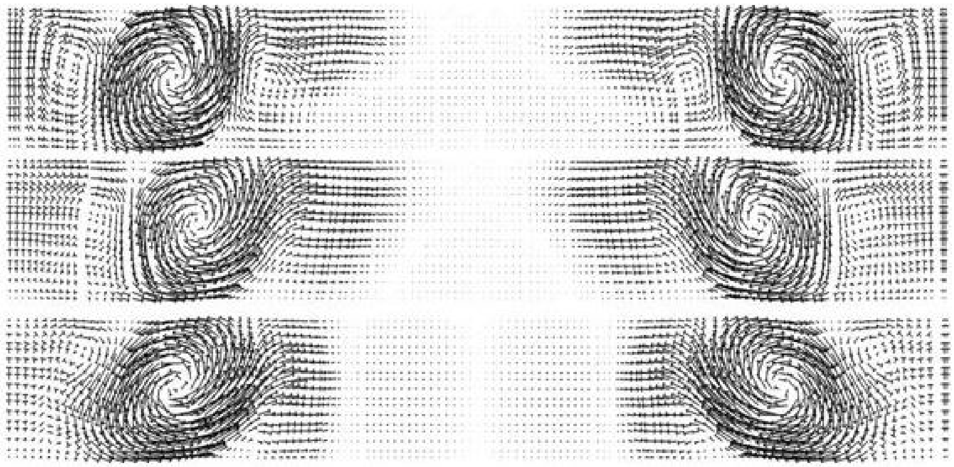

Figure 5.5: Velocity vectors at a cross-section at (i) x = 0.025 m, (ii) x = 0.045 m, and (iii) x = 0.07 m at Re = 200 for inline tubes of winglet attack angle 160°for the aqueous solution of CMC (2000 ppm)

of the tubes in the presence and absence of the RWPs respectively. Fig. 5.4a depicts the extensive recirculation that takes place behind the tubes, leading to a significant reduction in heat transmission. A passageway resembling a nozzle is formed between the tube and the vortex generator when the CFU configurations of VG are placed near the tubes. The addition of the rectangular winglet no longer most effectively generates a longitudinal vortex; however, additionally creates a nozzle-like acceleration region that reduced the wake zone in the rear of the tube compared to the base channel. It can be observed from Fig. 5.4b that the thermal gradient in the area behind the tube is greater when a VG is present compared to the base channel. The exit fluid temperature is higher in the channel with winglets compared to the base channel, leading to an improved heat transfer efficiency.

Figs. 5.5 and 5.6 represent the velocity vector for inline and staggered placement of the tubes at various cross sections along the axial direction. It is evident from Fig. 5.5 that the presence of RWPs generates strong vortices, but these vortices do not interact with each other in inline arrangements of tubes with winglets, while Fig. 5.6 depicts that the generated vortices interact with each other resulting in better intermixing of fluid in the staggered arrangement of the tubes with winglets. Hence a better intermixing of fluid was seen in staggered cases with the highest temperature of the fluid at the exit of the channel. These local variations of Nu_{sa}, f_{app}, and Q_f in the channel are mainly attributed to the presence of tubes and winglets. The availability of winglets and cylinders within the rectangular channel

(i)
(ii)
(iii)
(iv)
(v)
(vi)

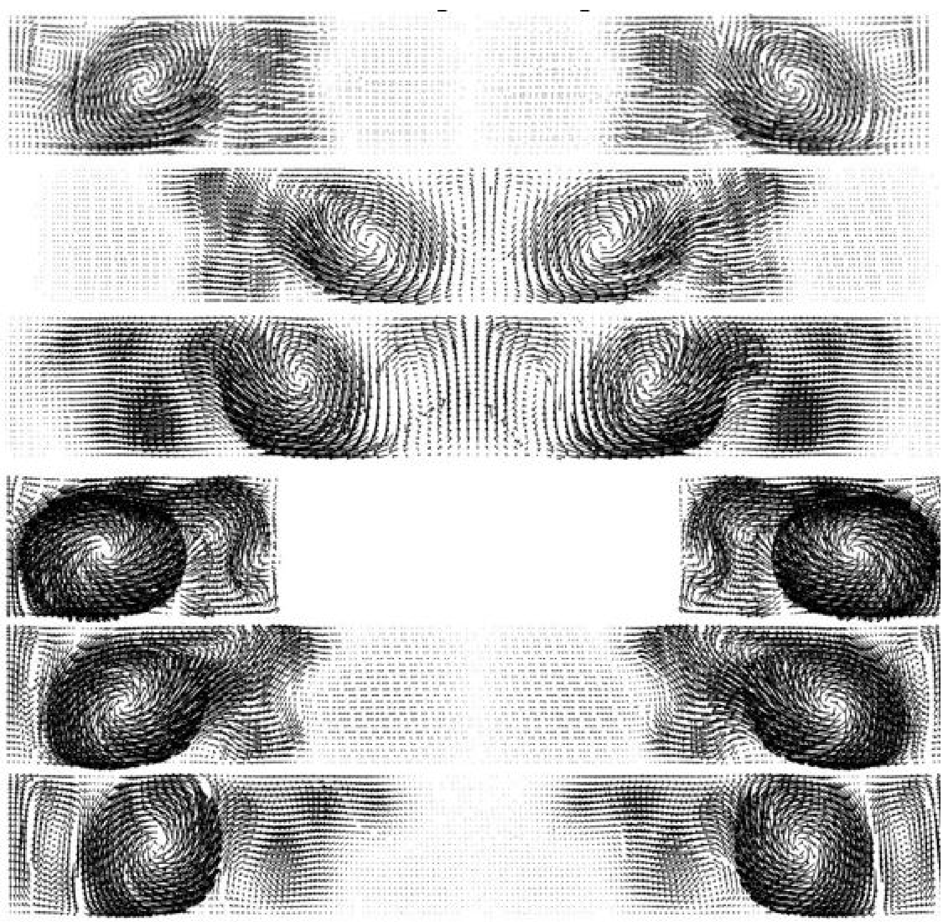

Figure 5.6: Velocity vectors at a cross-section at (i) x = 0.025 m, (ii) x = 0.045 m, (iii) x = 0.051 m, (iv) x = 0.065, (v) x = 0.07 m and (vi) x = 0.077 at Re = 200 for staggered tubes of winglet attack angle 160°for the aqueous solution of CMC (2000 ppm)

provides a variable area of flow for the fluid which in turn generates a local alteration in performance parameters such as Nu, f_{app}, and Q_f.

Figs. 5.7 and 5.8 demonstrate the effect of the angle of attack on a span-wise variation of Nu_{sa}, f_{app}, and Q_f of inline and staggered configurations of the tubes along with the base channel (without VG). It was observed that the value of Nu_{sa}, for the inline and staggered cases is significantly higher than the base channel. The occurrence of VGs in the flow domain generates more shear stress, and shear stress greatly influences the transmission of heat and fluid flow behavior. However, at the same time, the presence of VGs also increases the pressure drop in the channel due to the drag generated by the winglets exceeding that of the base channel. Employing VGs in the channel enhances the heat transfer but at the same time

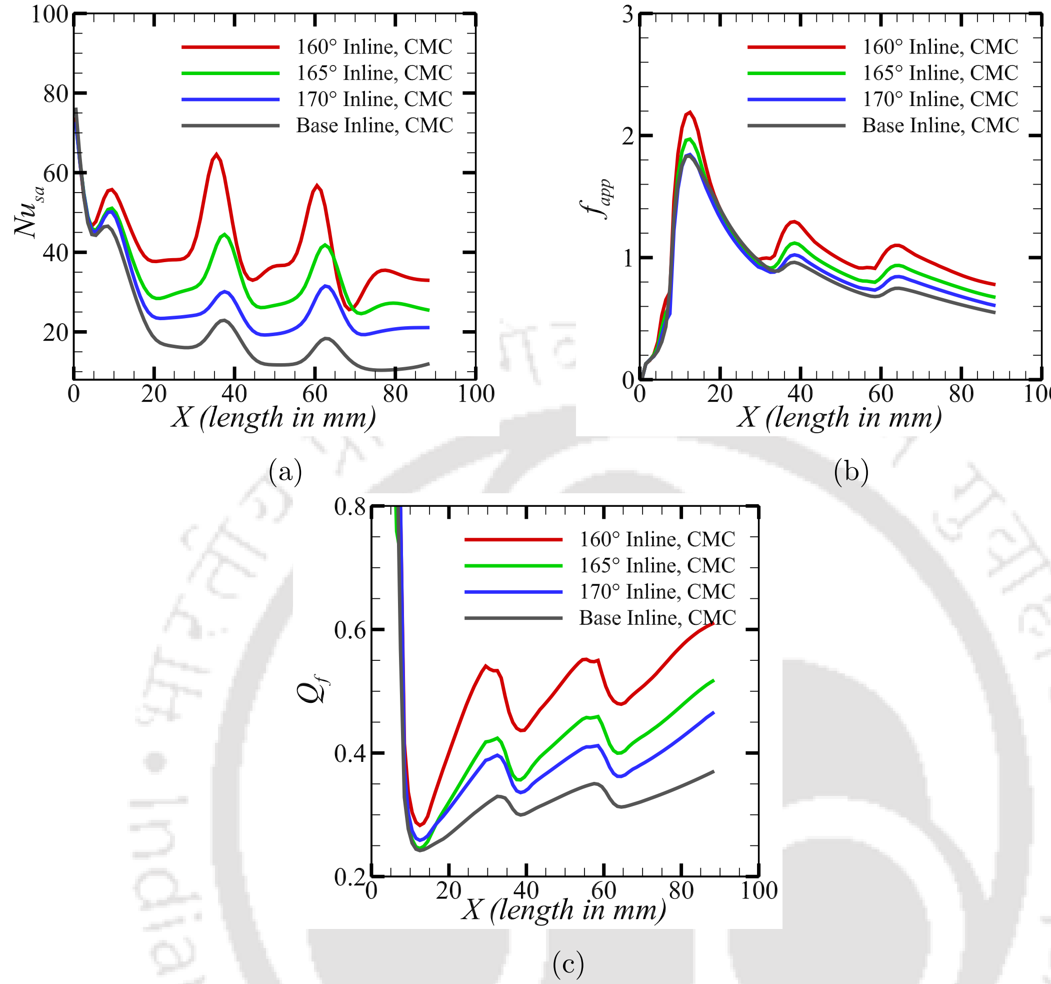

Figure 5.7: Span average variation of combined (a) Nu, (b) f_{app}, and (c) Q_f for different configurations of RWPs and without RWPs in a channel for CMC (2000 ppm) at $Re = 200$ for inline configuration of the tubes.

enhances the pressure drop too, compared to the base channel. It requires an overall performance comparison of the channel including the effect of heat transfer and pressure loss. The combined effect of heat transmission and frictional loss of the channel including the vortex generator is defined by the quality factor (Q_f) as the ratio of mean Colburn factor (j) and friction factor (f). This Q_f shows that, whether the effect of heat transfer is a dominant factor or pressure penalty, compared to the other configurations. The Q_f for the channel including VGs is significantly higher compared to the base channel. The value of Nu_{sa}increases with a reduction in the attack angle. Heat transmission is boosted to a greater extent at the smaller attack angle. Variable cross-sectional areas are present along the

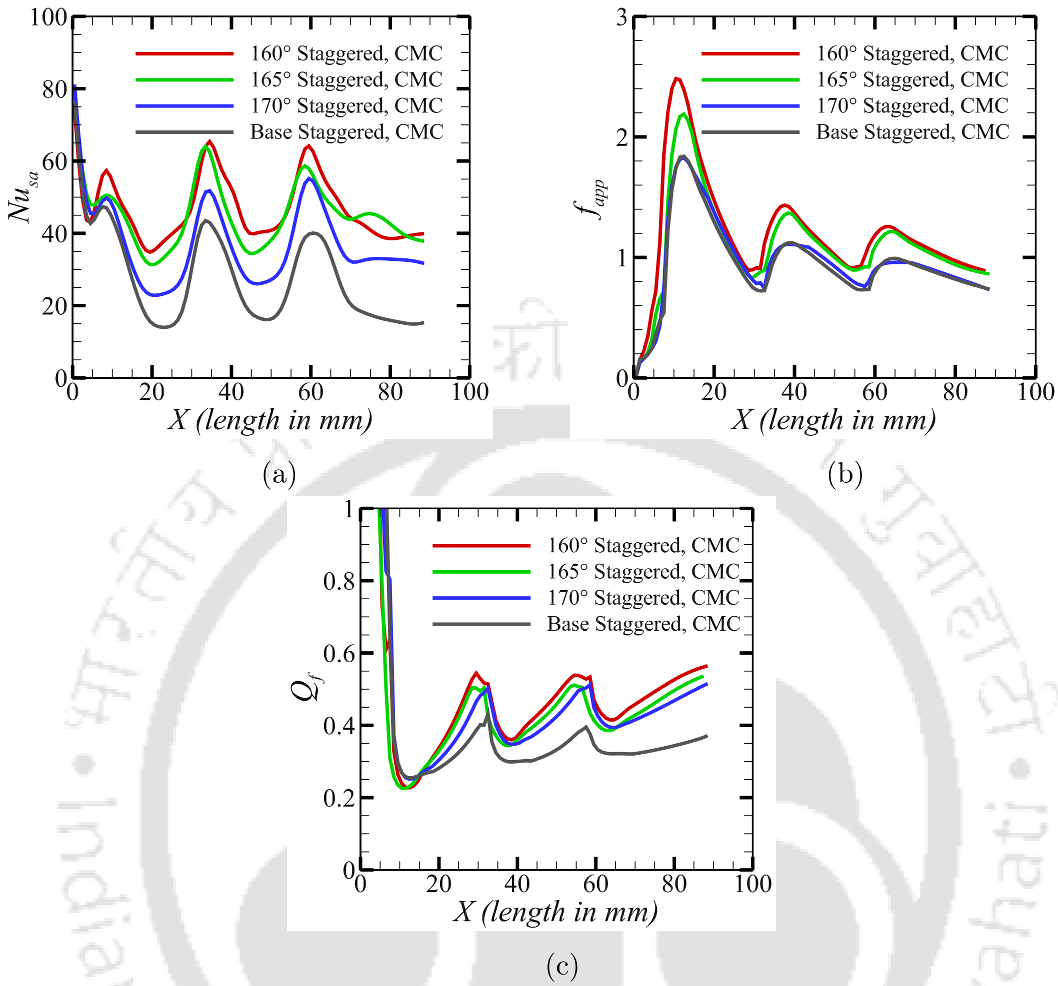

Figure 5.8: Span average variation of combined (a) Nu, (b) f_{app}, and (c) Q_f for different configurations of RWPs and without RWPs in a channel for CMC (2000 ppm) at $Re = 200$ for staggered configuration of the tubes.

flow channel encompassing the winglet, contingent upon the angle of attack; as a result, heat transmission improves when the angle of attack decreases [131]. Figs. 5.7b and 5.8b represent the span-average f_{app} for inlet and staggered configurations, respectively. It is evident from the figures that the span-average f_{app} for inline and staggered configurations increases with a decrease in attack angle. The values escalate as the angles of attack diminish. The rectangular winglet prompts the detachment of the flow and the form drag of the rectangular winglet results in an upsurge in drag [132]. Figs. 5.7c and 5.8c represent the Q_f for inline and staggered configurations. It can be seen from both the figures, the Q_f increases as the attack angle decreases. Therefore, the channel with winglets at 160° performs

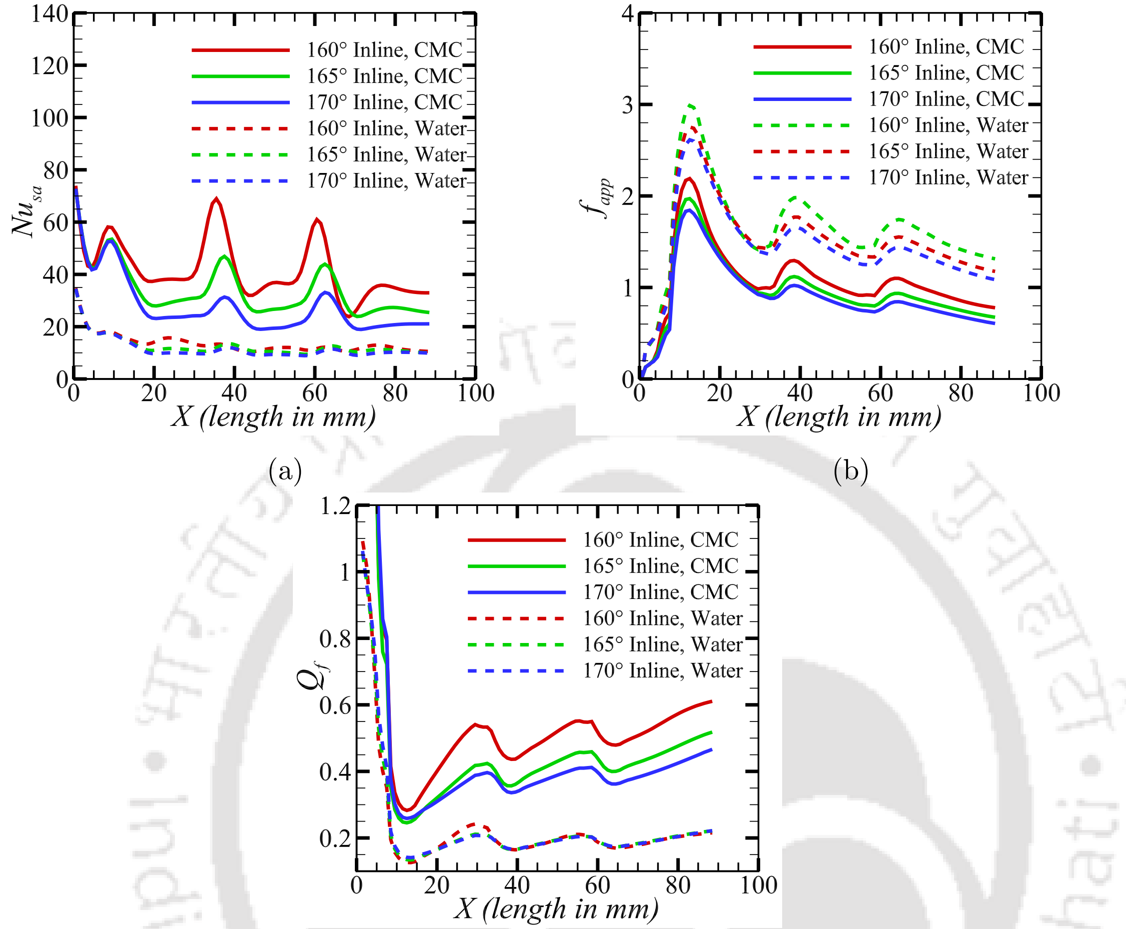

(a) (b)

(c)

Figure 5.9: Impact of various RWPs orientation on the span average variation of (a) *Nu*, (b) f_{app}, and (c) Q_f in a channel for CMC (2000 ppm) and water at *Re* = 200 for inline configuration of the tubes.

better compared to other attack angles of VGs.

Figs. 5.9 and 5.10 represent the span-wise variation of Nu_{sa}, f_{app}, and Q_f of the inline and staggered configurations of the tubes for an aqueous solution of CMC (2000 ppm w/v) and water at different attack angles. Figs. 5.9a and 5.10a both indicate a higher value of Nu_{sa} and Q_f for the CMC solution than for water for all attack angles. The thermal conductivity of water is less than that of the CMC [7], therefore, the CMC can transfer more heat from the heated wall. The Prandtl number of the CMC is higher than that of water as the former fluid is more viscous. Therefore, Momentum diffusivity rather than thermal diffusivity dominates the flow behavior in the case of CMC. Convection, related to conduction,

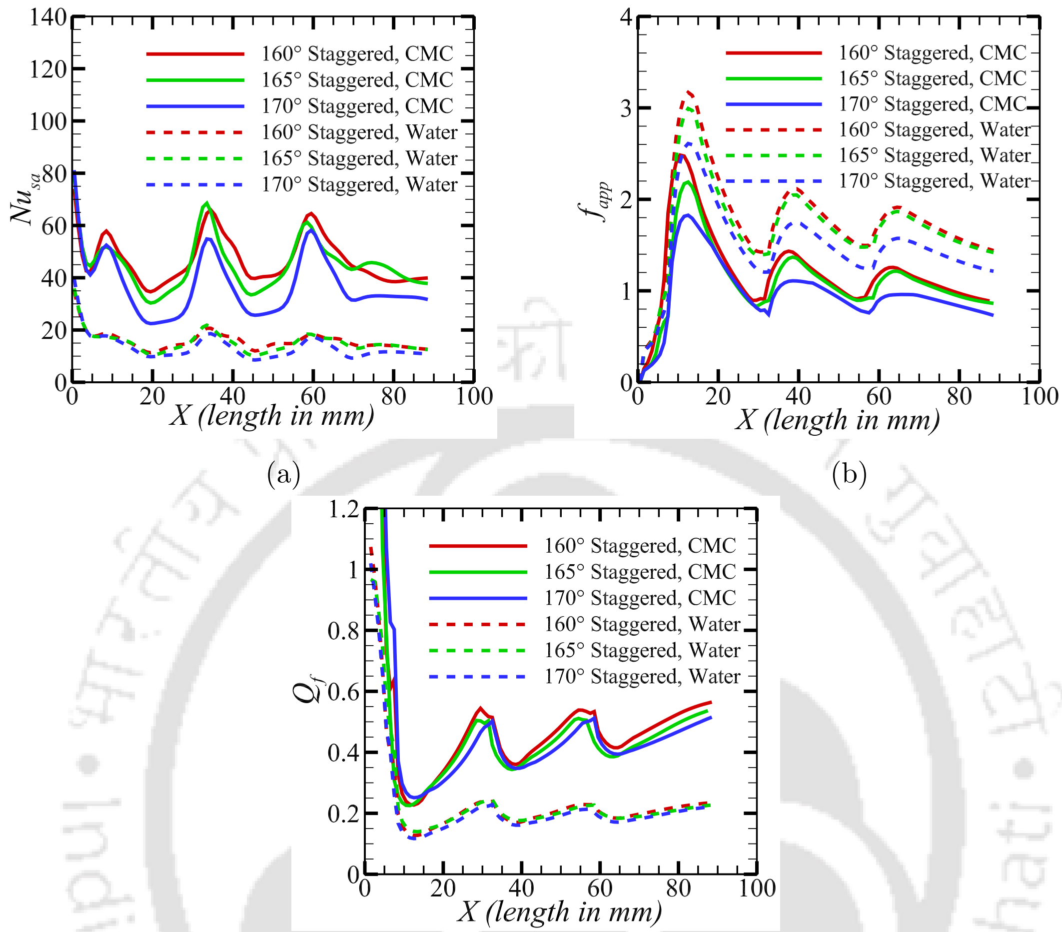

(a) (b) (c)

Figure 5.10: Impact of various RWPs orientation on the span average variation of (a) Nu, (b) f_{app}, and (c) Q_f in a channel for CMC (2000 ppm) and water at Re = 200 for staggered configuration of the tubes.

dominates the energy delivery in the channel with higher CMC concentrations (2000 ppm) [6]. It was observed from Figs. 5.9b and 5.10b, in both the inline and staggered cases, the f_{app} values for water are comparatively superior to the CMC (2000 ppm). The arrangement of CMC molecules in an aqueous solution is micelles shaped like cylinders or rods. These micelles have larger lengths and flexibility, and their creation is connected to the emergence of viscoelasticity and drag-lessening features in the solution. As the CMC concentration increases, the spherical micelles transform into rod-shaped micelles, leading to an increase in the number and flexibility of rod-shaped micelles, which in turn improves the elasticity of the fluid and reduces losses due to friction [133–137]. Figs. 5.9c and 5.10c show a better overall performance (Q_f) by combining both heat transfer and friction loss using the aqueous CMC solution as a working medium compared to water.

Fig. 5.11 displays the variation in the average Nusselt number (Nu_m), the average friction factor (f_{app}), and the average Quality factor (Q_f) with respect to Re for the inline and staggered configuration of tubes at different attack angles. Fig. 5.11a shows that Nu_m increases with an increase in Re. As Re increases, the velocity of the fluid increases, resulting in a reduction in boundary layer thickness. This, in turn, enhances the contact area of the fluid-solid interface. The reduction in the thickness of the thermal and hydraulic boundary layers is responsible for an increase in the heat transfer rate. The thickness of the hydraulic and thermal boundary layers decreases as the Reynolds number increases, boosting the heat transfer rate and Nu. The velocity gradients have a more significant impact on the viscosity of the shear-thinning fluid. CMC yields a higher velocity at a constant Re compared to water. The higher velocity CMC produces a high strain rate and helps to properly mix the fluid [6].

Fig. 5.11b shows that the average f_{app} reduces with increasing Re for both the inline and staggered configurations of the tubes. Fluid velocity increases, with increasing Re. At higher velocities, an aqueous solution of CMC acts as an effective medium for reducing frictional losses. At an increased Reynolds number, the dissolvability of the CMC solution rises as a consequence of the elongation of the polymer chain, which in turn leads to a decreased friction coefficient. As can be seen from Figs. 5.11a and 5.11b the Nu_m increases with an increase in Re and at the same time the f_{app} decreases with an increase in Re for the aqueous solution of CMC, favors the increase in overall performance Q_f with an increase in Re represented by Fig. 5.11c. The Nu_m and average friction factor (f_{app}) values of the present study were compared with the Nu_m and average friction factor (f_{app}) values of a rectangular channel inbuilt with rectangular winglets in the absence of cylinders[6] and it was found that the Nu_m and average friction factor (f_{app}) values of present setup were increased by 25% and 15% respectively compared to the average Nu_m and average friction factor (f_{app}) values given by [6]. It was also observed from Fig. 5.11, that the staggered arrangement is superior to inline arrangements in terms of Nu_m, average f_{app}, and average Q_f.

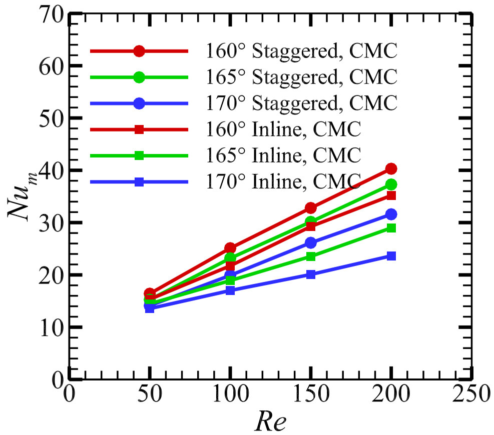

(a)

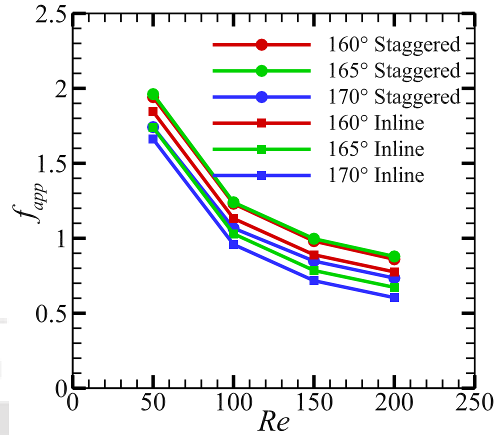

(b)

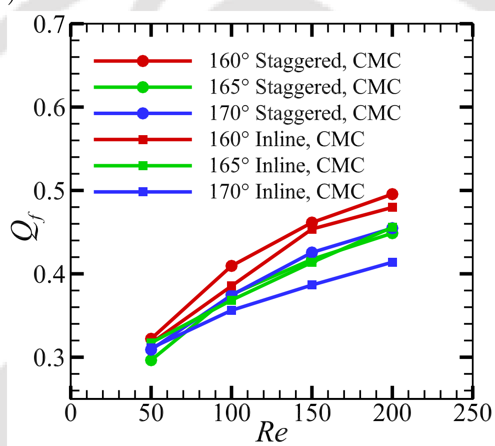

(c)

Figure 5.11: Variations of (a) Nu_m, (b) average f_{app} and (c) average Q_f for different configurations of tubes and RWPs for CMC (2000 ppm) with Re.

The CFU-CFD-CFU combination of VG placement favors the formation of strong vortices in the staggered arrangements of the tubes. These strong vortices make the flow unstable and help the fluid in a better intermixing on the cost of an enhancement in the pressure loss compared to the inline arrangement of the tube. In the staggered configuration of the tubes, the first pair of rectangular winglets in the CFU configuration directs the fluid into the following CFD configuration of VG, and that CFD configuration pushes that fluid further toward the third pair of CFU configurations of VG. This CFU-CFD-CFU combination of VGs allows the vortices to travel in a flow direction, and these vortices impart their energy to the flowing fluid, producing strong longitudinal vortices further in the axial direction and a better intermixing of fluid takes place. The combination of RWPs with CFU-CFD-CFU in staggered tubes creates upward and downward fluid flow zones, intensifying fluid mixing and improving heat transmission. Similarly, this combination of VG placement in CFU-CFD-CFU arrangement is supposed to create more obstacles in the flow route, causing an alteration in the flow pattern and resulting in larger form drag causing the friction factor augmentation. However, the value of f_{app} for the staggered configuration is greater than the inline configuration, but at the same time, the Nu_m value for the staggered configuration is also higher than the inline configuration. Therefore, enhancement in Nu dominates over the f_{app} in a staggered configuration, resulting in better overall performance (Q_f) compared to the inline configurations.

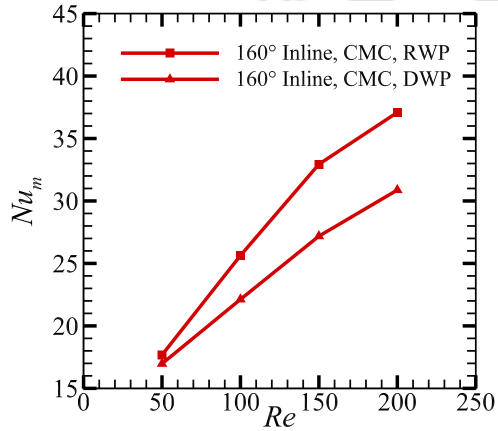

(a)

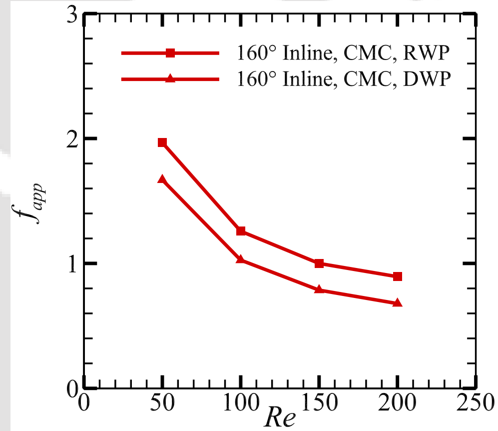

(b)

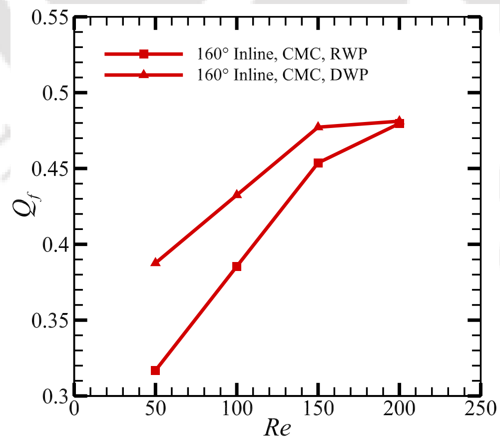

(c)

Figure 5.12: Average variation of (a) Nu_m, (b) f_{app}, and (c) Q_f for the channel equipped with DWVGs and RWVGs at an attack angle of 160° for CMC (2000 ppm) at various Re

Fig. 5.12 represents the comparison of Nu_m, f_{app}, and Q_f for RWVG and DWVG at various Re and an attack angle of 160°. It was observed from Fig. 5.12a, that at the lower Re, particularly at $Re = 50$, the Nu_m values for DWVGs and RWVGs are similar. While increasing the Re the difference in Nu_m between DWVGS and RWVGs also increases. The channel equipped with RWVGs outperforms the DWVGs when considering only the heat transfer. This is because the uniform and large surface area of RWVGs allows large volumes of liquid to come into contact with the heated surface helping the fluid absorb more amount of heat, increasing the heat transfer. As Re increases, RWVG provides a larger velocity gradient compared to DWVG, resulting in better fluid mixing near the wake zone and enhanced heat transfer. However, RWVG has a larger surface area and therefore produces a higher pressure drop than DWVG represented by Fig. 5.12b. In Fig. 5.12c, it can be observed that the channel containing DWVGs exhibits superior performance in both heat transfer and pressure drop when compared to the channel containing RWVGs. It was observed that the Nu_m, average f_{app} and Q_f increases with a decrease in the

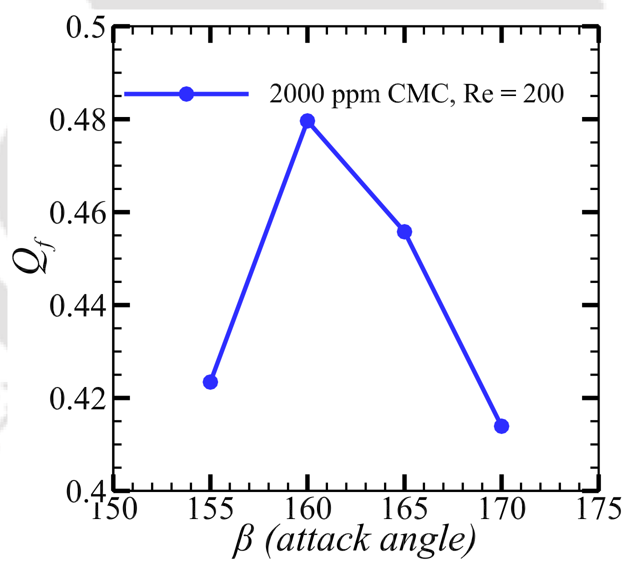

Figure 5.13: Variation in Q_f with attack angles for an inline configuration of tubes

attack angle of the winglet, but this decrease in attack angle up to what extent to obtain the best performance factor, that is Q_f. The thermohydraulic performance of the channel was calculated for one more case with an attack angle of 155° and compared with the Q_f of other attack angles. It was observed that the combined effect of heat transmission and frictional loss of the channel including the vortex generator is defined by the quality factor (Q_f) increases with a decrease in the attack angle, up to a certain extent but beyond that, it decreases. Fig. 5.13 depicts the optimum attack angle at which the channel gives the best overall performance, which is 160°.

5.5 Summary

The primary objective of this study was to inspect the effect of tube arrangement and VG placement on the thermal-hydraulic performance of the FTHE using shear-thinning non-Newtonian fluid as a working medium. Numerical simulations were carried out in a channel with the inline and staggered configuration of tubes with RWVGs half of the channel height using an aqueous solution of CMC (2000 ppm) as a non-Newtonian fluid. The thermal and hydraulic performance of the FTHE is affected by the inclusion of VG and is assessed by comparing the Nu, f_{app}, and Q_f of the channel with and without the VGs. Including VG in the channel produces strong longitudinal vortices, destabilizes the thermal boundary layer, and enhances the proper mixing of fluids, resulting in better heat transfer. The presence of VGs produces upwash and downwash regions along the flow inside the channel, causing a local variation of the thermohydraulic parameters. All VG cases produce a high f_{app} compared to the base channel. The staggered arrangements of the tube produce better Nu_m and a higher f_{app} compared to the inline arrangement due to the positioning of the VGs in the CFU-CFD-CFU configurations. Employing CMC as a working fluid improves Nu_m, decreases f_{app}, and therefore enhances Q_f of the channel. The Nu_m value increases with an increase in the *Re*, while f_{app} decreases with an increase in the *Re*. The Nu_m, average Q_f, and average f_{app} value of the channel with a staggered arrangement of the tubes equipped with VGs at 160° is increased by 89%, 19%, and 59% respectively compared to the base channel. The Nu_m and average Q_f value of the channel with a staggered arrangement of the tubes equipped with VGs at 160° and CMC (2000 ppm) as a working fluid is increased by 186%, and 133% respectively while the average f_{app} decreases by 65% compared to the water. Decreasing the attack angle of the VG improves Nu_m, vorticity, f_{app}, and Q_f of the channel up to 160°, beyond 160° it decreases. VG with a staggered arrangement of the tube with 160° attack angle performs best compared to other configurations.

Using CMC water solution as a coolant in rectangular channels is a wise course of action to improve heat transfer performance, but these coolants are suited for situations where pumping power is not a snag because the increased heat transfer is accompanied by a considerable pressure loss. It is not advisable to use the aqueous solution of CMC in the external flow because it is highly viscous and highly sensitive to the shear force. It can only be applied to the internal flow.

Chapter 6

Effect of shear-thinning fluid and curved vortex generators on the performance of fin-tube heat exchanger

Energy usage, efficiency optimization, and compactness improvement are crucial to reducing the continuously increasing power requirements of an FTHE to maintain its heat transmission capacity. To meet these above-mentioned requirements, continuous and timely modification is essential in the field of heat exchangers. Occasionally, it involves altering the geometry; other times, it involves utilizing different passive devices; and still other times, it involves using effective coolant to enhance the performance of the heat exchanger. A vortex generator (VG) is a passive technique to enhance heat transmission using various shapes of wings and winglets. Recently, as the research interest in curved VG has increased, many attempts have been made to develop new types of VG.

6.1 Introduction

In their numerical study, Gong *et al.*[75] used a curved rectangular winglet vortex generator (CRWVG) in an FTHE heat exchanger and reported an enhanced heat transfer performance while reducing the wake zone behind the tubes. Shi *et al.* [73] have numerically discussed the impact of the position of curved winglet VGs on the thermal-hydraulic performance of a FTHE. It has been observed that the frictional loss of the curved VGs is comparatively lesser than that of the equivalent plane VG. Lu and Zhai [111] discussed the impact of CRWVG on the thermo-fluid behavior of FTHE. At varied attack angles, the effectiveness of VGs with diverse curvatures is assessed. Additionally, the impacts of variables like location, extent, and attack angle are also examined. The numerical outcome demonstrates that the value of overall performance increases with the surge in Re, indicating that for the current investigation, a larger Re yields superior thermal-hydraulic performance. Additionally, it is discovered that VGs with a curvature of 0.25 work best thermally and hydraulically, and the greatest value of overall performance 1.06 is attained at an inclination angle of 15°. A better heat transfer performance can be obtained by using a CRWVG with considerably less pressure loss owing to its efficient design.

Meanwhile, There has been a great deal of attention given to research on thermohydraulic performance of non-Newtonian fluids all around the world. Shear-thinning fluid is utilized as a coolant across various industries, including distilleries, pharmaceutical and drug industries, food industries, petrochemical industries, and food and biological industries. The aqueous solution of CMC functions as a non-Newtonian shear-thinning fluid, and using it for heat removal applications results in superior outcomes [6, 77]. Kumar and Dalal [90] numerically simulated an FTHE using an aqueous solution of CMC and reported an enhancement in Nu by 124-186%. Additionally, the shear thinning property of the CMC solution impacted the shape of the vortices, resulting in improved heat transfer efficiency of a heat exchanger [7, 55, 91].

The research literature on the thermohydraulic performance of varying channel shapes and sizes, along with a CRWVG utilizing Newtonian fluid as a working medium, has been extensively studied. However, there has been comparatively less research conducted on rectangular winglet vortex generators (RWPs) with non-Newtonian fluid, in FTHE. The surveyed literature review concluded that the thermohydraulic performance of a channel with CRWVGs outperformed straight RWPs. Nonetheless, as per the knowledge of the author, no studies have yet been conducted to investigate the impact of shear-thinning fluids on the thermohydraulic performance of the FTHE with inbuilt CRWVGs. Therefore, a thorough investigation is required to understand the behavior of the shear-thinning fluid on the heat transfer and frictional loss of an FTHE using CRWVGs.

6.2 Problem definition

The present numerical investigation focuses on the impact of the CRWVG on the heat transfer and pressure drop of a heat exchanger with fin-tubes. Three-dimensional numerical simulations have been carried out for a rectangular channel equipped with three rows of inbuilt cylinders and punched CRWVG in the arrear of these cylinders with aqueous CMC solution as a working fluid. These winglets are mounted at various distances (r/R) away from the center of the cylinders with various angles of inclination from the direction of flow. The study focused on a Re interval between 50 and 200, using an aqueous solution containing 2000 parts per million (ppm) of CMC. The purpose of this research is to investigate the heat transfer and frictional loss in an FTHE equipped with punched CRWVGs and also to determine the optimal position of winglets inside the channel. The performance of this channel is compared with the base channel and the channel with RWPs of the same base length. In addition, a comparative analysis is conducted to examine the heat transfer and pressure drop characteristics of flow channels using CMC aqueous solutions compared to water. The outcome of this research is expected to provide significant insights into the selection of suitable winglets based on specific requirements.

6.2.1 Computational model

The chord length (l_{vg}), height (h), and thickness (t) of the CRWVGs are $2.93H$, $0.5H$, and $0.027H$, respectively. The winglets are located at various distances (r/R) away from the center of the cylinders. The CRWVG surface has an inclination angle (α) of 105°, 120°, and 135° with regard to the direction of fluid flow entering the channel. The distance between the front edge of the first and second sets of winglets and the front edge of the second and third sets of winglet pairs is $7.06H$ respectively. The hydraulic diameter ($2H$) of the channel defines the Re. The computational model for the inline and staggered FTHE along with the CRWVGs are shown in Figs. 6.1 and 6.2

The solid surfaces of the computational domain, winglets, and cylinders are maintained at a fixed temperature of 330 K, while the fluid temperature at the inlet of the channel is kept at a fixed temperature of 300 K. The material properties are considered to be invariant in temperature due to the minimal temperature fluctuations along the channel (less than 30 K), as per [6].

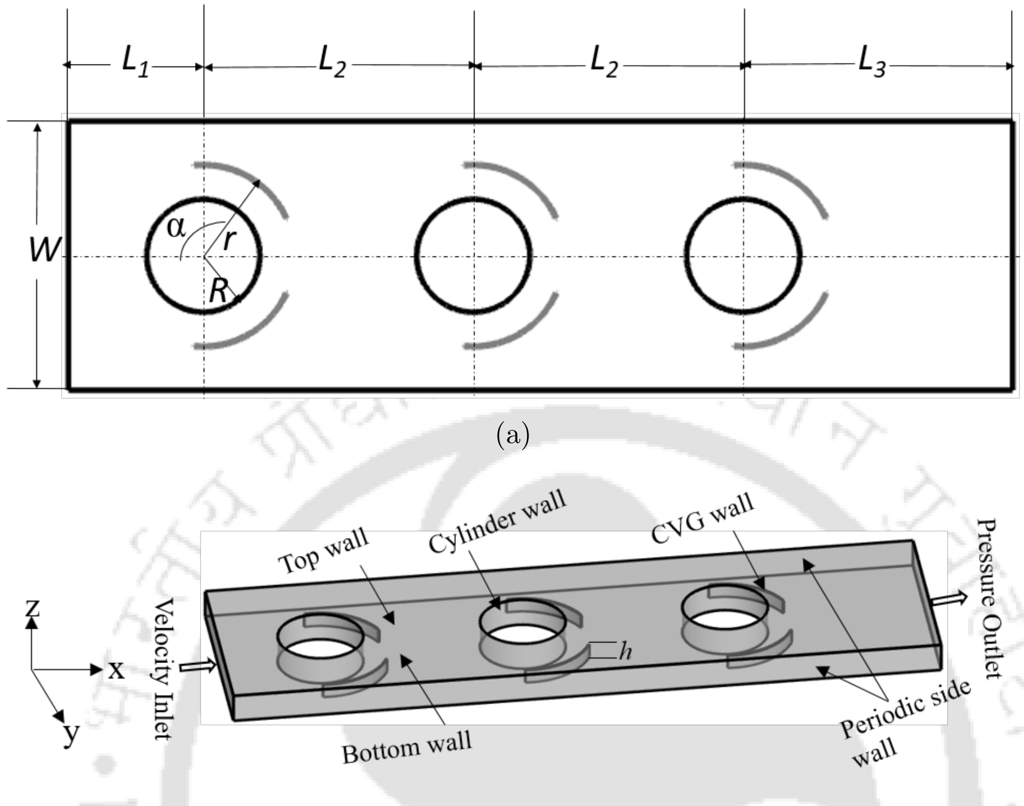

Figure 6.1: Computational domain with CRWVGs with inline tube configurations (a) Schematic view and (b) Isometric view

6.2.2 Boundary conditions

The comparison of the thermohydraulic performance between a non-Newtonian shear-thinning CMC solution and water is the main focus of this analysis.

At the inlet of the channel, a fully developed velocity profile is maintained in the flow path, while the outlet of the channel is maintained under pressure-outlet boundary conditions. The top and bottom walls of the channel, the wall of the cylinders, and the VG walls are maintained under isothermal and no-slip boundary conditions. Side walls are maintained at periodic boundary conditions. The boundary conditions for various part of the channel is mathematically represented in Table 6.1. Where, n represents the direction normal to the boundary. (x_1, y_1, z_1) and (x_2, y_2, z_2) are corresponding points on the opposite boundaries.

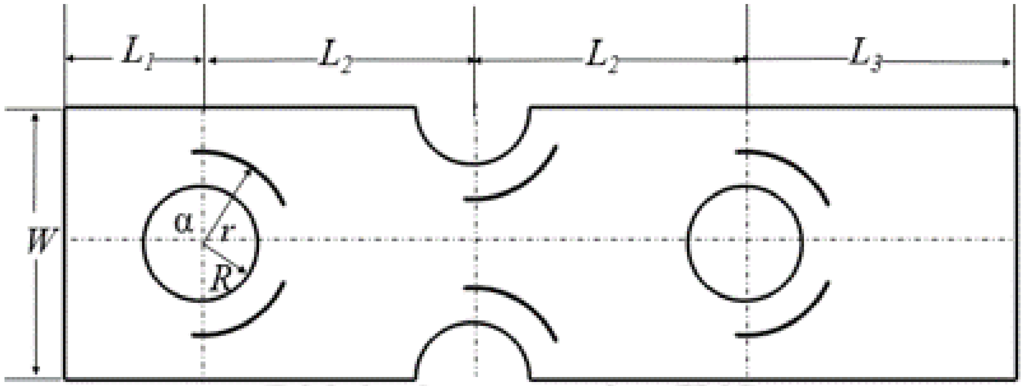

(a)

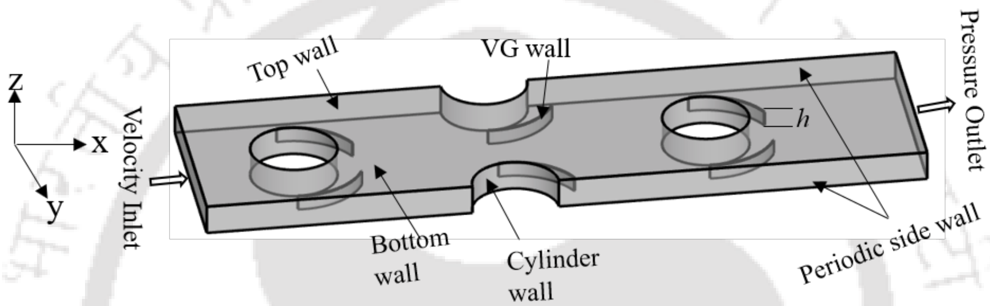

(b)

Figure 6.2: Computational domain with CRWVGs with staggered tube configuration (a) Schematic view and (b) Isometric view

6.3 Mesh generation and grid independency test

The flow domain discretization is composed of a non-uniform, unstructured mesh made up of multi-zone hexahedral cells that follow the flow direction, as shown in Fig. 6.3. These cells were made to cluster around the winglets, particularly in regions with steep gradients. To ensure the accuracy and investigate the influence of cell size, five different meshes were generated, each with a varying number of cells. Based on the findings presented in Table 6.2, it was observed that the system with the cell counts 1345205 and 1817205 provides the least variations in Nu_m and f_{app}. However, it was found that the mesh comprising 1345205 cells can produce satisfactory results maintaining a reasonable simulation time. Therefore, the mesh with the cell count 1817205 was chosen for additional analysis. The calculations were carried out on an HP machine with 8 CPU cores, each with 3 GB memory, with each case taking approximately 6 to 8 hours to compute.

Table 6.1: Boundary conditions are used in different parts of the channel

Boundary name	Boundary conditions
Entry	$u = u(z)$, $v = w = 0$, $T_{in} = 300$ K, $\frac{\partial p}{\partial n} = 0$
Exit	$p = 0$, $\frac{\partial T}{\partial x} = \frac{\partial u}{\partial x} = \frac{\partial v}{\partial y} = \frac{\partial w}{\partial z} = 0$
top, bottom, DWPs, and cylinder walls	$u = v = w = 0$, $T_w = 330$ K, $\frac{\partial p}{\partial n} = 0$
Side walls	$u(x_1, y_1, z_1) = u(x_2, y_2, z_2)$ and $p(x_1, y_1, z_1) = p(x_2, y_2, z_2)$

Table 6.2: Results of a mesh independence study on the flow of 2000 ppm aqueous CMC solution in a channel equipped with DWPs. at $Re = 200$

element counts	f_{app}	% Diff.	Nu_m	% Diff.
763470	0.8066	-	31.0139	-
1018640	0.8051	0.19	30.8944	0.39
1345205	0.8041	0.12	30.8184	0.25
1817205	0.8039	0.02	30.7961	0.07

6.4 Results and discussion

The study involved determining the average changes in performance parameters such as the Nusselt number (Nu), the apparent friction factor (f_{app}), and the quality factor (Q_f) caused by the addition of CRWVGs to the FTHE at various angles of attack (β) and radius ratios. Then, these data were compared to the performance of a similar channel with RWPs and with the base channel (without the winglets). Additionally, the performance of the channel was compared for Newtonian as well as non-Newtonian fluid.

Fig. 6.4 shows the velocity and temperature distribution of an FTHE equipped with RWVGs and CRWVGs and the base channel at the midplane ($z = 0.5H$). Using the CRWVGs in FTHE reduces the size of the poor wake zone compared to the base channel and channel with RWVGs. The shape and placement of the CRWVGs are such that, they guide the fluid to pass through the wake zone formed behind the cylinder which further enhances the contact of fluid at the back portion of the cylinders and enhances heat transfer. The addition of CRWVGs near the tubes of a heat exchanger creates a passageway resembling a nozzle between the tube and the VG. The presence of CRWVGs not only generates a longitudinal vortex but

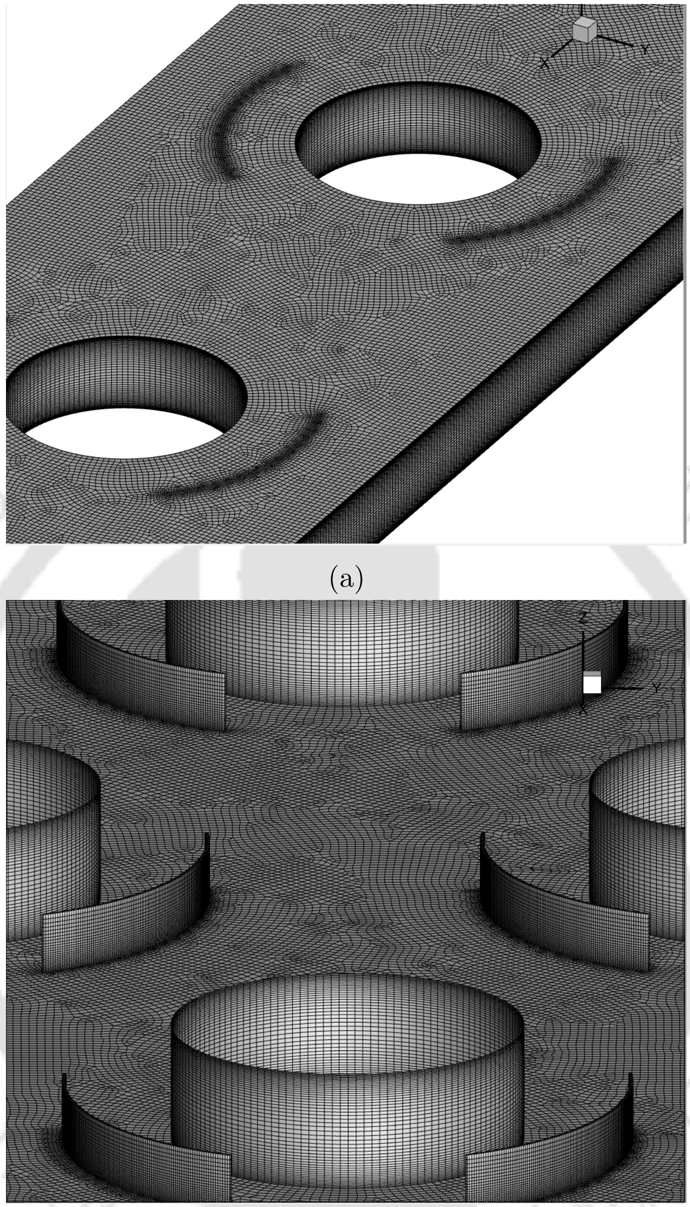

(a)

(b)

Figure 6.3: Magnified representation of the computational grid (a) Isometric view and (b) Schematic cut view

also creates a nozzle-like acceleration region. This region reduces the wake zone in the rear of the tube, resulting in improved heat transfer. The observations in Fig. 6.4b show that when a CRWVG is present, the temperature gradient in the area behind the tube is larger than in the base channel and channels containing RWVGs. The position of CRWVGs in staggered tube configuration is such that it

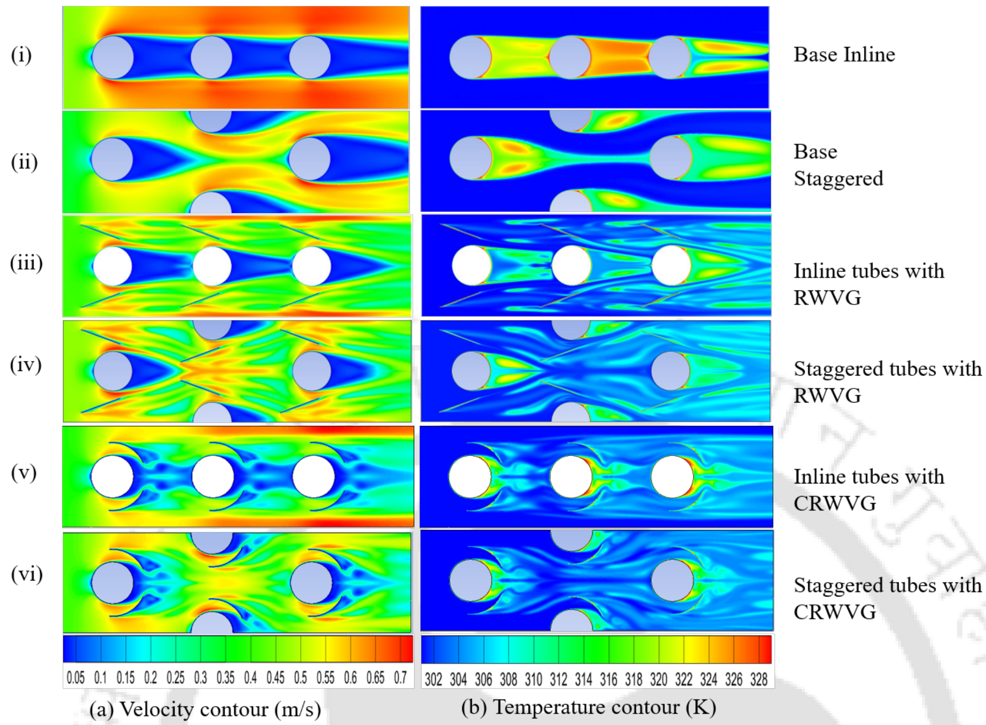

Figure 6.4: Comparison of (a) velocity (m/s) distribution and (b) temperature (K) distribution at a cross-section z = 0.5H and Re = 200 for (i) base inline, (ii) base staggered, (iii) inline tube row with RWP, (iv) staggered row with RWP (angle of attack = 160°), (v) inline tube row with CRWP, and (vi) staggered tube row with CRWP for the aqueous solution of CMC (2000 ppm)

allows better mixing of fluids resulting in better heat transfer compared to the inline configuration. Additionally, the exit fluid temperature is higher in the channel with curved winglets in staggered configurations compared to the base staggered channel and the staggered FTHE with rectangular winglets, leading to further improved heat transfer efficiency. These findings suggest that the use of CRWVG in FTHE can be an effective way to enhance heat transfer.

The optimal angle of inclination of the VG at which the channel performs best is of critical importance for future investigations of performance parameters such as average Nu, f_{app}, and Q_f. Fig. 6.5 depicts the fluctuation of Nu, f_{app}, and Q_f with attack angle for a channel with CRWVGs positioned at a radius ratio of 1.6 for both inline and staggered tube designs at Re = 200. As shown in Fig. 6.5, inline and staggered arrangements of tubes with CRWVG function best at an angle of inclination (α) = 120°. At this particular value of α, the system generates

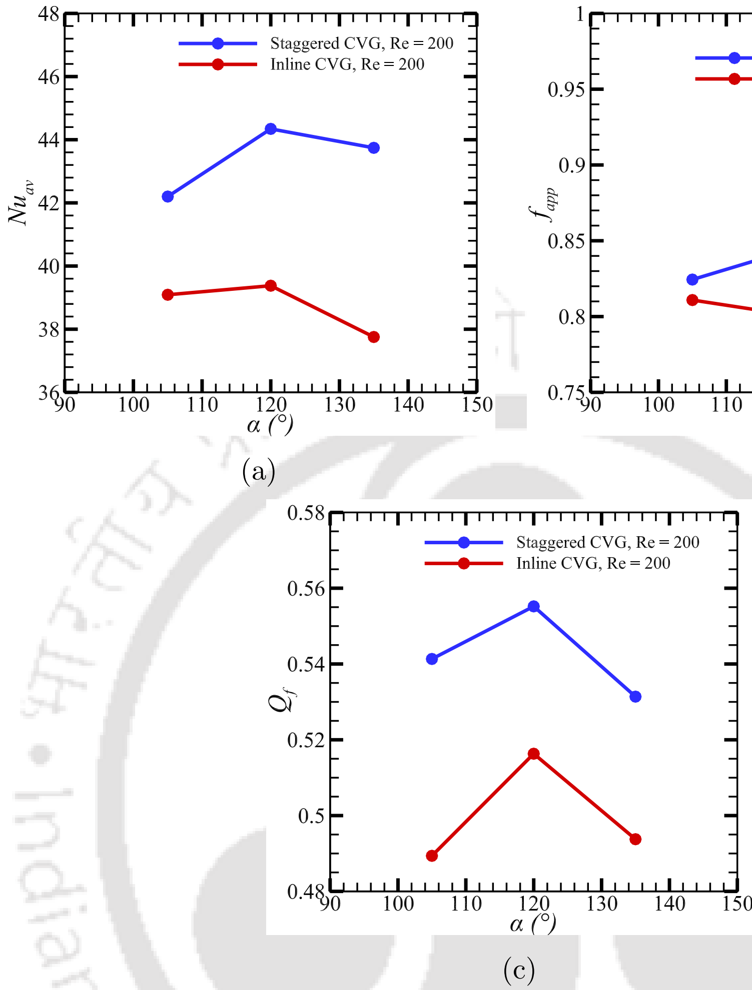

Figure 6.5: Variation of average (a) Nu_{av}, (b) f_{app}, and (c) Q_f with inclination angle α of a FTHE with CRWVGs for CMC (2000 ppm)

maximum heat transfer while incurring the least pressure loss resulting best overall performance. The FTHE with CRVGs at $\alpha = 120°$ is used for further investigation.

Once the optimal inclination angle is defined, the optimal distance between the CRWVGs and the center of the tube must be determined. Fig. 6.6 represents the average variation of Nu, f_{app}, and Q_f with radius ratio (r/R) for an FTHE with inline and staggered tube configurations at $\alpha = 120°$ for the flow of an aqueous solution of CMC. The average value of Nu and f_{app} increase with the increase in the value of r/R for both the inline and staggered tube configurations represented by Figs. 6.6a and 6.6b respectively. Increasing the r/R allows the fluid to be in contact with the CRWVG surface for a longer time resulting the heat transfer enhancement. However, increasing the r/R costs on the larger pressure drop which

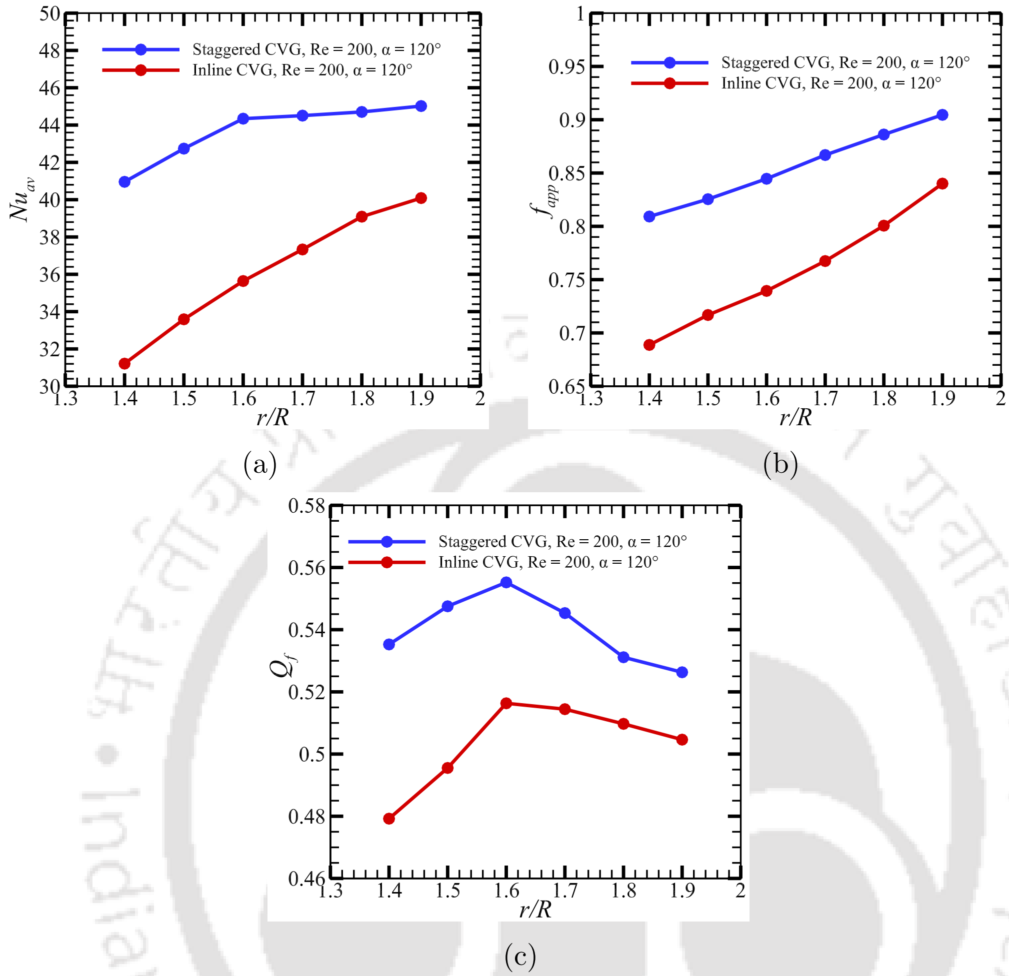

Figure 6.6: Average variation of (a) Nu, (b) f_{app}, and (d) Q_f with r/R for a FTHE with CRWPs at an inclination angle (α) of 120° for CMC(2000 ppm)

further increases the frictional loss. It is necessary to establish an optimal value of r/R for further examination of the performance parameters of the channel. A combined effect of heat transfer and frictional factor is defined by the quality factor (Q_f) and its variation with r/R is shown in Fig. 6.6c. It was observed that the overall performance of the channel is highest at a particular value of $r/R = 1.6$ for both the inline and staggered tube configurations of FTHE.

Now, the FTHE with CRVGs at $r/R = 1.6$ and $\alpha = 120°$ is the basis for future investigations. The average variations of Nu, f_{app}, and Q_f with Re for inline and staggered configurations of the base channel, channel with RVGs, and channel with CRVGs are represented by Fig. 6.7. It was observed from Fig. 6.7a with an increase in Re, average Nu increases for all cases. Higher Re yields larger velocity which

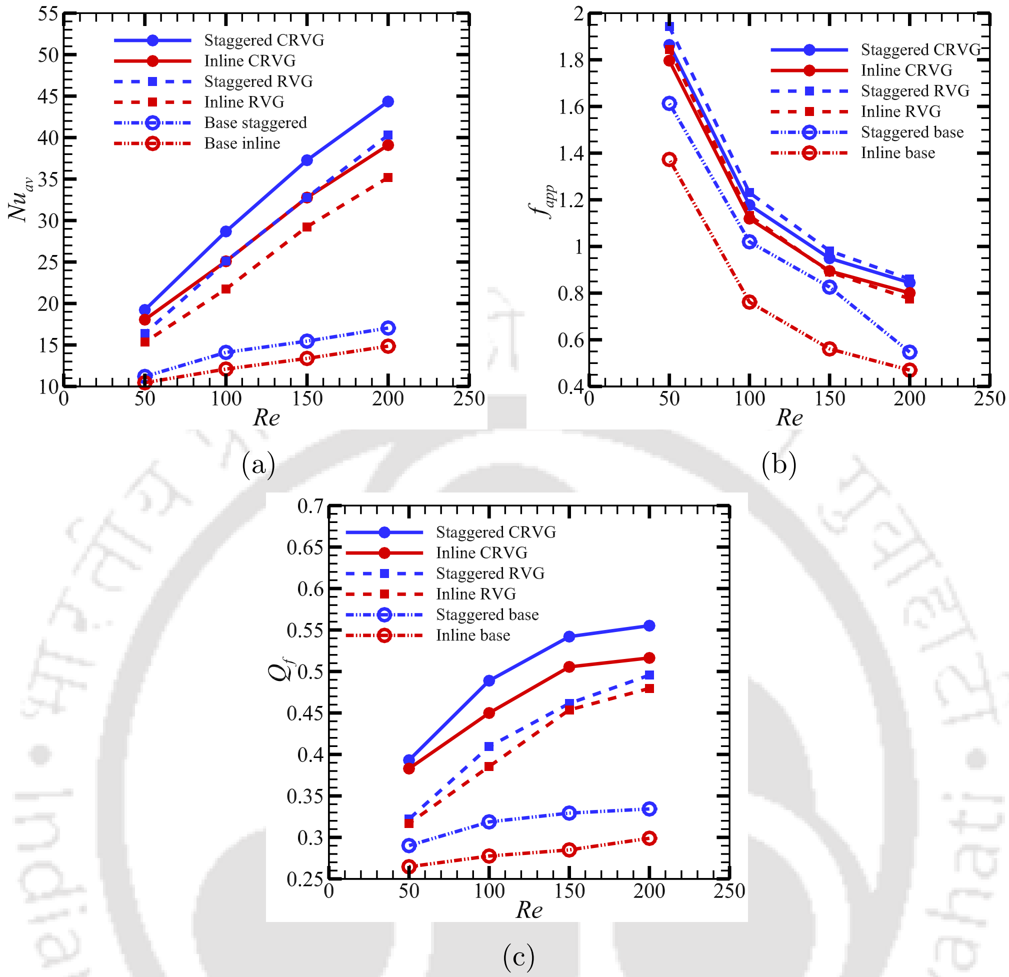

Figure 6.7: Variation of Nu_{av}, average f_{app}, and average Q_f of a CRVG, RVG, and base channel with Re for various tube configurations at ($r/R = 1.6$ for staggered and inline tube with CRVG) $\alpha = 120°$

further generates stronger vortices resulting in higher heat transfer. Fluid at higher Re generates a higher rate of shear strain, which further reduces the viscosity of an aqueous solution of CMC as it shows shear-thinning behaviour. The fluid near the cylinder and winglets surfaces suffer from the higher shear strain with reduced viscosity and fluid away from these surfaces has lesser shear strain with elevated viscosity mixed with each other resulting in high heat transfer. It was observed that the average Nu for an FTHE using CRVGs is highest compared to the conventional straight RVGs and base channel. The geometry and location of the CRVGs are such that, they can produce guiding effects as well as secondary flow effects to enhance the heat transfer. When CRVGs are placed on the arrear of the tubes it can guide the fluid to penetrate the poor heat transfer zone. When comparing the flow characteristics of CRVGs and RVGs, it can be seen that, for the CRVGs, the influence of flow guiding was greater than that of secondary flow. Fig. 6.7b clearly shows that the average f_{app} for straight RVGs is highest compared to the CRVGs and base channel. The CRVGs produce less pressure loss owing to the efficient stream-lined design of its surface that guides the fluid to move in the wake zone with relatively less pressure drop compared to the conventional straight RVGs. The f_{app} decreases with an increase in Re for all cases when considering the laminar flow of an aqueous solution of CMC. When the combined effects of heat transfer and friction loss are taken into account, the channel equipped with CRVGs performs better overall. For every scenario, it also rises as Re increases. In all circumstances, the staggered tube arrangements perform better than the inline configuration when average Nu, average f_{app}, and average Q_f are taken into account. CRWVG in an FTHE heat exchanger increases the Nu_{av}, and Q_f by 10-18% and 8-22% respectively, and decreases the f_{app} by 1-5% compared to the RVGs.

Fig. 6.8 represents the average variation of Nu, f_{app}, and Q_f with Re for inline and staggered configurations of the FTHE with CRVGs for the aqueous solution of CMC and water. It was shown in Fig. 6.8a that the average Nu for the channel using CMC as a working fluid is quite higher than the water. CMC water solutions are better thermal conductors than water, so they can absorb more heat from hot surfaces. CMC is more viscous than water, so its Prandtl number is higher than that of water. Therefore, the flow behavior of the CMC is dominated by momentum diffusion rather than thermal diffusion. Convection instead of conduction dominates energy transfer in channels with high CMC concentration (2000 ppm). CMC with a variable viscosity under the effect of variable rate of shear strain enhances the mixing, and results in higher heat transfer compared to water. Fig. 6.8b shows the f_{app} through the FTHE with CRVGs using an aqueous solution of water is lesser than the water. The molecular orientation of an aqueous solution of CMC is such that they have a wetting effect on the fluid, which acts as a drag reducer and reduces frictional loss compared to water. The combined effect of heat transfer and pressure loss in the channel using an aqueous solution of CMC exhibits a better performance compared to water. Using an aqueous solution of CMC in FTHE with CRVGs increases the Nu_{av}, and Q_f by 123-178% and 95-127% respectively, and decreases the f_{app} by 37-49% compared to the RVGs.

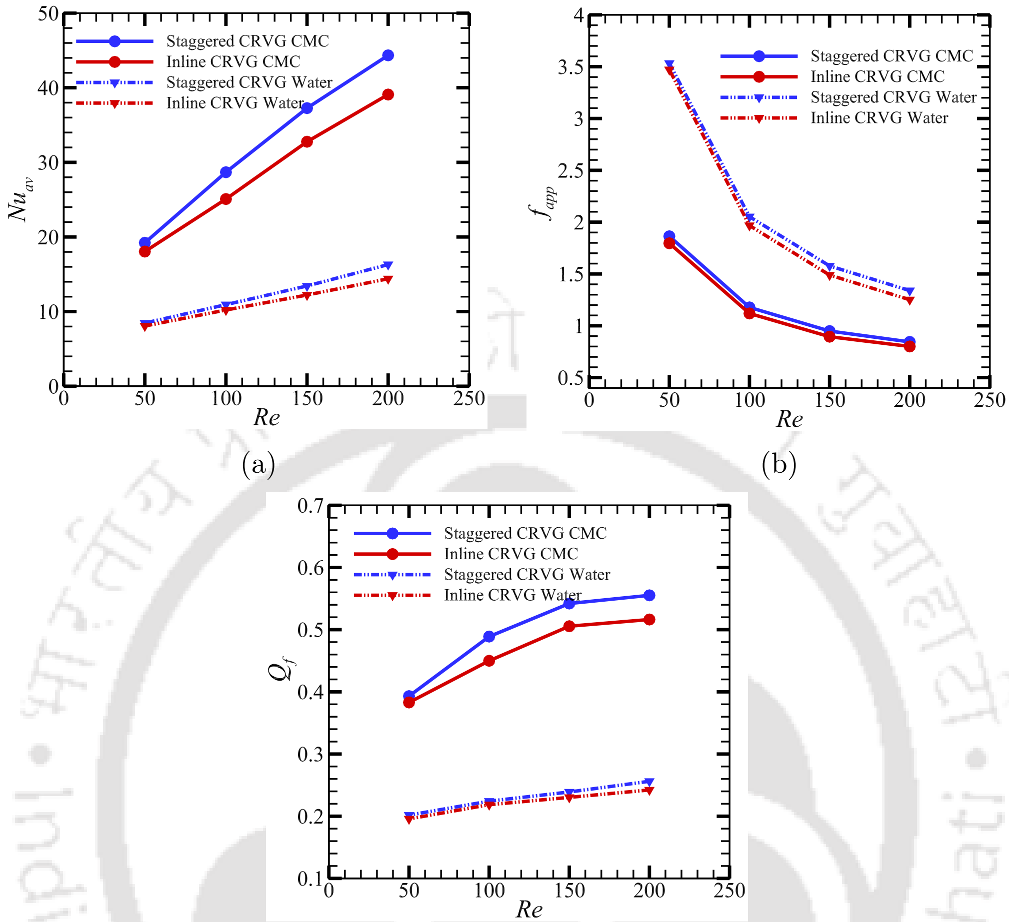

(a) (b)

(c)

Figure 6.8: Variation of Nu_{av}, average f_{app}, and average Q_f with Re for an aqueous solution of CMC and water for various tube configurations at (r/R =1.6 for staggered and inline configurations of tubes

6.5 Summary

A FTHE heat exchanger equipped with CRWVGs outperforms the conventional RWVGs considering overall performance. CRWVG in an FTHE heat exchanger increases the Nu_{av} and Q_f by 10-18% and 8-22% respectively and decreases the f_{app} by 1-5% compared to the RWVG. The inline and staggered configuration of the tube performs best at r/R = 1.6 whereas, both the configuration of the tube performs best at an angle ($\alpha = 120°$). The staggered tube configuration outperforms the inline tube configuration considering the heat transfer and pressure drop. Additionally, employing aqueous solutions of CMC as a working fluid in the channel with winglet improves the average Nu_m and the Q_f and reduces the f_{app} compared to the water.

Chapter 7

Conclusions and scope of future work

7.1 Conclusions

The primary objective of this thesis was to investigate the effect of winglets on the thermal and flow properties of shear-thinning fluid in a fin-tube heat exchanger. A detailed investigation of the thermal-hydraulic performance of FTHE was conducted through a series of numerical simulations using a commercial CFD solver ANSYS FLUENT. The simulations were carried out for the laminar flow at a range of Re 50 to 200, using various shapes and sizes of winglets, and an aqueous solution of CMC as a working fluid. The study aimed to investigate the effect of tube placement (inline and staggered), winglet inclination, and winglet placement (common flow up and common flow down) on the performance of FTHE. The results of the simulations provide valuable insights into the impact of these design parameters on the heat transfer coefficient, pressure drop, and thermal performance of FTHE. The thermal and hydraulic performance of the FTHE is affected by the inclusion of VG and is assessed by comparing the Nu, f_{app}, and Q_f of the channel with and without the VGs. Including VG in the channel produces strong longitudinal vortices, destabilizes the thermal boundary layer, and enhances the proper mixing of fluids, resulting in better heat transfer. The presence of VGs produces upwash and downwash regions along the flow inside the channel, causing a local variation of the thermohydraulic parameters. In this chapter, the important findings of each chapter are summarized below.

Thermo-hydraulic performance of a rectangular channel equipped with delta winglet pairs and an aqueous solution of CMC of concentration 2000 ppm as a working fluid was analysed and discussed in Chapter 3. The main conclusions from Chapter 3 are as follows:

- All VG cases produce a high Nu_m, f_{app} and Q_f compared to the base channel.
- A rectangular channel equipping RWPs outperforms DWPs considering only heat transfer at higher attack angles. However, RWPs lead to a larger pressure drop and hence require more pumping power to pump the fluid compared to the DWPs.
- The overall performance of the channel considering the combined effect of heat transfer and friction loss, DWPs outperform RWPs.
- The Nu_m and f_{app} rise as the angle of attack rises, whereas the Q_f rises as the angle of attack lowers up to a certain value. The channel with DWPs shows best overall performance at an attack angle of 30°.
- Using an aqueous solution of CMC in the channel as a working medium improves the Nu_m by 116% to 143% while reducing the friction coefficient of 56% to 68% compared to water.

The analysis of heat transfer and pressure drop of a FTHE with punched DWPs using an aqueous solution of CMC of concentration 2000 ppm as a working fluid was analysed and discussed in Chapter 4. The main conclusions from Chapter 4 are as follows:

- The Nu_m and Q_f value increase with an increase in the Re, while f_{app} decreases with an increase in the Re
- The Nu_m, average Q_f, and average f_{app} value of the channel with an inline configuration of the cylinders punched with DWVGs at $\beta = 160°$ is enhanced by 81%, 33%, and 36%, respectively compared to the channel without the DWVGs.
- The Nu_m and average Q_f value of the channel with an inline arrangement of the cylinders punched with DWVGs at $\beta = 160°$ employing an aqueous

solution of CMC (2000 ppm) is enhanced by 147%, and 104% respectively whereas, the average f_{app} reduced by 40% in comparison to the water.

- The Nu_m, f_{app} and Q_f value increase with an increase in the attack angle. Out of all configurations examined, DWVGs with $\beta = 160°$ perform best considering the overall performance of the channel.

Analysis of the thermal and hydraulic parameters of a FTHE using shear-thinning fluid and rectangular winglet is discussed in Chapter 5. Additionally, thermal and hydraulic performance of the FTHE using RWPs compared with the FTHE with DWPs and the base FTHE. The salient conclusions from Chapter 5 are as follows:

- If heat transfer is the only criterion to select the type of VGs, then RWVGs outperform the DWVGs by 24%, at the same time, f_{app} also increases by 34% compared to DWVGs. But when considering the overall performance of the channel, DWVGs outperform RWVGs by 9%.
- The staggered arrangements of the tube produce better Nu_m and a higher f_{app} compared to the inline arrangement due to the positioning of the VGs in the CFU-CFD-CFU configurations.
- The Nu_m, average Q_f, and average f_{app} value of the channel with a staggered arrangement of the tubes equipped with VGs at 160° is increased by 89%, 19%, and 59% respectively compared to the base channel.
- The Nu_m and average Q_f value of the channel with a staggered arrangement of the tubes equipped with VGs at 160° and CMC (2000 ppm) as a working fluid is increased by 186%, and 133% respectively while the average f_{app} decreases by 65% compared to the water.
- Decreasing the attack angle of the VG improves Nu_m, vorticity, f_{app}, and Q_f of the channel up to 160°, beyond 160° it decreases. VG with a staggered arrangement of the tube with 160° attack angle performs best compared to other configurations.

Effect of shear-thinning fluid and curved vortex generators on the performance of fin-tube heat exchanger were analysed and discussed in Chapter 6. The performance of FTHE equipped with CRWVGs is compared with the FTHE equipped with

RWVGs of same base length. Some important conclusions of Chapter 6 are as follows:

- A FTHE heat exchanger equipped with CRWVGs outperforms the conventional RWVGs considering overall performance. CRWVG in an FTHE heat exchanger increases the Nu_{av} and Q_f by 10-18% and 8-22% respectively and decreases the f_{app} by 1-5% compared to the RWVG.

- The inline and staggered configuration of the tube perform best at $r/R = 1.6$ whereas, both the configuration of the tube perform best at an angle $(\alpha) =$ 120°.

- Using CMC water solution as a coolant in rectangular channels is a wise course of action to improve heat transfer performance, but these coolants are suited for situations where pumping power is not a snag because the increased heat transfer is accompanied by a considerable pressure loss. It is not advisable to use the aqueous solution of CMC in the external flow because it is highly viscous and highly sensitive to the shear force. It can only be applied to the internal flow.

7.2 Scope of future work

The present research work numerically examines a limited types of winglets to analyze the thermal and hydraulic performance of fin-tube heat exchanger. The present work makes an honest attempt to give a detailed explanation of winglet mechanism on the thermal and flow parameter of shear-thinning fluid in a fin-tube heat exchanger. However, various optimized shapes and sizes of winglets are yet to be explored to optimize the performance of fin-tube heat exchnager. In this regard, a few possible extensions that may form the basis of future research are mentioned as future scope below:

- Heat transfer analysis of fin-tube heat exchnager using shear-thinning fluid and winglet with punched holes can also be explored.

- Heat transfer analysis of fin-tube heat exchnager using shear-thinning fluid and trapezoidal winglet might be a good options to explore to enhance the thermal hydraulic performance.

- Angle type of winglets can also be explored to enhance the thermohydraulic performnace of fin-tube heat exchanger using shear-thinning fluids.

References

[1] Lu G. and Zhou G. (2016) 'Numerical simulation on performances of plane and curved winglet–pair vortex generators in a rectangular channel and field synergy analysis', *International Journal of Thermal Sciences*, vol. 109, pp. 323–333.

[2] Maradiya C., Vadher J., and Agarwal R. (2018) 'The heat transfer enhancement techniques and their thermal performance factor', *Beni-Suef University Journal of Basic and Applied Sciences*, vol. 7(1), pp. 1–21.

[3] Awais M. and Bhuiyan A.A. (2018) 'Heat transfer enhancement using different types of vortex generators (vgs): A review on experimental and numerical activities', *Thermal Science and Engineering Progress*, vol. 5, pp. 524–545.

[4] Fiebig M., Kallweit P., Mitra N., and Tiggelbeck S. (1991) 'Heat transfer enhancement and drag by longitudinal vortex generators in channel flow', *Experimental Thermal and Fluid Science*, vol. 4(1), pp. 103–114.

[5] Lotfi B., Sundén B., and Wang Q. (2016) 'An investigation of the thermo-hydraulic performance of the smooth wavy fin-and-elliptical tube heat exchangers utilizing new type vortex generators', *Applied Energy*, vol. 162, pp. 1282–1302.

[6] Ebrahimi A., Naranjani B., Milani S., and Javan F.D. (2017) 'Laminar convective heat transfer of shear-thinning liquids in rectangular channels with longitudinal vortex generators', *Chemical Engineering Science*, vol. 173, pp. 264–274.

[7] Li P., Xie Y., and Zhang D. (2016) 'Laminar flow and forced convective heat transfer of shear-thinning power-law fluids in dimpled and protruded

microchannels', *International Journal of Heat and Mass Transfer*, vol. 99, pp. 372–382.

[8] Datta A., Sanyal D., and Das A.K. (2016) 'Numerical investigation of heat transfer in microchannel using inclined longitudinal vortex generator', *Applied Thermal Engineering*, vol. 108, pp. 1008–1019.

[9] Oneissi M., Habchi C., Russeil S., Bougeard D., and Lemenand T. (2016) 'Novel design of delta winglet pair vortex generator for heat transfer enhancement', *International Journal of Thermal Sciences*, vol. 109, pp. 1–9.

[10] Deshmukh P., Prabhu S., and Vedula R. (2016) 'Heat transfer enhancement for laminar flow in tubes using curved delta wing vortex generator inserts', *Applied Thermal Engineering*, vol. 106, pp. 1415–1426.

[11] Wu X., Liu D., Zhao M., Lu Y., and Song X. (2016) 'The optimization of fin-tube heat exchanger with longitudinal vortex generators using response surface approximation and genetic algorithm', *Heat and Mass Transfer*, vol. 52, pp. 1871–1879.

[12] Sohankar A. (2007) 'Heat transfer augmentation in a rectangular channel with a vee-shaped vortex generator', *International journal of heat and fluid flow*, vol. 28(2), pp. 306–317.

[13] Wu J. and Tao W. (2008) 'Numerical study on laminar convection heat transfer in a channel with longitudinal vortex generator. part b: Parametric study of major influence factors', *International Journal of Heat and Mass Transfer*, vol. 51(13-14), pp. 3683–3692.

[14] Wu J. and Tao W. (2012) 'Effect of longitudinal vortex generator on heat transfer in rectangular channels', *Applied Thermal Engineering*, vol. 37, pp. 67–72.

[15] Kotcioglu I., Caliskan S., Cansiz A., and Baskaya S. (2010) 'Second law analysis and heat transfer in a cross-flow heat exchanger with a new winglet-type vortex generator', *Energy*, vol. 35(9), pp. 3686–3695.

[16] Khoshvaght-Aliabadi M., Zangouei S., and Hormozi F. (2015) 'Performance of a plate-fin heat exchanger with vortex-generator channels: 3d-cfd simulation

and experimental validation', *International Journal of Thermal Sciences*, vol. 88, pp. 180–192.

[17] Abdollahi A. and Shams M. (2015) 'Optimization of shape and angle of attack of winglet vortex generator in a rectangular channel for heat transfer enhancement', *Applied Thermal Engineering*, vol. 81, pp. 376–387.

[18] Abdollahi A. and Shams M. (2015) 'Optimization of heat transfer enhancement of nanofluid in a channel with winglet vortex generator', *Applied Thermal Engineering*, vol. 91, pp. 1116–1126.

[19] Tang L., Chu W., Ahmed N., and Zeng M. (2016) 'A new configuration of winglet longitudinal vortex generator to enhance heat transfer in a rectangular channel', *Applied Thermal Engineering*, vol. 104, pp. 74–84.

[20] Samadifar M. and Toghraie D. (2018) 'Numerical simulation of heat transfer enhancement in a plate-fin heat exchanger using a new type of vortex generators', *Applied Thermal Engineering*, vol. 133, pp. 671–681.

[21] Dey P. (2022) 'Optimal position of square cylinder vortex generator in channel is not a function of ordinate only–a heat transfer and optimization study', *Engineering Science and Technology, an International Journal*, vol. 28, p. 101013.

[22] Vasudevan R., Eswaran V., and Biswas G. (2000) 'Winglet-type vortex generators for plate-fin heat exchangers using triangular fins', *Numerical Heat Transfer: Part A: Applications*, vol. 38(5), pp. 533–555.

[23] Zhou G. and Ye Q. (2012) 'Experimental investigations of thermal and flow characteristics of curved trapezoidal winglet type vortex generators', *Applied Thermal Engineering*, vol. 37, pp. 241–248.

[24] Garimella S. and Eibeck P. (1991) 'Enhancement of single phase convective heat transfer from protruding elements using vortex generators', *International journal of heat and mass transfer*, vol. 34(9), pp. 2431–2433.

[25] Khoshvaght-Aliabadi M., Naeimabadi N., Barzoki F.N., and Salimi A. (2021) 'Experimental and numerical studies of air flow and heat transfer due to

insertion of novel delta-winglet tapes in a heated channel', *International Journal of Heat and Mass Transfer*, vol. 169, p. 120912.

[26] Dogan S., Darici S., and Ozgoren M. (2019) 'Numerical comparison of thermal and hydraulic performances for heat exchangers having circular and elliptic cross-section', *International Journal of Heat and Mass Transfer*, vol. 145, p. 118731.

[27] Kondepudi S.N. and O'Neal D.L. (1993) 'Performance of finned-tube heat exchangers under frosting conditions: I. simulation model', *International Journal of Refrigeration*, vol. 16(3), pp. 175–180.

[28] Tso C., Cheng Y., and Lai A. (2006) 'An improved model for predicting performance of finned tube heat exchanger under frosting condition, with frost thickness variation along fin', *Applied Thermal Engineering*, vol. 26(1), pp. 111–120.

[29] Sun L. and Zhang C.L. (2014) 'Evaluation of elliptical finned-tube heat exchanger performance using cfd and response surface methodology', *International Journal of Thermal Sciences*, vol. 75, pp. 45–53.

[30] Jacobi A. and Goldschmidt V. (1990) 'Low reynolds number heat and mass transfer measurements of an overall counterflow, baffled, finned-tube, condensing heat exchanger', *International journal of heat and mass transfer*, vol. 33(4), pp. 755–765.

[31] Hsieh C.T. and Jang J.Y. (2012) 'Parametric study and optimization of louver finned-tube heat exchangers by taguchi method', *Applied Thermal Engineering*, vol. 42, pp. 101–110.

[32] Gu L., Min J., Wu X., and Yang L. (2017) 'Airside heat transfer and pressure loss characteristics of bare and finned tube heat exchangers used for aero engine cooling considering variable air properties', *International Journal of Heat and Mass Transfer*, vol. 108, pp. 1839–1849.

[33] Nemati H., Moghimi M., Sapin P., and Markides C. (2020) 'Shape optimisation of air-cooled finned-tube heat exchangers', *International Journal of Thermal Sciences*, vol. 150, p. 106233.

[34] Chen H.T., Chiu Y.J., Liu C.S., and Chang J.R. (2017) 'Numerical and experimental study of natural convection heat transfer characteristics for vertical annular finned tube heat exchanger', *International Journal of Heat and Mass Transfer*, vol. 109, pp. 378–392.

[35] Singh A., Maiya M., and Murthy S.S. (2017) 'Experiments on solid state hydrogen storage device with a finned tube heat exchanger', *International Journal of Hydrogen Energy*, vol. 42(22), pp. 15226–15235.

[36] Gray D. and Webb R.L., 'Heat transfer and friction correlations for plate finned-tube heat exchangers having plain fins', in 'International Heat Transfer Conference Digital Library', (Begel House Inc., 1986).

[37] Kim Y. and Kim Y. (2005) 'Heat transfer characteristics of flat plate finned-tube heat exchangers with large fin pitch', *International Journal of Refrigeration*, vol. 28(6), pp. 851–858.

[38] Taler D., Taler J., and Trojan M. (2020) 'Thermal calculations of plate–fin–and-tube heat exchangers with different heat transfer coefficients on each tube row', *Energy*, vol. 203, p. 117806.

[39] Qiu G., Sun J., Nie L., Ma Y., Cai W., and Shen C. (2020) 'Theoretical study on heat transfer characteristics of a finned tube used in the collector/evaporator under solar radiation', *Applied thermal engineering*, vol. 165, p. 114564.

[40] Bezaatpour M. and Rostamzadeh H. (2020) 'Heat transfer enhancement of a fin-and-tube compact heat exchanger by employing magnetite ferrofluid flow and an external magnetic field', *Applied Thermal Engineering*, vol. 164, p. 114462.

[41] Ravi R., Pachamuthu S., and Kasinathan P. (2020) 'Computational and experimental investigation on effective utilization of waste heat from diesel engine exhaust using a fin protracted heat exchanger', *Energy*, vol. 200, p. 117489.

[42] Abolfathi S., Lavasani A.M., Mobedi P., and Afshar K.S. (2021) 'Experimental study on flow around a tube in mixed tube bundles comprising cam-shaped and

circular cylinders in in-line arrangement', *International Journal of Thermal Sciences*, vol. 163, p. 106812.

[43] Mobedi P., Mirabdolah Lavasani A., Abolfathi S., and Afshar K.S. (2022) 'The aspect ratio effect on the performance of a cam-shaped cylinder in crossflow of air', *Experimental Heat Transfer*, vol. 35(4), pp. 500–515.

[44] Salehi Afshar K., Mirabdolah Lavasani A., Abolfathi S., and Mobedi P. (2023) 'The angle of attack effect on thermal-hydraulic performance of a cam-shaped tube with constant heat flux in crossflow', *Experimental Heat Transfer*, vol. 36(4), pp. 548–563.

[45] Hu D., Zhang Q., Song K., Gao C., Zhang K., Su M., and Wang L. (2023) 'Performance optimization of a wavy finned-tube heat exchanger with staggered curved vortex generators', *International Journal of Thermal Sciences*, vol. 183, p. 107830.

[46] Aktas A.E., Kuru M.N., Erdinc M.T., Aydin O., and Bilgili M. (2023) 'Optimizing the tube geometry to enhance thermohydraulic performance of tube bank heat exchanger', *International Journal of Thermal Sciences*, vol. 193, p. 108460.

[47] Skullong S., Promvonge P., Jayranaiwachira N., and Thianpong C. (2016) 'Experimental and numerical heat transfer investigation in a tubular heat exchanger with delta-wing tape inserts', *Chemical Engineering and Processing-Process Intensification*, vol. 109, pp. 164–177.

[48] Behfard M. and Sohankar A. (2016) 'Numerical investigation for finding the appropriate design parameters of a fin-and-tube heat exchanger with delta-winglet vortex generators', *Heat and Mass Transfer*, vol. 52, pp. 21–37.

[49] Majumder A. and Pal D. (2016) 'Numerical study of fin-tube type heat exchanger with delta winglets', *Frontiers in Heat and Mass Transfer (FHMT)*, vol. 7(1).

[50] Awais M. and Bhuiyan A.A. (2019) 'Enhancement of thermal and hydraulic performance of compact finned-tube heat exchanger using vortex generators (vgs): a parametric study', *International Journal of Thermal Sciences*, vol. 140, pp. 154–166.

[51] Wang C.C., Lo J., Lin Y.T., and Wei C.S. (2002) 'Flow visualization of annular and delta winlet vortex generators in fin-and-tube heat exchanger application', *International Journal of Heat and Mass Transfer*, vol. 45(18), pp. 3803–3815.

[52] Salviano L.O., Dezan D.J., and Yanagihara J.I. (2016) 'Thermal-hydraulic performance optimization of inline and staggered fin-tube compact heat exchangers applying longitudinal vortex generators', *Applied Thermal Engineering*, vol. 95, pp. 311–329.

[53] Lei Y., Zheng F., Song C., and Lyu Y. (2017) 'Improving the thermal hydraulic performance of a circular tube by using punched delta-winglet vortex generators', *International Journal of Heat and Mass Transfer*, vol. 111, pp. 299–311.

[54] Valencia A., Fiebig M., and Mitra N. (1996) 'Heat transfer enhancement by longitudinal vortices in a fin-tube heat exchanger element with flat tubes', .

[55] Biswas G., Torii K., Fujii D., and Nishino K. (1996) 'Numerical and experimental determination of flow structure and heat transfer effects of longitudinal vortices in a channel flow', *International Journal of Heat and Mass Transfer*, vol. 39(16), pp. 3441–3451.

[56] Gentry M. and Jacobi A.M. (2002) 'Heat transfer enhancement by delta-wing-generated tip vortices in flat-plate and developing channel flows', *J. Heat Transfer*, vol. 124(6), pp. 1158–1168.

[57] Kumar A. and Layek A. (2020) 'Nusselt number and friction characteristics of a solar air heater that has a winglet type vortex generator in the absorber surface', *Experimental Thermal and Fluid Science*, vol. 119, p. 110204.

[58] Ramanathan S., Thansekhar M., Kanna P.R., and Gunnasegaran P. (2020) 'A new method of acquiring perquisites of recirculation and vortex flow in sudden expansion solar water collector using vortex generator to augment heat transfer', *International Journal of Thermal Sciences*, vol. 153, p. 106346.

[59] Fu H., Sun H., Yang L., Yan L., Luan Y., and Magagnato F. (2023) 'Effects of the configuration of the delta winglet longitudinal vortex generators and channel height on flow and heat transfer in minichannels', *Applied Thermal Engineering*, vol. 227, p. 120401.

[60] Tian L.T., He Y.L., Lei Y.G., and Tao W.Q. (2009) 'Numerical study of fluid flow and heat transfer in a flat-plate channel with longitudinal vortex generators by applying field synergy principle analysis', *International Communications in Heat and Mass Transfer*, vol. 36(2), pp. 111–120.

[61] Kong Y., Yang L., Du X., and Yang Y. (2016) 'Effects of continuous and alternant rectangular slots on thermo-flow performances of plain finned tube bundles in in-line and staggered configurations', *International Journal of Heat and Mass Transfer*, vol. 93, pp. 97–107.

[62] Sinha A., Chattopadhyay H., Iyengar A.K., and Biswas G. (2016) 'Enhancement of heat transfer in a fin-tube heat exchanger using rectangular winglet type vortex generators', *International Journal of Heat and Mass Transfer*, vol. 101, pp. 667–681.

[63] Jacobi A. and Shah R. (1995) 'Heat transfer surface enhancement through the use of longitudinal vortices: a review of recent progress', *Experimental Thermal and Fluid Science*, vol. 11(3), pp. 295–309.

[64] Zolfaghari A., Aminian E., and Saffari H. (2022) 'Numerical investigation on entropy generation in the dropwise condensation inside an inclined pipe', *Heat Transfer*, vol. 51(1), pp. 551–577.

[65] Eiamsa-Ard S. and Promvonge P. (2011) 'Influence of double-sided delta-wing tape insert with alternate-axes on flow and heat transfer characteristics in a heat exchanger tube', *Chinese Journal of Chemical Engineering*, vol. 19(3), pp. 410–423.

[66] Sun Z., Zhang K., Li W., Chen Q., and Zheng N. (2020) 'Investigations of the turbulent thermal-hydraulic performance in circular heat exchanger tubes with multiple rectangular winglet vortex generators', *Applied Thermal Engineering*, vol. 168, p. 114838.

[67] Zhang K., Sun Z., Zheng N., and Chen Q. (2020) 'Effects of the configuration of winglet vortex generators on turbulent heat transfer enhancement in circular tubes', *International Journal of Heat and Mass Transfer*, vol. 157, p. 119928.

[68] Liu H.l., Li H., He Y.l., and Chen Z.t. (2018) 'Heat transfer and flow characteristics in a circular tube fitted with rectangular winglet vortex

generators', *International Journal of Heat and Mass Transfer*, vol. 126, pp. 989–1006.

[69] Tiggelbeck S., Mitra N., and Fiebig M. (1994) 'Comparison of wing-type vortex generators for heat transfer enhancement in channel flows', .

[70] Fiebig M., Valencia A., and Mitra N.K. (1993) 'Wing-type vortex generators for fin-and-tube heat exchangers', *Experimental Thermal and Fluid Science*, vol. 7(4), pp. 287–295.

[71] Liu H.l., Fan C.c., He Y.l., and Nobes D.S. (2019) 'Heat transfer and flow characteristics in a rectangular channel with combined delta winglet inserts', *International Journal of Heat and Mass Transfer*, vol. 134, pp. 149–165.

[72] Song K., Xi Z., Su M., Wang L., Wu X., and Wang L. (2017) 'Effect of geometric size of curved delta winglet vortex generators and tube pitch on heat transfer characteristics of fin-tube heat exchanger', *Experimental Thermal and Fluid Science*, vol. 82, pp. 8–18.

[73] Shi W., Liu T., Song K., Zhang Q., Hu W., and Wang L. (2021) 'The optimal longitudinal location of curved winglets for better thermal performance of a finned-tube heat exchanger', *International Journal of Thermal Sciences*, vol. 167, p. 107035.

[74] Modi A.J., Kalel N.A., and Rathod M.K. (2020) 'Thermal performance augmentation of fin-and-tube heat exchanger using rectangular winglet vortex generators having circular punched holes', *International Journal of Heat and Mass Transfer*, vol. 158, p. 119724.

[75] Gong B., Wang L.B., and Lin Z.M. (2015) 'Heat transfer characteristics of a circular tube bank fin heat exchanger with fins punched curve rectangular vortex generators in the wake regions of the tubes', *Applied Thermal Engineering*, vol. 75, pp. 224–238.

[76] Naik H., Harikrishnan S., and Tiwari S. (2018) 'Numerical investigations on heat transfer characteristics of curved rectangular winglet placed in a channel', *International Journal of Thermal Sciences*, vol. 129, pp. 489–503.

[77] Nejat A., Mirzakhalili E., Aliakbari A., Niasar M.S.F., and Vahidkhah K. (2012) 'Non-newtonian power-law fluid flow and heat transfer computation across a pair of confined elliptical cylinders in the line array', *Journal of Non-Newtonian Fluid Mechanics*, vol. 171, pp. 67–82.

[78] Jain A., Biswas G., and Maurya D. (2003) 'Winglet-type vortex generators with common-flow-up configuration for fin-tube heat exchangers', *Numerical Heat Transfer: Part A: Applications*, vol. 43(2), pp. 201–219.

[79] Torii K., Kwak K., and Nishino K. (2002) 'Heat transfer enhancement accompanying pressure-loss reduction with winglet-type vortex generators for fin-tube heat exchangers', *International Journal of Heat and Mass Transfer*, vol. 45(18), pp. 3795–3801.

[80] Zeeshan M., Nath S., Bhanja D., and Das A. (2018) 'Numerical investigation for the optimal placements of rectangular vortex generators for improved thermal performance of fin-and-tube heat exchangers', *Applied Thermal Engineering*, vol. 136, pp. 589–601.

[81] Tiwari S., Maurya D., Biswas G., and Eswaran V. (2003) 'Heat transfer enhancement in cross-flow heat exchangers using oval tubes and multiple delta winglets', *International Journal of Heat and Mass Transfer*, vol. 46(15), pp. 2841–2856.

[82] Sommers A. and Jacobi A. (2005) 'Air-side heat transfer enhancement of a refrigerator evaporator using vortex generation', *International journal of refrigeration*, vol. 28(7), pp. 1006–1017.

[83] Islam M.S., Hino R., Haga K., Monde M., and Sudo Y. (1998) 'Experimental study on heat transfer augmentation for high heat flux removal in rib-roughened narrow channels', *Journal of nuclear science and technology*, vol. 35(9), pp. 671–678.

[84] Ahmed H.E., Ahmed M.I., and Yusoff M.Z. (2015) 'Heat transfer enhancement in a triangular duct using compound nanofluids and turbulators', *Applied Thermal Engineering*, vol. 91, pp. 191–201.

[85] Ebrahimi A., Roohi E., and Kheradmand S. (2015) 'Numerical study of liquid flow and heat transfer in rectangular microchannel with longitudinal vortex generators', *Applied Thermal Engineering*, vol. 78, pp. 576–583.

[86] Wang Q., Chen Q., Wang L., Zeng M., Huang Y., and Xiao Z. (2007) 'Experimental study of heat transfer enhancement in narrow rectangular channel with longitudinal vortex generators', *Nuclear Engineering and Design*, vol. 237(7), pp. 686–693.

[87] Kurnia J.C., Sasmito A.P., and Mujumdar A.S. (2014) 'Laminar heat transfer performance of power law fluids in coiled square tube with various configurations', *International Communications in Heat and Mass Transfer*, vol. 57, pp. 100–108.

[88] Esmaeilnejad A., Aminfar H., and Neistanak M.S. (2014) 'Numerical investigation of forced convection heat transfer through microchannels with non-newtonian nanofluids', *International Journal of Thermal Sciences*, vol. 75, pp. 76–86.

[89] Sasmal C. and Chhabra R. (2011) 'Laminar natural convection from a heated square cylinder immersed in power-law liquids', *Journal of Non-Newtonian Fluid Mechanics*, vol. 166(14-15), pp. 811–830.

[90] Kumar D. and Dalal A. (2024) 'A numerical study of the thermal and hydraulic parameters of a finned tube heat exchanger using shear-thinning fluid and rectangular winglet', *International Journal of Thermal Sciences*, vol. 195, p. 108653.

[91] Ebrahimi A. and Kheradmand S. (2012) 'Numerical simulation of performance augmentation in a plate fin heat exchanger using winglet type vortex generators', *International Journal of Mechanical Engineering and Mechatronics*, vol. 1(2), pp. 109–121.

[92] Pereira E., Bhattacharya M., and Moray R. (1989) 'Modeling heat transfer to non-newtonian fluids in a double tube heat exchanger', *Transactions of the ASAE*, vol. 32(1), pp. 256–0262.

[93] Al-Rashed A.A., Shahsavar A., Entezari S., Moghimi M., Adio S.A., and Nguyen T.K. (2019) 'Numerical investigation of non-newtonian

water-cmc/cuo nanofluid flow in an offset strip-fin microchannel heat sink: thermal performance and thermodynamic considerations', *Applied Thermal Engineering*, vol. 155, pp. 247–258.

[94] He Z., Fang X., Zhang Z., and Gao X. (2016) 'Numerical investigation on performance comparison of non-newtonian fluid flow in vertical heat exchangers combined helical baffle with elliptic and circular tubes', *Applied Thermal Engineering*, vol. 100, pp. 84–97.

[95] Lin C.X., Ko S.Y., and Tsou F. (1996) 'Laminar heat transfer in square duct flow of aqueous cmc solutions', *International journal of heat and mass transfer*, vol. 39(3), pp. 503–510.

[96] Muthamizhi K. and Kalaichelvi P. (2015) 'Development of nusselt number correlation using dimensional analysis for plate heat exchanger with a carboxymethyl cellulose solution', *Heat and Mass Transfer*, vol. 51, pp. 815–823.

[97] Shin H.K., Park M., Kim H.Y., and Park S.J. (2015) 'Thermal property and latent heat energy storage behavior of sodium acetate trihydrate composites containing expanded graphite and carboxymethyl cellulose for phase change materials', *Applied thermal engineering*, vol. 75, pp. 978–983.

[98] Varnaseri M. and Peyghambarzadeh S. (2020) 'Comprehensive study of the effect of the addition of four drag reducing macromolecules on the pressure drop and heat transfer performance of water in a finned tube heat exchanger', *Journal of Macromolecular Science, Part B*, vol. 59(11), pp. 747–773.

[99] Tso C.P., Sheela-Francisca J., and Hung Y.M. (2010) 'Viscous dissipation effects of power-law fluid flow within parallel plates with constant heat fluxes', *Journal of Non-Newtonian Fluid Mechanics*, vol. 165(11-12), pp. 625–630.

[100] Pimenta T.A. and Campos J. (2012) 'Friction losses of newtonian and non-newtonian fluids flowing in laminar regime in a helical coil', *Experimental Thermal and Fluid Science*, vol. 36, pp. 194–204.

[101] Poh H.J., Kumar K., Chiang H.S., and Mujumdar A.S. (2004) 'Heat transfer from a laminar impinging jet of a power law fluid', .

[102] Siavashi M., Bahrami H.R.T., and Aminian E. (2018) 'Optimization of heat transfer enhancement and pumping power of a heat exchanger tube using nanofluid with gradient and multi-layered porous foams', *Applied Thermal Engineering*, vol. 138, pp. 465–474.

[103] Aminian E., Moghadasi H., and Saffari H. (2020) 'Magnetic field effects on forced convection flow of a hybrid nanofluid in a cylinder filled with porous media: A numerical study', *Journal of Thermal Analysis and Calorimetry*, vol. 141, pp. 2019–2031.

[104] Aminian E., Moghadasi H., Saffari H., and Gheitaghy A.M. (2020) 'Investigation of forced convection enhancement and entropy generation of nanofluid flow through a corrugated minichannel filled with a porous media', *Entropy*, vol. 22(9), p. 1008.

[105] Shah M., Petersen E., and Acrivos A. (1962) 'Heat transfer from a cylinder to a power-law non-newtonian fluid', *AIChE Journal*, vol. 8(4), pp. 542–549.

[106] Tanner R.I., *Engineering rheology*, vol. 52 (OUP Oxford, 2000).

[107] Barquín K. and Valencia A. (2021) 'Comparison of different fin and tube compact heat exchanger with longitudinal vortex generator in cfu-cfd configurations', *Journal homepage: http://iieta. org/journals/ijht*, vol. 39(5), pp. 1523–1531.

[108] Manual U. (2021) 'Ansys fluent 21r1', *Theory Guide*, vol. 67.

[109] Fiebig M. (1995) 'Embedded vortices in internal flow: heat transfer and pressure loss enhancement', *International Journal of Heat and Fluid Flow*, vol. 16(5), pp. 376–388.

[110] Wang C.C. and Chi K.Y. (2000) 'Heat transfer and friction characteristics of plain fin-and-tube heat exchangers, part i: new experimental data', *International Journal of Heat and Mass Transfer*, vol. 43(15), pp. 2681–2691.

[111] Lu G. and Zhai X. (2019) 'Effects of curved vortex generators on the air-side performance of fin-and-tube heat exchangers', *International Journal of Thermal Sciences*, vol. 136, pp. 509–518.

[112] Sara O., Pekdemir T., Yapici S., and Yilmaz M. (2001) 'Heat-transfer enhancement in a channel flow with perforated rectangular blocks', *International Journal of Heat and Fluid Flow*, vol. 22(5), pp. 509–518.

[113] Liu J., Xie G., and Simon T.W. (2015) 'Turbulent flow and heat transfer enhancement in rectangular channels with novel cylindrical grooves', *International Journal of Heat and Mass Transfer*, vol. 81, pp. 563–577.

[114] Sahel D., Ameur H., Benzeguir R., and Kamla Y. (2016) 'Enhancement of heat transfer in a rectangular channel with perforated baffles', *Applied Thermal Engineering*, vol. 101, pp. 156–164.

[115] Japar W.M.A.A., Sidik N.A.C., and Mat S. (2018) 'A comprehensive study on heat transfer enhancement in microchannel heat sink with secondary channel', *International Communications in Heat and Mass Transfer*, vol. 99, pp. 62–81.

[116] Alfarawi S., Abdel-Moneim S., and Bodalal A. (2017) 'Experimental investigations of heat transfer enhancement from rectangular duct roughened by hybrid ribs', *International Journal of Thermal Sciences*, vol. 118, pp. 123–138.

[117] Neil Jordan C. and Wright L.M. (2013) 'Heat transfer enhancement in a rectangular (ar= 3: 1) channel with v-shaped dimples', *Journal of Turbomachinery*, vol. 135(1), p. 011028.

[118] Ghani I.A., Sidik N.A.C., Mamat R., Najafi G., Ken T.L., Asako Y., and Japar W.M.A.A. (2017) 'Heat transfer enhancement in microchannel heat sink using hybrid technique of ribs and secondary channels', *International Journal of Heat and Mass Transfer*, vol. 114, pp. 640–655.

[119] Vengadesan E., Thameenansari S., Manikandan E.J., and Senthil R. (2022) 'Experimental study on heat transfer enhancement of parabolic trough solar collector using a rectangular channel receiver', *Journal of the Taiwan Institute of Chemical Engineers*, vol. 135, p. 104361.

[120] Chen Y., Fiebig M., and Mitra N. (1998) 'Heat transfer enhancement of a finned oval tube with punched longitudinal vortex generators in-line', *International Journal of Heat and Mass Transfer*, vol. 41(24), pp. 4151–4166.

[121] Chen Y. and Fiebig M., 'Effect of fin heat conduction on the performance of punched winglets in finned oval tubes', in 'Heat Transfer Enhancement of Heat Exchangers', (Springer, 1999), pp. 107–122.

[122] Brockmeier U., Fiebig M., Güntermann T., and Mitra N.K. (1989) 'Heat transfer enhancement in fin-plate heat exchangers by wing type vortex generators', *Chemical engineering & technology*, vol. 12(1), pp. 288–294.

[123] Brockmeier U., Guentermann T., and Fiebig M. (1993) 'Performance evaluation of a vortex generator heat transfer surface and comparison with different high performance surfaces', *International journal of heat and mass transfer*, vol. 36(10), pp. 2575–2587.

[124] Biswas G., Mitra N., and Fiebig M. (1989) 'Computation of laminar mixed convection flow in a channel with wing type built-in obstacles', *Journal of Thermophysics and Heat Transfer*, vol. 3(4), pp. 447–453.

[125] Bergman T.L., Lavine A.S., Incropera F.P., and DeWitt D.P., *Introduction to heat transfer* (John Wiley & Sons, 2011).

[126] Gunter A. and Shaw W. (1945) 'A general correlation of friction factors for various types of surfaces in crossflow', *Transactions of the American Society of Mechanical Engineers*, vol. 67(8), pp. 643–656.

[127] Siavashi M., Bahrami H.T., Aminian E., and Saffari H. (2019) 'Numerical analysis on forced convection enhancement in an annulus using porous ribs and nanoparticle addition to base fluid', *Journal of Central South University*, vol. 26(5), pp. 1089–1098.

[128] Fiebig M. (1998) 'Vortices, generators and heat transfer', *Chemical Engineering Research and Design*, vol. 76(2), pp. 108–123.

[129] Bejan A., *Convection heat transfer* (John wiley & sons, 2013).

[130] Saffari H., Kamali M., Vatanjoo E., and Aminian E. (2023) 'Theoretical investigation on microstructured hybrid surface heat transfer characteristics with marangoni convection effect', *Numerical Heat Transfer, Part A: Applications*, vol. 84(7), pp. 675–694.

[131] He Y.L. and Zhang Y., 'Advances and outlooks of heat transfer enhancement by longitudinal vortex generators', in 'Advances in Heat Transfer', vol. 44 (Elsevier, 2012), pp. 119–185.

[132] Li L., Du X., Zhang Y., Yang L., and Yang Y. (2015) 'Numerical simulation on flow and heat transfer of fin-and-tube heat exchanger with longitudinal vortex generators', *International Journal of Thermal Sciences*, vol. 92, pp. 85–96.

[133] Koch S. (1997) 'Formation of the shear-induced state in dilute cationic surfactant solutions', *Rheologica acta*, vol. 36, pp. 639–645.

[134] Oda R., Narayanan J., Hassan P., Manohar C., Salkar R., Kern F., and Candau S. (1998) 'Effect of the lipophilicity of the counterion on the viscoelasticity of micellar solutions of cationic surfactants', *Langmuir*, vol. 14(16), pp. 4364–4372.

[135] Davies T.S., Ketner A.M., and Raghavan S.R. (2006) 'Self-assembly of surfactant vesicles that transform into viscoelastic wormlike micelles upon heating', *Journal of the American Chemical Society*, vol. 128(20), pp. 6669–6675.

[136] Samuel M., Card R., Nelson E., Brown J., Vinod P., Temple H., Qu Q., and Fu D. (1999) 'Polymer-free fluid for fracturing applications', *SPE Drilling & Completion*, vol. 14(04), pp. 240–246.

[137] Virk P.S. (1975) 'Drag reduction fundamentals', *AIChE Journal*, vol. 21(4), pp. 625–656.

LIST OF PUBLICATIONS

International Journal

1. **Dheeraj Kumar**, Amaresh Dalal, A numerical study of the thermal and hydraulic parameters of a finned tube heat exchanger using shear-thinning fluid and rectangular winglet, *International Journal of Thermal Sciences*, vol. 915, A88, 2024.

2. **Dheeraj Kumar**, Amaresh Dalal, Computational analysis of heat transfer and frictional loss of FTHE with delta winglet and shear-thinning fluid, *International Journal of Thermal sciences*, *Communicated*.

3. **Dheeraj Kumar**, Amaresh Dalal, Heat transfer analysis of a rectangular channel with delta winglets and shear-thinning fluid, *International Journal of Heat and Mass Transfer*, *Communicated*.

4. **Dheeraj Kumar**, Amaresh Dalal, Effect of shear-thinning fluid and curved vortex generators on the performance of finned-tube heat exchanger, *Under preparation*.

International Conference

1. **Dheeraj Kumar**, Amaresh Dalal, Heat Transfer Analysis of Finned Tube Heat Exchanger with Non-Newtonian fluid and Longitudinal Vortex Generator, *International Heat and Mass Transfer Conference* (IHMTC), IIT Madras, 17th - 20th December, 2021.

2. **Dheeraj Kumar**, Amaresh Dalal, A Numerical Study Of Thermohydraulic Performance Of A Finned Tube Heat Exchanger Using An Aqueous Solution Of Carboxymethyl Cellulose And Rectangular Winglet Pair, *International Heat Transfer Conference* (IHTC), Cape Town, South Africa, 14-18 August 2023.

3. **Dheeraj Kumar**, Amaresh Dalal, Heat Transfer And Pressure Drop Analysis Of Fin-Tube Heat Exchanger With Delta Winglet And Shear-Thinning Fluid, *International Conference on Computational Heat and Mass Transfer* (ICCHMT), Düsseldorf, Germany, 4-8 September 2023.